Investigation of the Occurrence of Ice Jams on the Lower Red River in Manitoba

by

Morgann Becket

A thesis submitted to the Faculty of Graduate Studies of

The University of Manitoba

In partial fulfillment of the requirements of the Degree of

Master of Science

Department of Civil Engineering

University of Manitoba

Winnipeg, Manitoba, Canada

Abstract

The Lower Red River in Manitoba regularly experiences ice jam flooding, with the most severe events occurring between Lockport and Netley Lake. This research investigates the timing and frequency of ice jamming on this section of the Lower Red River, the relationship between ice jams and antecedent conditions, and different ice jam prediction methods and their suitability for the study area. By gaining a better understanding of ice jamming trends in the area, this research provides accessible prediction methods that can help guide decisions related to the risk and severity of spring ice jamming.

A database of ice jam events was developed with each event given a severity rating from 1-5, based on the resulting flood from the ice jam. Out of 54 ice jam events from 1962-2017, the most common event locations were found to be Sugar Island, Selkirk Bridge, and the Netley Creek Confluence. All ice jam events occurred when the peak spring flow exceeded 1000 cms and all severe events (severity 3+) occurred when peak spring flows exceeded 1500 cms.

Three different ice jam prediction models including a threshold model, regression model, and discriminate function analysis (DFA) were developed using meteorological and hydrometric parameter data. The threshold model proved to be the best tool to predict severe events, as its predictions differentiated all severe event years from non-event years with only one false positive result. The quadratic three-outcome DFA had success in predicting minor ice jam years (severity 1-2) and differentiating them from severe ice jam or no ice jam years and is therefore recommended to use alongside the threshold model. The regression model was not as effective as the threshold model or DFA in predicting ice jamming.

Acknowledgments

First, I would like to thank my advisors Dr. Karen Dow and Dr. Shawn Clark for allowing me to pursue a project I was passionate about and giving me the freedom to take it in the direction I found most beneficial. The guidance and expertise you both provided me with was invaluable and I am thankful for the opportunity to work with you both.

I would also like to thank everyone in our water resources group who assisted me in any way. Whether it was a friendly chat, brainstorming session, or help with fieldwork, the encouragement from this group was much appreciated.

I would also like to acknowledge the funding contribution from the Natural Sciences and Engineering Research Council of Canada, Manitoba Hydro, the University of Manitoba, and Manitoba Infrastructure. Additionally I would like to thank Environment and Climate Change Canada and Manitoba Infrastructure for the data and knowledge contribution to the project.

Lastly, I would like to thank my friends and family, especially my parents who have supported me along the way. A special thank you to my friend Katy who always had a kind word and a good edit. Finally, I would like to thank my fiancé Greg who has always encouraged me in everything I do.

Disclaimer

Table of Contents

List of Figures

List of Tables

Nomenclature

Symbol	Units	Description
$\boldsymbol{E_m}$	[Wm^{-2}]	Net heat flux acting on the ice cover
$\boldsymbol{E_{si}}$	[Wm^{-2}]	Net solar radiation
$\boldsymbol{E_{li}}$	[Wm^{-2}]	Net long wave radiation
$\boldsymbol{E_{ei}}$	[Wm^{-2}]	Net latent heat flux
$\boldsymbol{E_{hi}}$	[Wm^{-2}]	Net flux of sensible heat
$\boldsymbol{E_{pi}}$	[Wm^{-2}]	Heat flux from precipitation
$\boldsymbol{E_w}$	[Wm^{-2}]	Heat flux from the water
$\boldsymbol{h_i}$	[Wm^{-2}°C];	Heat transfer coefficient between the ice and air
$\boldsymbol{T_i}$	[°C]	Temperature of the ice
$\boldsymbol{T_a}$	[°C]	Temperature of the air
$\boldsymbol{t_i}$	[m]	Ice thickness
$\boldsymbol{\alpha}$	[m°C$^{-1/2}$]	Stefan equation coefficient
$\boldsymbol{ADDF}$	[°C]	Accumulated degree days of freezing
$\boldsymbol{ADDT}$	[°C]	Accumulated degree days of thawing
$\boldsymbol{ADAT}$	[°C]	Average daily air temperature
$\boldsymbol{T_b}$	[°C]	Base air temperature
$\boldsymbol{\eta}$	[m]	Ice thickness
$\boldsymbol{\eta_0}$	[m]	Ice thickness just before thaw begins
$\boldsymbol{\varepsilon}$	[m°C^{-1}day]	Site specific heat transfer coefficient

sc	Wm^{-2}	Solar insolation
so	m	Incident solar radiation
a_2		Location dependant empirical constants
b_2		Location dependant empirical constants
$\frac{n}{N}$		Ratio of bright sunshine hours
α_1		Albedo
RSE		Residual standard error
R^2		Coefficient of determination
$Adjusted\ R^2$		Adjusted coefficient of determination

Chapter 1: Introduction

1.1 Background

River ice breakup is experienced annually on rivers in northern climates. The breakup process can be unpredictable at times and events like rainfall or rapid snowmelt can lead to the formation of ice jams. Breakup ice jams can result in a significant rise in upstream water levels and when released, discharge a surge of water and ice downstream. In Manitoba, the water levels experienced from ice jamming has threatened entire communities on multiple occasions and since ice jams usually occur with little warning, the resulting evacuations can be a race against the clock. Locations near the City of Selkirk have experienced millions of dollars of damages due to ice jam flooding and the Province of Manitoba currently spends over $1,000,000 annually to mitigate ice jamming in this area (Hoye, 2019).

At present there is no tried and true method to predict if and/or when an ice jam will occur based on antecedent conditions such as over-winter or even early breakup meteorological and hydrometric data. No universal deterministic methods have yet been developed resulting in most modeling being highly empirical and site specific (White, 2003). This is because conditions that dictate the breakup processes and occurrence of ice jams are considered a local phenomenon and as such, causes and conditions attributed to one site may not be beneficial to other sites that experience ice jamming (White, 2003). Therefore, studying local ice jams can give insights to trends and anecdotal conditions that lead up to these events, which can be done through development of an ice jam database.

Ice jam databases can be used to provide insight into events in an area, such as when and where ice jams occur and how severe they can be. This data is invaluable as the ice-affected stage can be much harder to model than the open water stage due to the complicated ice processes that occur. Therefore, the historic stage and discharge values might be the best way to estimate the ice-impacted stage. Furthermore, when paired with meteorological and hydrological data, an ice jam database can be used to better understand local ice jamming trends and identify variables that influence ice jamming. Identifying these variables help us to understand the causes of local ice jams and are the building block to developing a prediction tool.

1.2 Study Area

The study area for this project is the Lower Red River between Lockport and Netley Lake as shown in Figure 1.1. This stretch of the river is approximately 33 km in length, running through the City of Selkirk and draining many creeks including Netley Creek just south of Netley Lake. Ice jams occur frequently in this area and are considered an annual threat to residents and infrastructure.

Chapter 1: Introduction

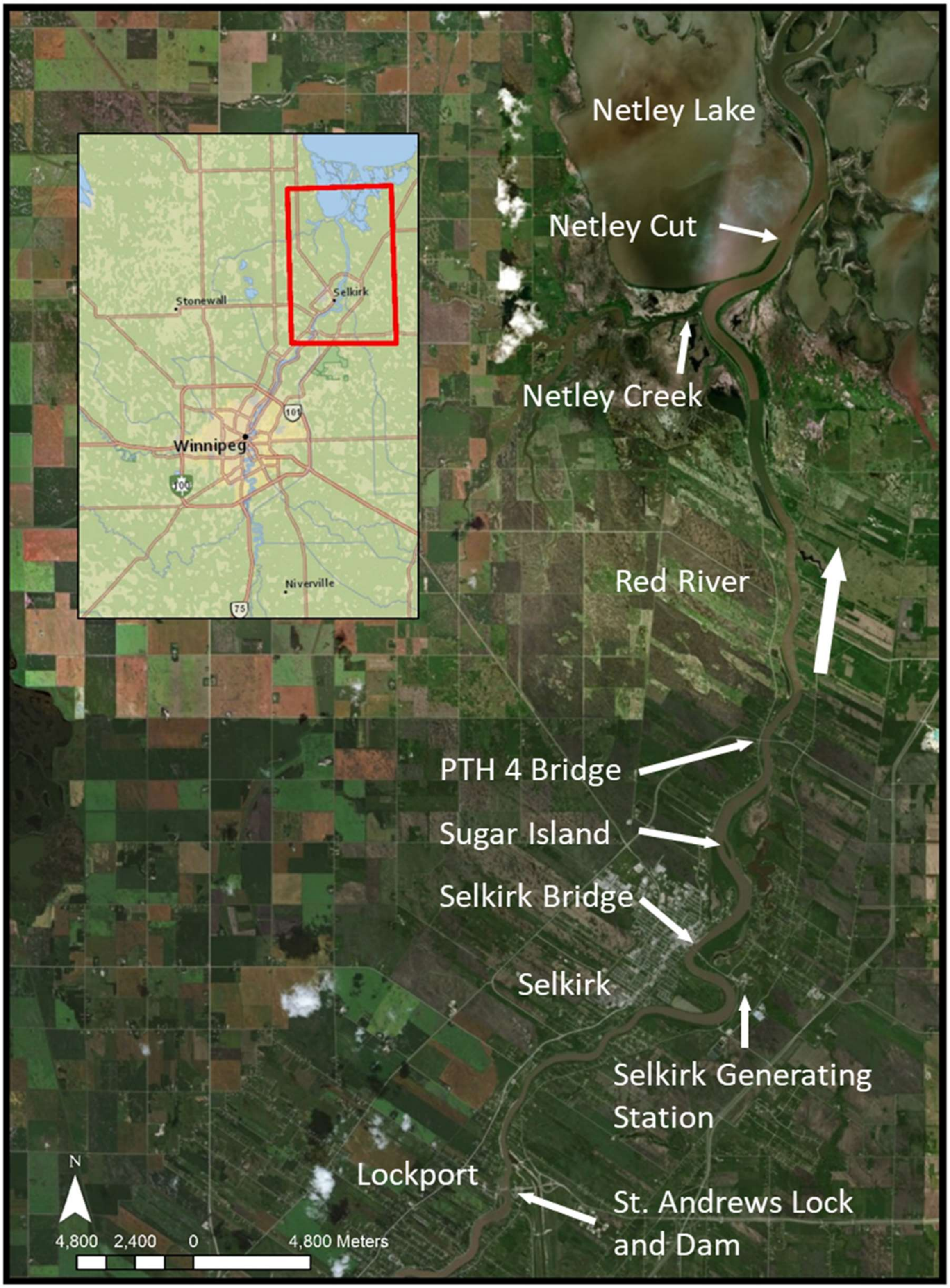

Figure 1.1: Map depicting relevant landmarks in the study area.

Chapter 1: Introduction

1.2.1 The Red River

The Red River watershed is a large watershed located in both Canada and the United States. The watershed, which is approximately 288,000 km^2 in size and includes the Assiniboine watershed, is the southern-most watershed of the Nelson River basin. The river is approximately 885 km long and is one of the few north-flowing rivers in North America. The river originates in South Dakota and then flows north between North Dakota and Minnesota, continuing to southern Manitoba where it empties into Lake Winnipeg.

The Red River is a meandering river that runs through the central prairie region and therefore has a very mild slope causing the river to be prone to extreme open water floods for several reasons. The mild slope of the river and overbank areas cause floodwaters to inundate much larger areas than most floodplains. The slope also results in the floodwater taking several weeks to dissipate, as the flood peak is very slow moving. Also, the gradients of the major tributaries are larger by a factor of 10 or more, resulting in more water being introduced to the main channel than can flow downstream (Rannie, 2016).

The Lower Red River stretches from the confluence of the Assiniboine River to Lake Winnipeg, running through cities such as Winnipeg, Lockport, and Selkirk. The river also runs through the Netley-Libau marsh, a delta system located just south of Lake Winnipeg, before emptying into the lake. Before it reaches the marsh, a portion of the flow short circuits through Netley Lake via the Netley Cut which was approximately 460 m in width in 2015 and continues to increase at a rate of 13.5 m each year (Kowal, 2019).

1.2.2 Water Control Structures

Due to the high population in the proximity of the river and its capacity for large flood events, many water control structures have been built to primarily reduce the risk of flooding to the area, especially the City of Winnipeg, but also to control water levels for navigation purposes. These include:

- The Shellmouth Dam: completed in 1972 on the Assiniboine River and includes a 56 km long reservoir to protect downstream areas from high flows;
- The Portage Diversion: running from the Assiniboine River near Portage La Prairie to Lake Manitoba, the diversion can remove up to ≈700 cms (25,000 cfs) from the Assiniboine in times of high flow;
- St Andrews Lock and Dam: located at the city of Lockport, the lock and dam were built in 1910 to drown upstream rapids and allow river navigation from Winnipeg to Lake Winnipeg; and
- The Red River Floodway: completed in 1968 and at the time was the second largest earth moving project in the world behind the Panama Canal. The water from the Red River is diverted into the floodway just south of Winnipeg and re-enters the river north of Lockport. After the devastating 1997 flood, the floodway was expanded and can now divert ≈4000 cms (140,000 cfs) and protect Winnipeg from a one-in-700 year flood (Government of Manitoba, 2015).

All the above structures have the potential to impact the water level on the Lower Red River.

1.2.3 Ice Processes

During the winter season, the Lower Red River forms a stable ice cover, usually lasting from November until April. Late season ice thicknesses in the area average 0.7 m but can reach up to 1.06 m. In the spring, breakup is initiated by warming temperatures and an influx of snowmelt runoff. Lower Red River ice breakup usually occurs in the range of flows from 990 cms to 1420 cms. At the most downstream reach of the river past Breezy Point it is likely that higher flows are needed to initiate breakup as this ice is more typical of lake ice (Acres, 2004). During spring breakup, ice jamming frequently occurs on the Lower Red River with the most severe jams occurring on the most downstream section between Lockport and Lake Winnipeg.

Some of the factors that make the Lower Red River prone to breakup ice jamming is its highly meandering channel and the location of infrastructure, where ice pieces can become juxtaposed. The very mild slope of the river also reduces the driving forces acting on lodged ice pieces allowing them to more easily stay in place. In addition, due to its south to north flow direction, the spring peak in the south extent of the river slowly moves north as the snow is still melting, amplifying the amount of flow reaching the north region where the ice could still be intact. Some examples of ice accumulation on the Lower Red River can be seen in Figure 1.2.

Figure 1.2: Ice accumulation on the Lower Red River during breakup.

Ice jams have been recorded on the Lower Red River since the area was first settled, with the most frequent ice jam locations at the Selkirk Bridge, Sugar Island, the PTH 4 Bridge, and north of PTH 4 (Acres, 2004). The occurrence of ice jams in this area is probably due to the extremely mild slope, as it is as low as 0.00001 m/m between Lockport and Lake Winnipeg, and the development of thick ice (K. E. Lindenschmidt, 2012). It is common for upstream ice jams to release and re-form downstream causing a cascading effect, resulting in multiple jams over the breakup season in this reach. In the Breezy Point area additional factors contribute to ice jam formation, such as an increase in the bed elevation (4-5 m consistently) just downstream of the Netley Creek confluence caused by sediment transport in Netley Creek. Also, the river's sharp meander just downstream of the confluence can reduce flow (K. E. Lindenschmidt, 2012). This increase in bed elevation can be seen in Figure 1.3.

Chapter 1: Introduction

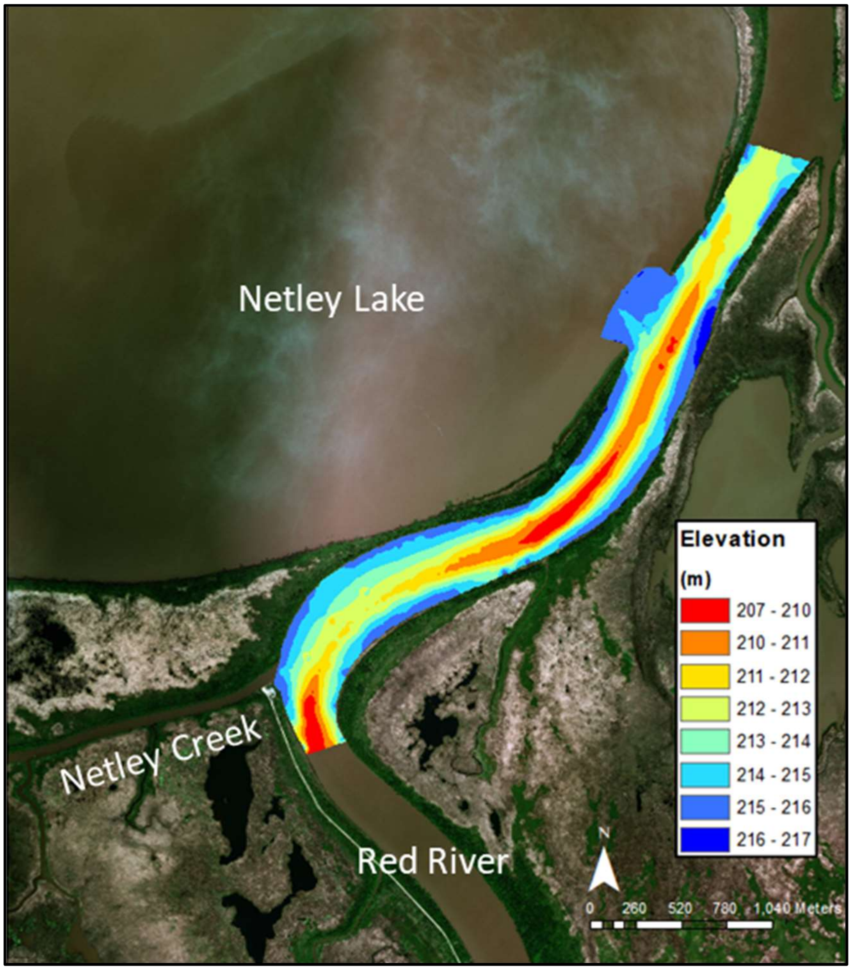

Figure 1.3: Bathymetry of the Red River between Netley Creek and Netley Lake. Bathymetry acquired by Manitoba Hydro in 2019.

Jamming along the Lower Red River occurs frequently with indications that jamming has become more severe and may continue to do so. Recent years of severe ice jam flooding on the Lower Red River occurred in 1995, 1996, 2004, 2005, 2007, 2009, and 2011 (K. Lindenschmidt et al., 2010). The most extreme event was in 2009 where high soil moisture and above average snowpack contributed to ice jam flooding, leading to a $4.4 million buyout of flood prone properties in the Breezy Point area just south of Netley Creek (Wazney & Clark, 2016).

1.2.4 Ice Jam Mitigation Program

Due to the frequency and severity of ice jamming on the Lower Red River, the Province of Manitoba has developed an ice jam mitigation program for the area. The program relies on a large machine called an Amphibex, which is similar to a backhoe but with the ability to float. This machine was initially designed for dredging, but instead is used to break up the ice. The excavator arm drags the Amphibex onto the ice where the weight of the machine causes the ice to break.

This unique program started in 2006 with the purchase of a used Amphibex and has since expanded to include an additional three Amphibexes as well as other supporting machinery (Hoye, 2019). Currently, the ice is broken from the Netley Cut to Selkirk in a six-week period, depending on ice conditions and weather, in February and March before natural breakup occurs. The program results in roughly the middle third of the river being broken, as seen in Figure 1.4. The goal of the program is to allow ice that would usually form ice jams to move through the river reach and into the Netley Cut during the spring flow peak.

Figure 1.4: Amphibex ice cutting pattern looking downstream from the PTH 4 Bridge.

The weight of an Amphibex can only shatter ice of less than 45 cm thickness. Therefore on the Red River, where thicknesses are typically double that, additional steps have to be taken (Hoye, 2019). First, an ice thickness survey on the Red River is conducted using ground penetrating radar (GPR). The survey measures thousands of points and is used to identify locations where the ice thickness exceeds the Amphibex's capabilities. In these areas, heavy duty saws are deployed to cut through the ice, however the ice is not cut all the way through to avoid water refreezing in the cut. Once cutting is completed, the Amphibexes are then deployed to break up the ice. As the number of Amphibexes and supporting equipment have increased so has the cost of the program, which is now approximately $1.5 million annually (Hoye, 2019).

1.2.5 Past Studies

There have been limited studies done on ice jamming on the Lower Red River. In 2004, as part of the Preliminary Engineering Report to expand the existing floodway, Acres Engineering reviewed water level data and local newspapers to determine years of possible ice jamming and the related flow conditions (Acres, 2004). This data was used to determine if the expanded floodway would impact the severity of ice jams on the Lower Red River in the Selkirk area, north of the floodway outlet, as there were many concerns that ice jamming had worsened since the completion of the floodway channel in 1968 (KGS et al., 2004). Additionally, an independent study was completed in 2005 on the effects of the proposed expanded floodway on ice jamming. Both reports concluded that the floodway does not increase ice jam flooding downstream of the floodway outlet (KGS et al., 2004; Northwest Hydraulics, 2005).

In 2012, Lindenschmidt modelled ice jamming along the Lower Red River between Lockport and Lake Winnipeg using the one-dimensional RIVICE modelling software. The data needs for this model included discharge and stage measurements, as well as ice thicknesses. The model was calibrated to the multiple ice jamming events that occurred in 2010 and at the time, produced the highest stage on record between Selkirk and the Netley Creek confluence. Simulation of the ice jamming was successful, with the authors stating the model would be a useful tool to investigate ice jam mitigation strategies in the reach.

1.3 Objectives

The objective of this research is to gain a greater understanding of the variables and conditions that are associated with ice jam formation on the Lower Red River. Although some work has been done to document and model past ice jams in the area, the author is unaware of any attempt to collect detailed information on past ice jam events or to try and distinguish conditions that lead up to these events. A detailed analysis of past ice jam events is the first step in predicting the risk of a future event. The ability to do this with confidence has many benefits for the area as it can help personnel to make informed decisions of when to invest in ice jam mitigation measures during low risk times and/or flood preparedness at high risk times. This could potentially lead to savings of both money and resources.

This research will investigate the occurrence of ice jamming on the Lower Red River as well as any relationship with antecedent conditions or a combination of these conditions that lead to ice jamming. The main objectives of this research are as follows:

1. Complete a historical review of ice jamming in the study area by gathering data on past ice jam events from various sources (e.g. reports and newspaper archives) to create a comprehensive ice jam database.
2. Determine if any antecedent conditions, such as over-winter or early breakup meteorological and hydrometric data correlate to the occurrence of an ice jam.
3. Investigate jam prediction methods and their suitability for the study area. This will be done by developing preliminary prediction models and evaluating their performance through hindcasting historical ice jam events.

Chapter 2: Background

River ice breakup and ice jamming are very complex physical processes and are difficult to study. This is further exacerbated since relevant data during the breakup period, such as ice strength, river flow, and ice jam thickness, is difficult and often dangerous to collect. The purpose of this chapter is to give the reader a basic understanding of the major processes that are central to this study which much of the methods and analysis are based on.

2.1 Heat Exchange

The main driver of any ice process is the heat exchange of the water or ice cover with the environment. During the ice formation process, the supercooling of water generates frazil ice particles, skim ice, border ice, and eventually results in a solid ice cover. Frazil ice particles can only form in areas of turbulent flow, which are uncommon on the Lower Red River as the freeze-up period is usually associated with low flow conditions. When frazil generation does occur, the disc-shaped particles stick together forming frazil pans and eventually result in a rougher ice cover. In the spring, when milder weather and increased solar radiation occur due to the change of seasons, the ice cover starts to deteriorate from both the bottom and top surface. The competence of the ice cover at the time of breakup determines whether a thermal or dynamic breakup occurs. There are three methods typically used for modeling heat exchange in relation to river ice, these will be discussed below.

2.1.1 Full Energy Budget

The full energy budget model includes all the possible heat fluxes, either positive or negative, that act on an ice cover. This is the most data intense method as it relies on very site-specific data that is either measured or quantified empirically. The energy budget is shown in Equation 2.1 with all terms expressed as Wm^{-2} (Beltaos, 2008):

$$E_m = E_{si} + E_{li} + E_{ei} + E_{hi} + E_{pi} + E_w \quad (2.1)$$

Where: E_m is the net heat flux [Wm^{-2}];

E_{si} is the net solar radiation [Wm^{-2}];

E_{li} is the net long wave radiation [Wm^{-2}];

E_{ei} is the net latent heat flux [Wm^{-2}];

E_{hi} is the net flux of sensible heat [Wm^{-2}];

E_{pi} is the heat flux from precipitation [Wm^{-2}]; and

E_w is the heat flux from the water [Wm^{-2}].

E_m represents the net heat flux to the combined ice and snow cover, if a layer of snow is present.

When applied in the context of river ice, the summed components of the energy budget can be attributed to ice growth (heat loss) or ice melt (heat gain). Some terms can be measured directly such as solar radiation, other terms must be calculated empirically and rely on calibrated parameters. Although the most precise method, the full energy budget is the most difficult to use as data requirements are large and often site-specific data for all terms is not available.

2.1.2 Linear Heat Transfer

As a more simplistic approach to the full energy budget, the linear heat transfer model assumes a linear relationship between two different bodies, either water and air, ice and air, or water and ice. Using this method the net heat flux (E_m) from water to ice can be calculated as (Beltaos, 2008):

$$E_m = h_i(T_i - T_a) \tag{2.2}$$

Where: h_i is the heat transfer coefficient between the ice and air [Wm^{-2}°C];

T_i is the temperature of the ice [°C]; and

T_a is the temperature of the air [°C].

The coefficient h_i is a site-specific calibrated parameter. For the heat transfer between ice and water as well as water and air, a different calibrated heat transfer coefficient would be used. Although the inputs for this method are much simpler, determining the heat transfer coefficient requires calibration of historic water temperature or ice temperature data which may not be available.

2.1.3 Degree Day Approach

The degree day approach simplifies the energy budget and assumes it is only air temperature dependent. In this approach, the average daily air temperature above or below a base threshold criteria is accumulated. Although there are many variations to this approach, the accumulation usually begins after five consecutive days of meeting the threshold criteria. Once accumulation starts, days that do not meet the criteria are either ignored or deducted. Accumulated degree days of freezing (ADDF) are accrued below 0°C and usually relate to ice growth or thickness. A well know version of correlating ADDF to ice thickness is the Stefan equation (Ashton, 1986):

$$t_i = \alpha\sqrt{ADDF} \tag{2.3}$$

Where: t_i represents the ice thickness [m];

α represents a site-specific coefficient [m°C$^{-1/2}$]; and

ADDF [°C] is calculated using equation 2.4:

$$ADDF = \sum(ADAT - T_b) \tag{2.4}$$

Where: ADAT represents the average daily air temperature [°C]; and

T_b represents the base air temperature [°C].

The coefficient α is calibrated with measured ice thickness data for a specific site or can be taken from the literature. Table 2.1 shows typical ranges of α depending on the ambient conditions. Areas with higher α values are windy areas or areas with little snow, due to its insulating effects. Rivers tend to have lower α value as the turbulent flow can hinder ice growth.

Table 2.1: Common values of α used in the Stefan equation (Michel, 1971)**.**

Conditions	α [m°C$^{-1/2}$]
Windy lakes, no snow	0.027
Average lake, with snow	0.017 – 0.024
Average river, with snow	0.014 – 0.017
Sheltered small stream with rapid flow	0.007 – 0.014

When looking at ice decay on rivers, accumulated degree days of thawing (ADDT) is used as an indicator of reduced ice thickness or strength. Bilello (1980) completed a historical analysis of the decay of river ice at six locations throughout Canada and the USA and recommended using a base air temperature of -5°C as the turbulence in rivers and increased solar radiation in the spring cause ice to erode prior to the air temperature reaching 0°C. The ice decay can be calculated as (Bilello, 1980):

$$\eta = \eta_0 - \varepsilon ADDT \tag{2.5}$$

Where: η represents the ice thickness [m];

η_0 represents the ice thickness just before thaw begins [m];

ε represents a site specific coefficient [m°C^{-1}day]; and

ADDT calculated similarly to Equation 2.4 [°C].

The degree day approach is highly empirical and simplistic and therefore is used more as an index, or indicator of the degree of ice growth or decay, rather than a means of accurate measurement. This is especially true for ice decay as a limitation of this approach is that it excludes solar radiation, which is the largest heat flux during the breakup season (Beltaos, 2008).

2.2 River Ice Breakup and Ice Jamming Processes

The occurrence of an ice jam is dependant on many factors such as river morphology, flow constrictions along the channel, and the available runoff in the spring freshet. However, the most extreme jams, causing large backwater levels, usually arise when thick ice is broken up and sent downstream. Although ice jams usually occur rapidly with little warning, the ice strength at breakup is dependant on the hydraulic and structural effects of the onset of milder weather in the pre-breakup period.

In general, increasing temperatures and solar radiation cause two things to occur: First, the resisting force of the ice cover decreases as the ice starts to melt. Second, the driving forces, such as hydrodynamic forces, on the ice cover increase as runoff increases flow. When the driving forces exceed the resisting forces, the ice cover breaks up and is set in motion. Normally breakup occurs after the ice cover experiences some thermal weakening and the water level has risen due to runoff, but there are two extreme scenarios known as a thermal and dynamic breakup. When there are very little driving forces applied to the ice cover and it's left to decay in place and gradually open up, it is referred to as a thermal breakup, seen in Figure 2.1(a). Thermal breakups usually occur when there is a small amount of precipitation in the winter and spring preceding breakup. Contrarily, if there is a large increase in runoff, usually due to rapid snowmelt or rain on snow events, the intact ice cover will become dislodged with little to no deterioration (and therefore very high strength), which is known as a dynamic breakup Figure 2.1(b).

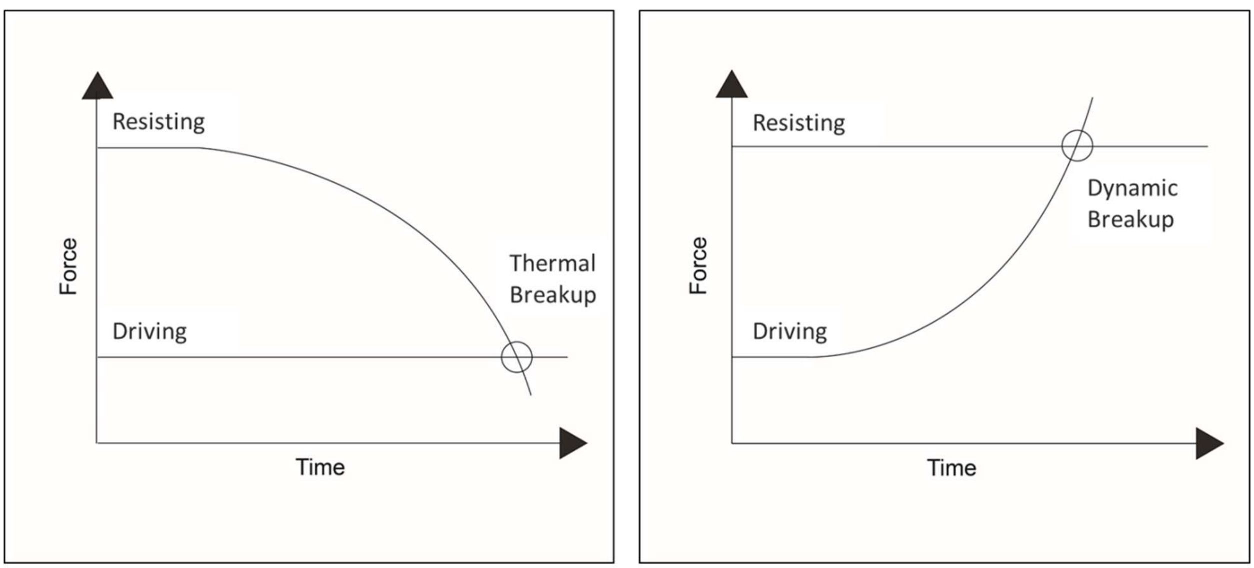

(a) (b)

Figure 2.1: Conceptual depiction of the interaction between the resisting forces of the ice cover and driving forces acting on the ice cover. Breakup occurs where the two forces meet, a thermal breakup occurs in (a) and a dynamic breakup occurs in (b). Adapted from Beltaos, 2008.

Chapter 2: Literature Review

Thermal weakening of the ice cover starts during the pre-breakup period, the ice cover starts to thin and lose strength as melt occurs both on the underside and top of the cover. Initially the temperature of the ice cover varies with the thickness of the ice. The temperature at the bottom of the ice cover is equal to the water temperature at the ice-water interface (roughly at 0°C), and the top ice surface temperature can be approximated as being equal to the atmospheric temperature. The melting of the underside of an ice cover is due to the heat transfer from water to ice. Initially the heat transfer from water reduces the temperature of the ice cover isothermally. Melting starts to occur when the heat transfer to the ice is greater than what is conducted vertically, with the greatest melt occurring when the ice cover temperature is close to zero. As bottom melt progresses, the smooth underside of the ice cover forms ripples which can increase the heat transferred to the ice by as much as 50% (Ashton, 1986).

The first stage of top melt, which is primarily driven by solar radiation and air temperature, begins as the layer of snow on the ice is melted. The snow and ice melt at different rates as snow has a higher albedo and therefore reflects a larger amount of solar radiation compared to ice. As the snow on the ice cover melts, an increased amount of solar radiation penetrates and is absorbed by the ice. This causes the ice temperature to rise to 0°C at which point it starts to melt. Many studies have related compressive ice strength decline to solar radiation absorption (Ashton, 1986; Bulatov, 1970; F. Hicks, Chen, & Andres, 1995). The ice crystals first start to melt at their boundaries where contaminates are stored, reducing the freezing point in these areas. The differential melt of the ice causes an increase in porosity and a reduction in ice strength (Bulatov, 1970). At an advanced stage the ice cover degrades to long columnar ice crystals called candle ice, that have near negligible strength.

Chapter 2: Literature Review

As the temperature increases, the snowpack starts to melt and produce runoff that combines with any rainfall within the drainage basin. Runoff increases the discharge, velocity, and stage of the river, which increases the shear stress and water pressure applied to the ice cover. To relieve the flexural stress caused by increasing water pressure, the ice cover fractures and forms hinge cracks that run longitudinally. In large rivers, two hinge cracks develop along the river banks; the water level then rises and the middle of the ice cover floats freely. The restriction of the meandering banks to ice cover movement and the applied shear stress of the flow cause bending stress, and if the bending stress exceeds the flexural strength, transverse cracking occurs (Beltaos, 2008).

Once the ice cover is in motion it quickly breaks into ice floes. The ice floes will continue downstream; however, ice jams can happen if the ice floes becomes restricted. This usually occurs during a dynamic breakup when floes are strong and thick. Ice jams commonly form when floes reach an intact ice cover, channel constriction or bend, locations of channel slope reduction, or infrastructure such as bridge piers. Ice floes become juxtaposed to form a layer of surface ice or, if the hydrodynamic forces are strong enough, some ice floes will become submerged forming a thickened jam. Thickened jams can grow to a thickness of several metres and greatly increase the hydraulic roughness (Beltaos, 2008).

Once the ice jam has been initiated it will continue to grow upstream as more ice floes accumulate. As the ice jam grows, the external forces on the ice jam increase, such as the weight of the ice jam and the shear force from the flow of water. If the external forces exceed the resisting internal frictional forces of the ice blocks, the jam will shove, condensing in size and increasing in thickness, and allowing it to now resist the forces acting on it.

There are three regions of a thickened ice jam, the most downstream reach is called the downstream transition and occurs adjacent to the cause of the ice jam such as an intact ice cover, channel constriction, or infrastructure. The downstream transition holds the toe of the jam – the location of the ice jams maximum thickness – which can either be floating or grounded. In this reach the water surface slope increases rapidly to meet the water level downstream of the toe. Further upstream is the equilibrium reach where the jam thickness is uniform. In this section the water surface slope is assumed to be equal to the open water surface slope. The upstream transition is at the head or upstream end of the jam where thickness decreases from the equilibrium reach as you move upstream.

As the jam increases in size, the thickness and backwater level continue to increase until the jam reaches equilibrium. Any additional ice floes added to an equilibrium jam will only increase the length of the equilibrium reach but not increase water depth or the length of the shouldering transitional reaches. If an equilibrium reach has not yet formed but the incoming supply of ice has stopped then the jam has reached a steady state where water levels remain constant. However, in this state there is still potential for the water levels to rise if additional ice is added (Beltaos, 2008). Ice jam stages are usually much higher than open water or even stable ice cover stages for the same discharge due to the dramatic reduction in the channel conveyance. Figure 2.2 shows the discharge impact on stage for different channel ice conditions.

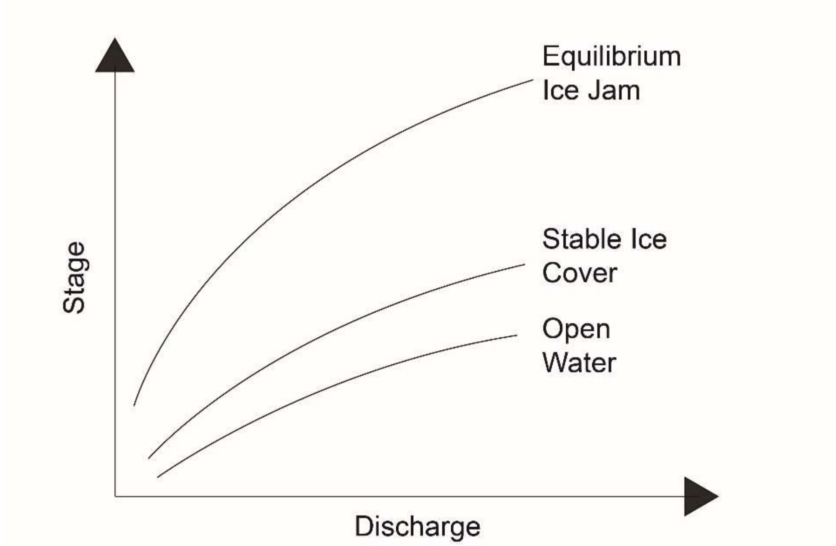

Figure 2.2: Stage and discharge relationship for open water, stable ice covered, and equilibrium ice jam conditions. Adapted from Beltaos, 2008.

Physical, hydraulic, or mechanical characteristics of ice jams are very difficult to determine. There is very little field data available for ice jams such as thickness and discharge occurring under the jam as acquiring that data can be dangerous due to the volatile nature of ice jams. There are some instances where a mid-winter breakup will occur and ice jams will refreeze making it safe to drill for ice thickness measurements. Shear walls can also be used to estimate jam thickness. A shear wall represents the portion of the jam along the river bank that was grounded and not subjected to the shear from flow. Usually the thicker the ice jam the greater the distance the shear wall spans. Therefore, the width of a shear wall increases closer to the jam toe. However, the thicknesses measured from a shear wall are just estimates since the release surge of a jam upstream can erode a shear wall or deposit ice pieces where no jam had occurred (Beltaos, 2008).

Chapter 2: Literature Review

There is no universal method to predict when an ice jam will occur as the process is physically complex and very site specific (Beltaos, 2008; White, 2003). Serious ice jamming occurs during a dynamic breakup when driving forces break up a strong ice cover. Therefore, possible indicators of a dynamic breakup can be used to predict if ice jamming will occur such as factors that lead to large driving forces, usually indicated by a rapid melt (high snow water equivalent, high spring temperatures and solar radiation), as well as factors that lead to a high resisting force, usually indicated by a thick ice cover (intenseness of winter). The many meteorological and hydrodynamic factors that contribute to dynamic breakups and ice jamming will be discussed further in Chapter 4.

Chapter 3: Ice Jam Database

Information on ice jam events can be difficult to obtain. The data is often scattered and of lower quality compared to open water floods, as ice events tend to impact smaller river reaches and last for shorter durations. Therefore, collecting ice jam data in the form of a database can be a useful tool, and could help to identify trends in location, timing, and severity of events. One of the largest ice jam databases in North America is the Cold Regions Research and Engineering Laboratories (CRREL) ice jam database. The database includes tens of thousands of entries from 1785 to present (Carr, Gaughan, George, & Mason, 2015; White, 1996a). White (1996) describes the CRREL database's ability to improve emergency response to ice jams by having past data readily available, such as past mitigation methods and their success, or past stage data and the resulting extent of flooding. As ice processes are complicated to model, especially in real-time, sometimes the best indication of future events comes from past data.

3.1 Database Development

The first step of developing an ice jam database for the Lower Red River was first to identify the exact dates and locations of ice jam events. The database ranges from 1962 to 2017: 1962 is when hydrometric data started to be recorded for the area and 2017 was the last year of corrected hydrometric data available at the time of this study. The data recorded for each ice jam event includes the year, start date, end date, location, UTM East coordinate, UTM north coordinate, a summary of the information found from media sources, the event severity, and any additional notes. The following sections detail how this data was acquired. A condensed database can be found in Appendix A.

Chapter 3: Ice Jam Database

3.1.1 Severity Rating

In addition to the temporal and spatial data of the physical ice jam, impacts to the surrounding area were included in the database. This information was used to assign a severity rating to each ice jam. The severity rating was adapted from the flash flood severity index introduced by Schroeder et al. 2016, as flash flood events relate well to ice jamming since they are both characterized by a rapid increase in water levels. The ice jam severity index developed for this project has five severity ratings that are based on the resulting flooding caused by the ice jam. The five severity ratings are defined similarly to those in Schroeder et al., with some adjustments to the impacts of each category. The modifications allowed for scaling of the severity index to better represent flooding and damages in the study area and find acceptable boundaries between each category. The ice jam severity index is shown in Table 3.1.

Chapter 3: Ice Jam Database

Table 3.1: Ice Jam severity index adapted from Schroeder et al., 2016.

Severity	Ice Jam Description
1	Concern: Ice jam caused water levels to rise but no/ little flooding occurred.
2	Moderate Flooding: Overland flooding, bridge or road closures, some damage to properties. Evacuation due to access issues but not due to concern of flood damage. Volunteer evacuations.
3	Serious Flooding: Homes evacuated due to flooding, homes flooded, garages and outbuildings flooded.
4	Severe Flood: Increased number of flooded properties. Vehicles and/or mobile homes swept away.
5	Catastrophic Flood: Buildings/large infrastructure submerged; permanent homes swept away.

Ice-impacted water levels were not used to determine the severity of jam events. While using water levels as an indication of the event severity is preferred as it is arguably less subjective, the study area is a 33 km long reach and water levels are only available at one location, Selkirk Generating Station, for a majority of the study years. Therefore, the severity of events that occur at Breezy Point, approximately 20 kilometres downstream, may not be reflected in magnitude by the water level at Selkirk. Additionally, the severity index incorporates other factors that may not be captured by water levels at just one location, such as flooding extent, road closures, damage to property, and evacuation requirements.

3.1.2 Historical Review

Historical information was acquired from archived media sources, predominately from newspapers or archived news releases from the Province of Manitoba. Table 3.2 lists the data sources used, as well as the years they were available. Referenced newspapers were from the Winnipeg and Selkirk area; both the Winnipeg Free Press and Winnipeg Tribune printed daily newspapers, while the Selkirk Enterprise and Selkirk Journal printed weekly. Much of the data in this study were from the Selkirk newspapers due to Selkirk's proximity to the study area. Additionally, the Province of Manitoba's news releases provided detailed ice jam information. News release archives date back to the 1940s, but detailed flood bulletins have only been available since 1995. All newspapers were accessed through the Winnipeg Public Library's subscription to Newspaperarchives.com.

Table 3.2: Data sources used for the review of ice jam events on the Lower Red River.

Data Source	Years Available
Winnipeg Free Press	1872 - Present
Winnipeg Tribune	1890 - 1965
Selkirk Enterprise	1908 - 1977
Selkirk Journal	1985 - Present
Manitoba News Releases	1995 - Present

Keyword searches were used to find articles relating to ice jamming in the study area every year between 1962 and 2017. The articles were used to specify locations, dates, and duration of ice events and – when possible – multiple sources were used to confirm events. Occasionally some estimations and assumptions were required when the information provided was vague or specific details were missing. Ice jam events were not always clearly labelled as such, especially for older events; sometimes only mentions of flooding and damages from ice floes were found, but such events can be assumed to have been caused by ice jamming.

Coordinates of the ice jam toe were also recorded. Toes that formed at a known landmark resulted in coordinates that used exact locations (e.g. Selkirk Bridge, PTH 4 Bridge). Most locations, however, were described in historical records using vague terms such as “near” and “area” (e.g. “near McIvor Lane”, “Breezy Point area”) that referred to a stretch of river. In these cases, one coordinate was chosen to represent the entire area being referenced. The year, event start date, event end date, name of location, and UTM coordinates were recorded for each event.

In addition to the spatial and temporal data collected, the database also includes summaries of important information from both the newspaper articles and Manitoba news releases. This data was used to determine the severity ratings, as discussed previously. Additionally, notes were kept on any estimations or assumptions made such as locations and dates.

3.1.3 Historical Water Levels

This thesis will demonstrate that the number of ***reported*** ice jam events has increased in recent years, especially Severity 1 (low severity) events. This is not necessarily an indication that ice jam events occur more frequently now than in the past, but rather that the increase of media outlets in the recent decades have led to more events being captured, especially small events that did not get as much media attention in the past. Therefore, the database may be biased to more recent events. To mitigate this potential bias, historical water level data can be used to identify ice jam events not previously captured through media sources. Acres (2004) reviewed the stage records at Manitoba Hydro's Selkirk Generating Station, which is located on the upstream stretch of the Red River that runs through Selkirk (location can be seen in Figure 1.1), and flagged dramatic increases in stage as indicative of possible ice jam events. A similar approach for the same dataset was used in this study.

Stage data from the Selkirk Generating Station was available from 1962 to 2017; however, some data was missing, including the spring hydrographs for 1974, 1977, 1979-1983, 2002-2003, 2006, and 2008. The spring hydrograph was reviewed for each year that the historical review did not flag an ice jam. Through this process, eight additional years (1965, 1970, 1976, 1984, 1989, 1992, 1994, 1998) were identified as having ice jam events. Figure 3.1 shows the 1965 spring hydrograph as an example year where an ice jam was flagged based on recorded water level without supporting news articles. Appendix B contains all Selkirk Generating Station water level data. Even with these measures, however, we cannot be certain that times with no recorded events are due to no events taking place, or just lack of data.

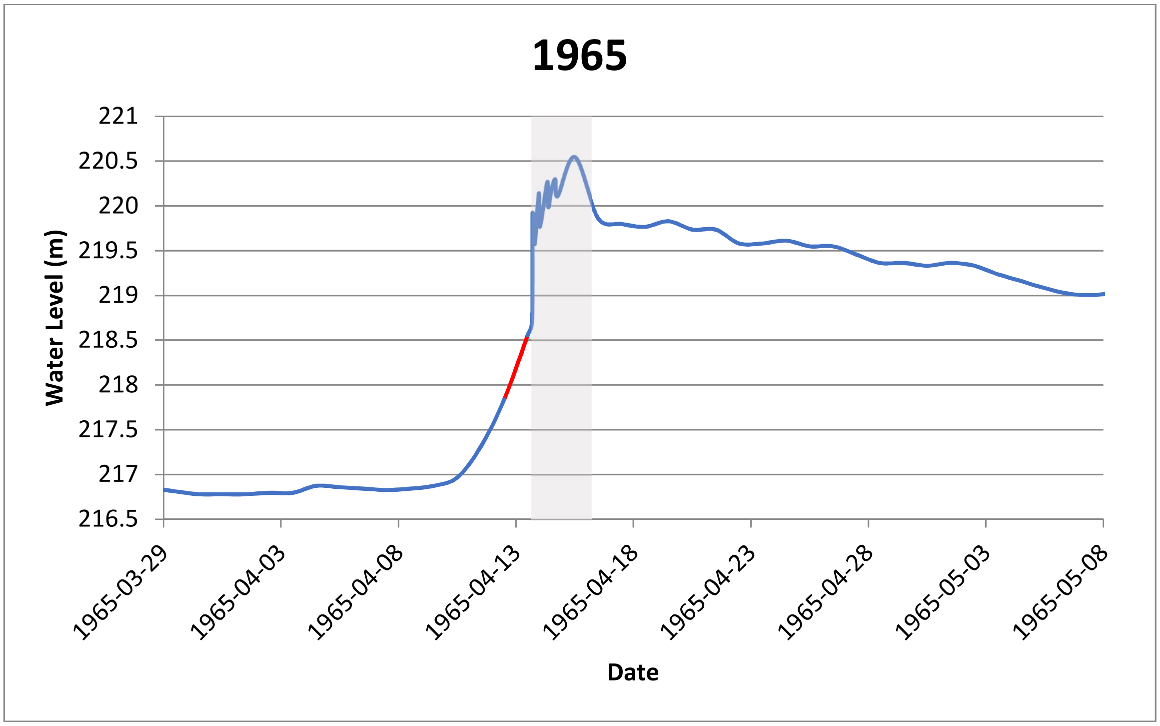

Figure 3.1: Spring hydrograph for the Selkirk Generating Station in 1965. The red section of the line is the assumed time of breakup. The grey section of the graph indicates when an ice jam occurred.

With the dates of newly-identified jams known from the stage records, an additional media search was done for any indication of flooding in the area during those times. Only 1965 had flooding during the time of the ice jam, correlating with a Severity 2 ice jam event in terms of severity. All the others were considered a Severity 1 event, or "concern". The locations of these jams were estimated based on the assumption that water from the Red River backs up into a small channel just south of Sugar Island during an ice jam. The backflow in this channel then floods Selkirk Park and Highway 204, causing the closure of the Selkirk Bridge as the east access is closed. Figure 3.2 shows the location of the backflow in relation to the bridge. Based on this assumption, the 1965 jam that resulted in flooding was assumed to be at Sugar Island, since this location would cause this flooding scenario. The other jams were assumed to occur at the Selkirk

Bridge, upstream from the inlet, as a jam at this location is not likely to cause backflow through the channel to Selkirk Park.

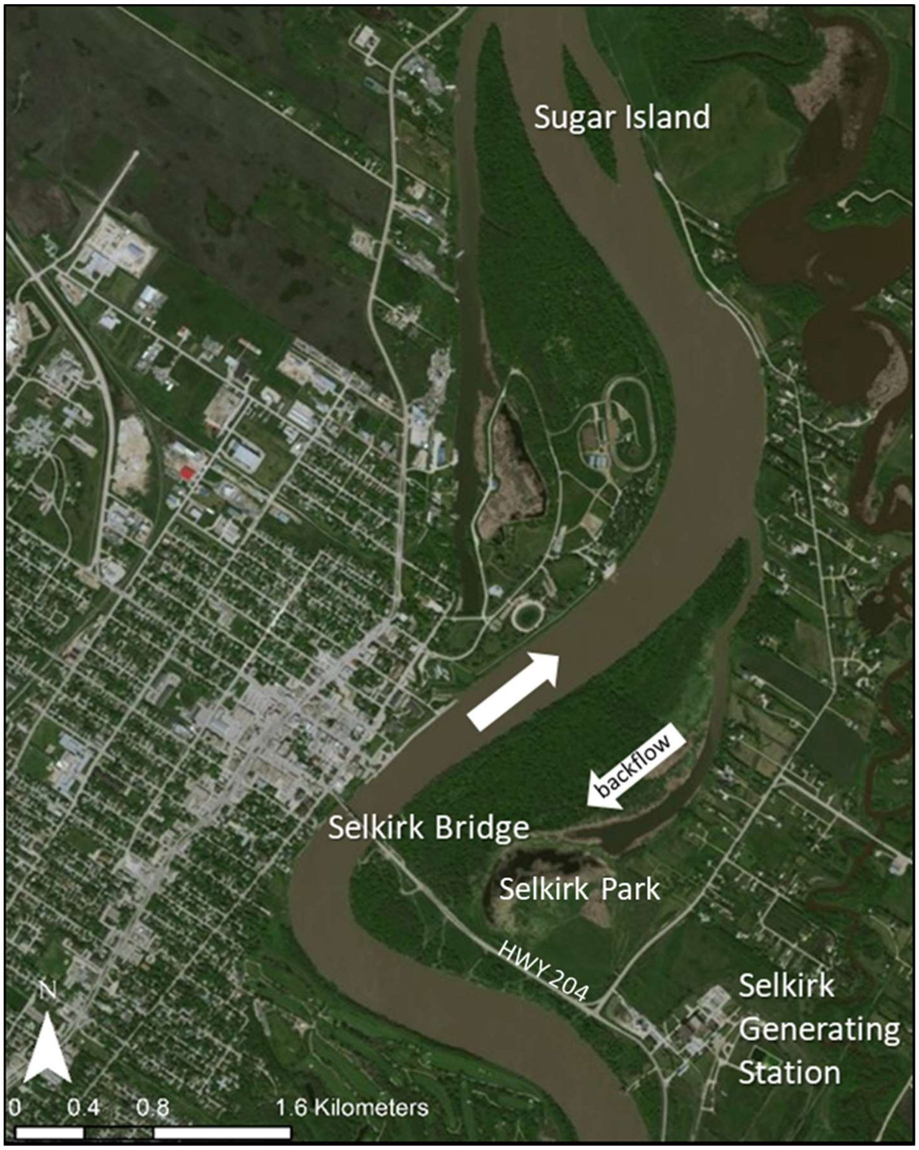

Figure 3.2: Location of backflow flooding at Selkirk Bridge.

3.2 Historic Ice Jam Events

From the historic review 54 ice jam events were identified, with 40 of them having a severity rating of 2 or higher. Some years had more than one event, as ice jams can form and release multiple times along the reach. For example, in 2009, ice flow down this stretch of river resulted in four jams from Lower Fort Garry to Breezy Point (see Appendix A for ice jam information). Table 3.3 and Figure 3.3 summarize the frequency of ice jams at each location. Sugar Island had the most events, with 13 recorded ice jams, followed by the Selkirk Bridge with 12. It should be noted that 7 of the 12 events recorded for the Selkirk Bridge were assumed to be Severity 1 events at that location, based on the water level records.

Table 3.3: Location and frequency of ice jams in the study area from 1962-2017.

Location	Frequency	Easting (m E)	Northing (m N)
Sugar Island	13	652240	5556513
Selkirk Bridge	12	652240	5556513
Netley Creek Confluence	10	652212	5573464
McIvor Lane	7	654633	5565507
PTH 4 Bridge	4	653992	5562031
Breezy Point	3	653390	5570837
Father Turney Road	2	653963	5561030
Lower Fort Garry	1	648039	5553053
South of Selkirk	1	653187	5554983
St. Clement Drive	1	650677	5554549

Chapter 3: Ice Jam Database

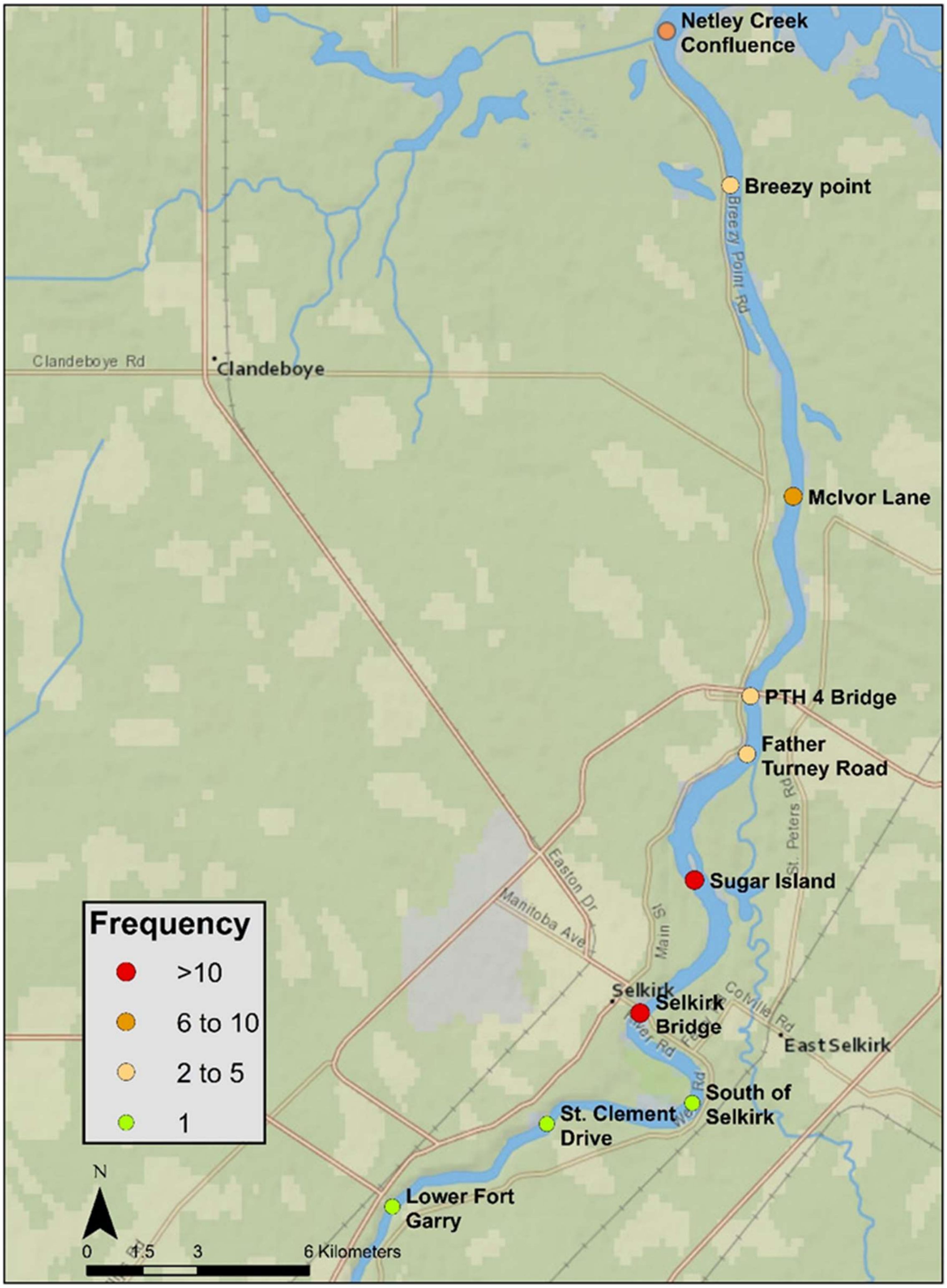

Figure 3.3: Frequency of ice jam events by location from 1962-2017.

One-time ice jam events exclusively occurred at the upstream section of the study area, south of Selkirk. All others occurred at well known ice jam locations, with the most severe events – Severity 3 ("serious flooding") or higher – occurring at the downstream portion of the study reach, as seen in Figure 3.4. Ice jams at Selkirk Bridge, Sugar Island, and PTH 4 Bridge can easily be attributed to the flow constrictions at these locations. Channel morphology may impact ice jam formation at the Father Turney Road, McIvor Lane, and Breezy Point locations, as they occur at meanders or where the channel is narrowed. The Red River at the Netley Creek Confluence consistently sees an increase in bed elevation of 4-5 meters due to the sediment transport from Netley Creek (see Figure 1.3), as well as the presence of thicker lake ice. These two factors may explain why this location is prone to more severe events (K. E. Lindenschmidt, 2012). It should be noted that these 13 events happened over 10 years with 1996, 2004, and 2011 each having two severe events.

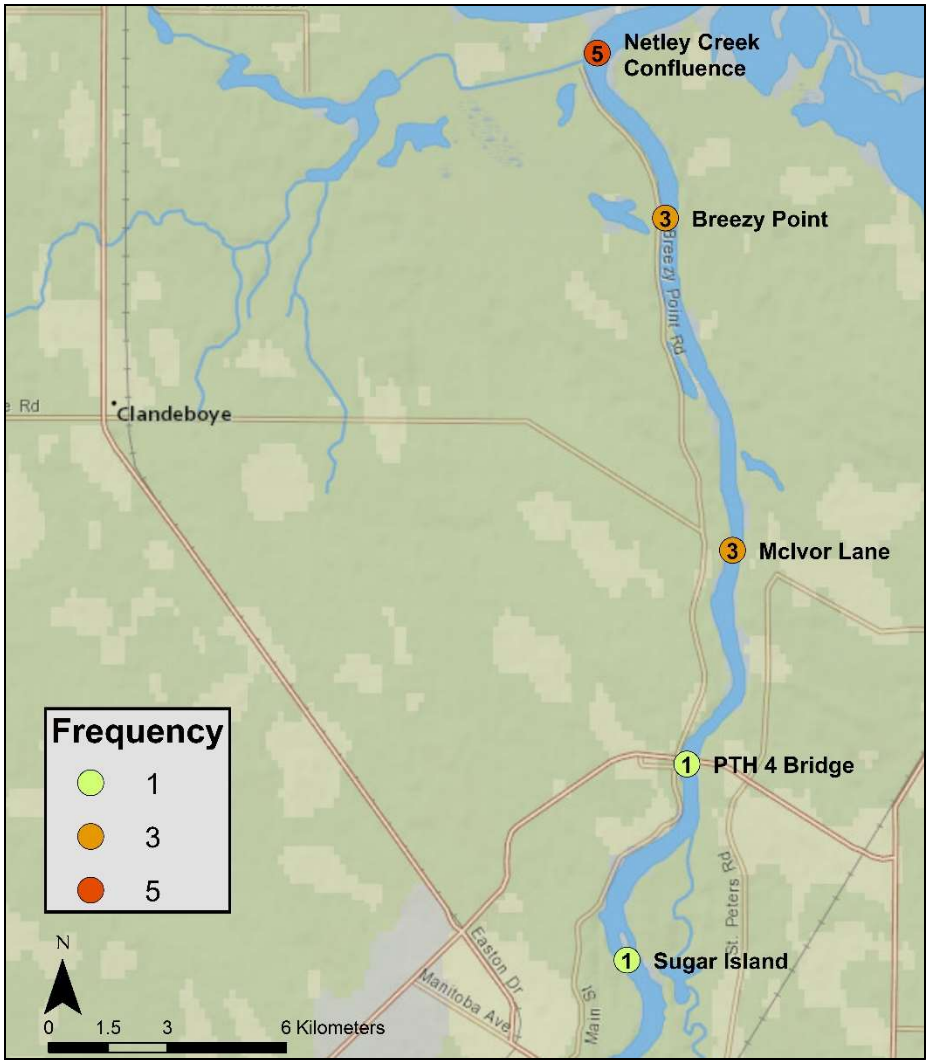

Figure 3.4: Frequency by location of Severity 3-5 events.

Figures 3.5 and 3.6 show the frequency of events per decade and years with events per decade. Using the 2009 ice jam events to illustrate the difference between the figures, that year four ice jam events occurred and would contribute four to the total number of events per decade, meanwhile adding one to the total number of years with events per decade. As discussed previously and shown in Figure 3.5, there has been an increase of events in more recent years. Figure 3.6, however, shows that the number of years with events is not increasing. Again, it is possible that this is due to an increase in media capturing lower-severity events in more recent years, especially from the Province of Manitoba news releases. These releases were available after 1995 and gave detailed information on smaller ice jams that did not always make it into the newspapers. Perhaps in the early years of the database only the most severe jams each spring were published.

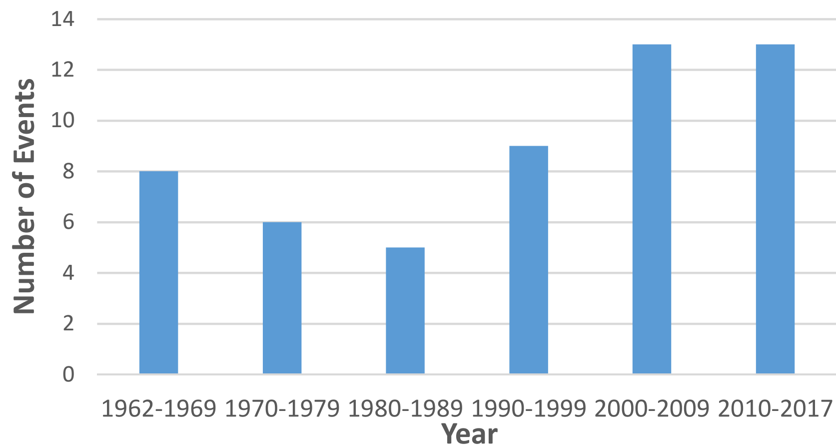

Figure 3.5: Frequency of events by decade. The periods 1962-1969 and 2010-2017 are only 8-year periods due to the start and end date of the study period.

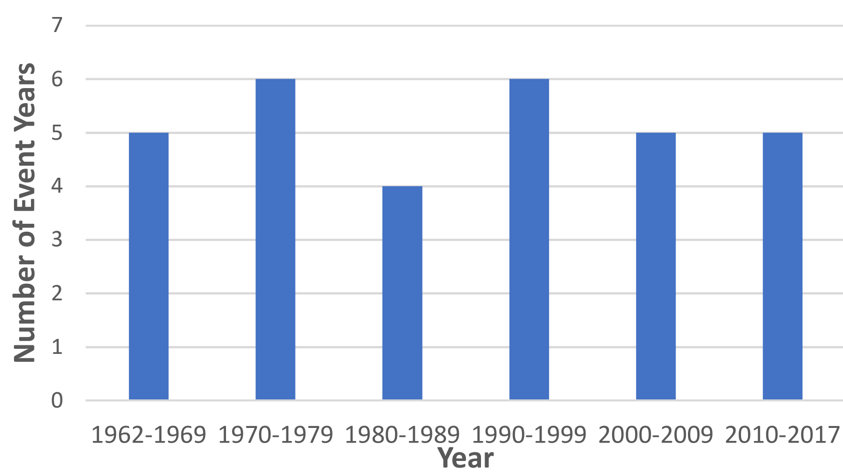

Figure 3.6: Frequency of event years by decade. 1962-1969 and 2010-2017 are only 8-year periods due to the start and end date of the study period.

The 1980-1989 time period had the lowest number of ice jam events and years. It should be noted that no flow records were available for 1980-1983 and only media sources could be relied on for this period. Lack of flow data may have resulted in an unidentified ice jam during this time frame, resulting in the lower numbers as the period of 1978-1984 had no ice jams identified and is the longest time stretch to do so.

3.3 Historic Ice Jam Events Trends

As part of the preliminary engineering report for the Red River Floodway environmental impact statement (EIS), a review of ice jam events north of the floodway was undertaken to determine the flow conditions that tend to lead to ice jamming. The EIS reported the following trends:

1. ice jams did not occur with flows over 2600 cms;
2. ice jams rarely occurred with flows over 2000 cms; and
3. ice jams occurred when the spring hydrograph was rising, or when the hydrograph peaked at flows less the 2600 cms (KGS et al., 2004).

Further investigation suggests that the EIS was referring only to the peak flow of the spring hydrograph during jam years, and not necessarily the flow during the ice jam event.

Table 3.4 shows the peak spring flow in the study area, ordered from largest to smallest. The table also includes the peak ice-impacted flow during the time of the ice jam, as identified by the ice jam database, as well as the severity of the ice jam event for each year. Table 3.4 shows that the data collected in this study prove that the trends reported in the EIS are now outdated. The years highlighted in yellow are those that contradict the reported trends. Apart from 1996 – where the spring flow could easily have been rounded to 2600 cms – all the highlighted years occurred after the report had been published. The years 2009, and 2011 had peak spring flows above 2600 cms, and the 2009 year had ice jam flows above 2600 cms.

Table 3.4: Yearly peak spring flow ordered from highest to lowest. Shaded years have a 0 severity and indicate no ice jam event. Years highlighted in yellow contridict the reported trends by KGS et al., 2004.

Year	Spring peak (cms)	Peak ice jam or ice impacted flow (cms)	Severity
1997	4320	1890	0
2009	3200	3090	5
1979	2780	1910	0
2011	2730	2370	3
1996	2610	1750	4
1966	2570	2380	2
2006	2430	2280	0
2017	2230	2230	2
1969	2200	1140	2
1974	2150	2140	3
1987	2120	2120	2
2001	2070	1580	2
1970	2040	1250	1
2004	2000	1840	4
2014	1970	1970	3
2010	1950	1670	2
2013	1950	538	0
1965	1890	1340	2
2005	1820	1152	3
1978	1810	1250	2
1995	1770	1770	4
1986	1760	1760	2
1962	1720	1290	0
1999	1660	1350	2
1967	1650	1520	3
2016	1620	1620	2
1983	1580	1580	0
1971	1580	1580	2

Year	Spring peak (cms)	Peak ice jam or ice impacted flow (cms)	Severity
1976	1530	1530	1
2007	1520	1520	3
1998	1500	1100	1
1975	1480	949	0
1989	1430	1220	1
1992	1350	1060	1
1982	1310	1190	0
1972	1130	946	2
1984	1100	1100	1
1980	1010	1010	0
1964	1000	1000	2
1994	980	980	1
1993	947	740	0
2008	919	850	0
1985	869	869	0
1963	782	544	0
2012	589	589	0
2002	585	450	0
1988	541	348	0
1973	535	535	0
2000	530	530	0
1968	490	490	0
2003	470	470	0
2015	470	439	0
1990	378	378	0
1991	325	223	0
1977	186	186	0
1981	160	160	0

The wording of the trends found in the EIS may also be misleading, as the years where spring flows were over 2000 cms were generally rare, but ice jams during these high flow years were very common. Looking at the peak spring flows in Table 3.4 (column 2), 20 of 31 ice jam event years had flows less than 2000 cms; however ice jams occurred 11 out of 14 years where flows were above 2000 cms. Looking at ice-impacted flows (column 3 of Table 3.4), most ice jams did occur when flows were under 2000 cms (25 of 31 ice jam event years) as well, however an ice jam did occur most years where the flow was above 2000 cms (6 of 7 years). It is challenging to discern any trends related to ice jamming and flow, apart from the fact that no ice jam has occurred with a spring peak flow less than 1000 cms. When peak flows are above 1000 cms, ice jam years are more common than non-event years; when the flow is greater than 2600 cms, only ice jams with a severity of 3 or above have occurred in event years.

Table 3.5 displays peak ice-impacted water levels from the Selkirk Generating Station over the study period, with the exclusion of 1974, 1977, 1979-1983, 2002-2003, 2006, and 2008 because water levels at this station were not available. The level data is given in metres above sea level (m a.s.l.) as all stations in the study area use this notation. Apart from 1997, all jam years had a water level higher than the non-jam years. In 1997, the threat of a major ice jam was believed to be so great that 45,000 holes were drilled in the ice of the Lower Red River as a prevention measure (IJC, 1997). For this reason, the year 1997 should perhaps be considered an anomaly, as it is possible that an ice jam could have occurred if no prevention had taken place. Excluding 1997, the lowest water level for an ice jam year was 219.99 m in 1998, and the highest water level for a non-jam year was 219.77 m in 2013.

From Table 3.5, the severity of the ice jam event does not necessarily correlate with the water levels at the gauge. Looking at the five years with the highest water levels, the lower-severity ice jams (2007 and 1986) were located closer to the gauge stations at the PTH 4 Bridge and Selkirk Bridge, respectively. The remaining three events were rated as Severity 4 or Severity 5 and were located at Breezy Point or the Netley Creek Confluence. As stated earlier, the impact of the event on the gauge depends not only on the severity but also on the distance to the gauge. This reinforces the use of the severity categories – as opposed to resulting water level – in order to determine the impact of an ice jam.

Table 3.5: Peak ice-impacted water level at the Selkirk Generating Station during the study period.

Jam Years			
Year	Date	m a.s.l.	Severity
2007	April 7, 2007	223.25	3
2009	April 10, 2009	223.07	5
1986	April 1, 1986	222.59	2
1996	April 18th-21st, 1996	222.50	4
2004	April 3, 2004	222.29	4
1995	March 26, 1995	222.13	4
1966	April 9, 1966	222.12	2
2011	April 8, 2011	222.10	3
2014	April 22, 2014	221.88	3
2016	March 19, 2016	221.86	2
2005	April 5, 2005	221.84	3
1978	April 11, 1978	221.82	2
2017	March 30, 2017	221.67	2
2010	March 28, 2010	221.64	2
1967	April 11, 1967	221.48	3
1987	April 7, 1987	221.31	2
1972	April 16, 1972	221.14	2
1971	April 12, 1971	221.11	2
1994	April 9, 1994	221.01	1
1999	April 5, 1999	221.01	2
2001	April 10, 2001	220.98	2
1984	April 8, 1984	220.82	1
1970	April 19, 1970	220.79	1
1965	April 15, 1965	220.55	2
1992	April 3, 1992	220.50	1
1989	April 19, 1989	220.34	1
1964	April 18, 1964	220.33	2
1969	April 13, 1969	220.02	2
1976	April 8, 1976	220.02	1
1998	March 29, 1998	219.99	1

Non-Jam Years		
Year	Date	m a.s.l.
1997	April 22, 1997	221.35
2013	May 5, 2013	219.77
1985	March 31, 1985	219.57
1993	April 6, 1993	219.17
1975	April 25, 1975	218.99
1973	March 29, 1973	218.93
1962	April 24, 1962	218.85
2015	March 23, 2015	218.48
1988	April 7, 1988	218.46
1963	April 9, 1963	218.38
1968	April 12, 1968	218.24
2012	March 21, 2012	218.07
1990	April 8, 1990	218.05
2000	March 27, 2000	217.94
1991	April 8, 1991	217.64

Chapter 4: Ice Jam Parameters

There are no universally-known parameters that signify whether or not ice jamming will occur. Conditions that dictate the breakup processes and occurrence of ice jams are considered local phenomena and, as such, models developed for one site may be useless at another (White, 2003). In 2007, Mahabir et al. applied both fuzzy logic and neuro-fuzzy logic models of the Athabasca River to the Hay River to determine the transferability of the models. The results indicated that the fuzzy logic model was transferable to the Hay River for "high" flood events only. The neuro-fuzzy logic model did not produce the same high level of accuracy seen for the Athabasca River, and did not give successful predictions. This indicates that the models' accuracy depended on the calibration of site-specific parameters (Mahabir et al. 2007). Although the exact parameter relationships may not be transferable from one study to the next, the parameters used are fairly similar, and are related either to the driving force or the resisting force of the ice cover. These include parameters related to air temperature, precipitation, hydrometric conditions, and energy balance.

Data availability is the main determinant of which parameters are used in a given study. Where direct data is not available, many parameters can serve as an index for the actual process related to ice jamming. For example, ice cover strength at time of breakup is directly related to the resisting force of the ice cover. It is highly unlikely, however, that study locations would have a record of breakup ice strength, as collecting this data is very dangerous. Ice strength can instead be inferred based on seasonal parameters. As spring ice strength is a function of the peak winter strength and the reduction of strength in the spring, parameters relating to ice thickness and winter temperatures can be used as indices for peak winter ice strength, and parameters relating to spring temperature and solar radiation can be used as indices for the reduction in ice strength in the spring.

4.1.1 Hydrometric and Meteorological Data Sources

All the hydrometric and meteorological data used for this study was acquired through existing hydrometric and weather stations. All weather station data was available through Environment and Climate Change Canada, except for the data from Manitoba Agriculture's weather station in Selkirk. All hydrometric stations are managed by either Water Survey of Canada (WSC) or Manitoba Infrastructure, with data available through WSC. Manitoba Hydro initially managed the hydrometric station at the Selkirk Generating Station, however Manitoba Infrastructure took over management of the station in 2004. Table 4.1 and Figure 4.1 summarize the hydrometric and weather stations used in this study.

Table 4.1: Hydrometric and weather stations used in this study.

Map ID	Name	Station Type	Station ID
1	Red River at Breezy Point	Hydrometric Station	05OJ022
2	Red River At Selkirk	Hydrometric Station	05OJ005
3	Red River At Selkirk Generating Station	Hydrometric Station	05OJ829
4	Red River Near Lockport	Hydrometric Station	05OJ010
5	Red River near Ste. Agathe	Hydrometric Station	05OC012
6	Red River at Emerson	Hydrometric Station	05OC001
7	Assiniboine River at Headingly	Hydrometric Station	05MJ001
8	Selkirk (Manitoba Agriculture)	Weather Station	
9	Selkirk	Weather Station	5022630
10	Stony Mountain	Weather Station	5022791
11	Oakbank	Weather Station	5022051
12	Winnipeg Richardson International Airport	Weather Station	5023222

Chapter 4: Ice Jam Parameters

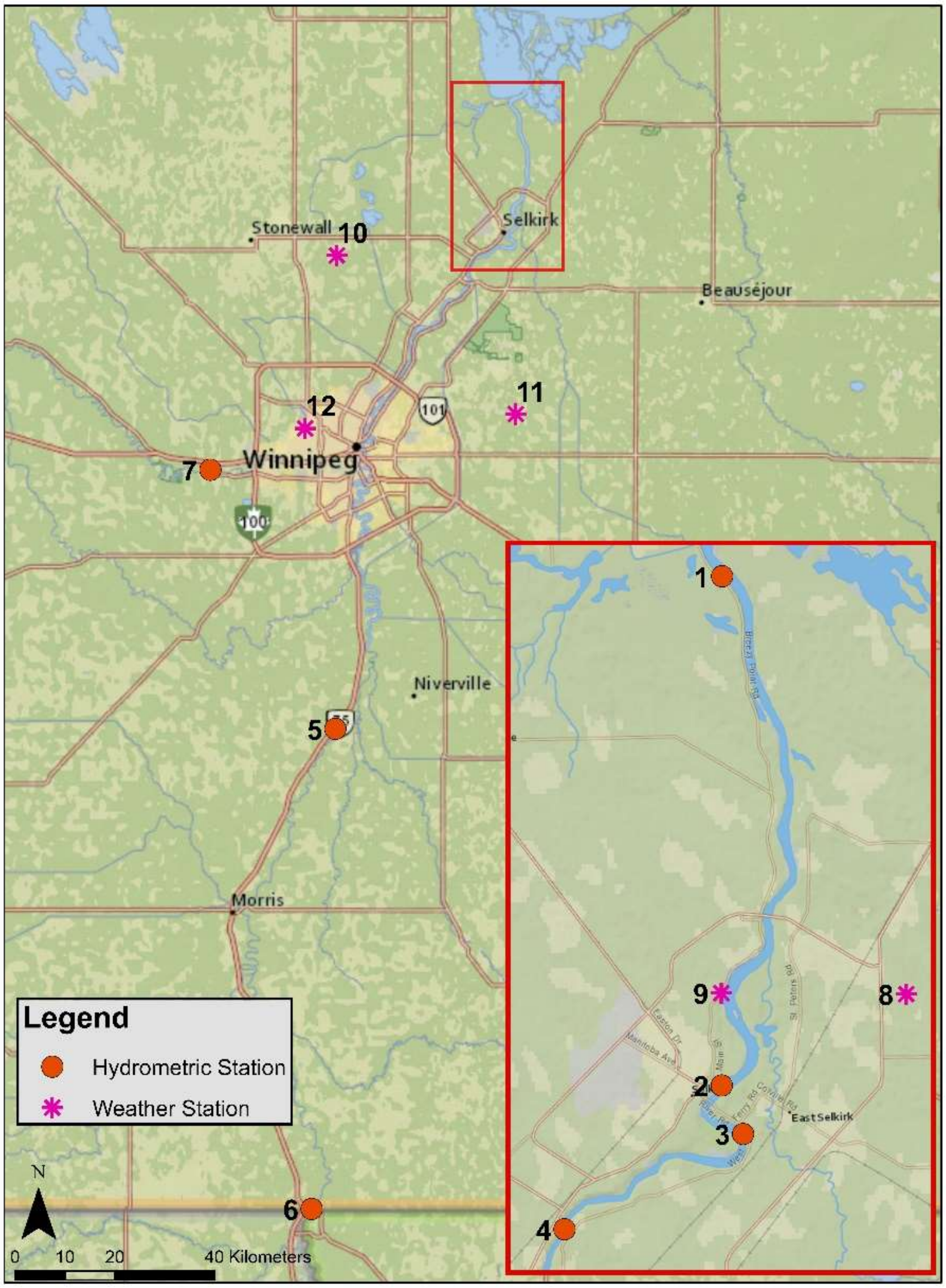

Figure 4.1: Locations of hydrometric and weather stations used in this study. Numbers beside the station refer to Map ID found in Table 4.1.

4.2 Breakup Initiation Date

For ice jam years, spring data could be collected in relation to when ice jams were recorded. No observed breakup data is available for non-jam years, though, so a consistent interval was needed as a reference for parameter data from year to year. When hydrometric data is impacted by ice conditions, that data is denoted with a B. The last B date in the spring water record – the last date when there are ice conditions impacting a station – was considered; however, it would reference conditions after an ice jam has occurred. Instead, an estimation of the initiation of breakup – that is, when the ice cover began to move downstream – was used. This method provided insight as to which conditions at breakup are related to ice jamming.

Breakup initiation is defined by Beltaos et al. (1990) as the first significant spike in spring water levels. The breakup initiation date can thus be determined through close analysis of the spring water level record (Beltaos et al., 1990; de Rham et al., 2019). As spring thaw is underway, the water level starts to rise from the mostly steady winter level. As the ice breaks up, the flow resistance decreases, resulting in spikes on the rising limb of the hydrograph. A clear spike is not always visible in the water level record due to steep rises of water levels or over-mature breakups. In these instances, a reasonable assumption (i.e. within 1-2 days) of the breakup initiation date can be estimated by analysing the rising limb of the hydrograph and determining the logical point that a stable ice cover would cease to be present (Beltaos et al., 1990).

Through the development of a river ice database, Environment and Climate Change Canada (ECCC) has determined the breakup initiation date for the Lockport and Selkirk hydrometric stations (see Table 4.1)(de Rham et al., 2019). This data was kindly provided by ECCC, and is the source of the majority of breakup initiation dates used in this study, although minor adjustments were made for some years. For years where no date was provided, usually due to missing records at the previously listed stations, the breakup initiation was determined from the Selkirk Generating Station (GS) water record. It was assumed that the Selkirk GS was in close enough proximity to both the Lockport and Selkirk stations that the breakup initiation would occur on the same date for all three stations. The breakup initiation can be seen on the yearly spring hydrograph for the Selkirk GS, found in Appendix B; a table listing the breakup initiation dates can be found in Appendix C.

4.3 Parameter Selection

Parameters were selected based on data available from the hydrometric and weather stations listed in Table 4.1. Each parameter was compared to the ice jam severity or the ice-impacted water level, given in metres above sea level (m a.s.l.), at the Selkirk GS. This comparison gives the option of using either a discrete (ice jam severity value from 1 to 5) or continuous (ice-impacted water level) number system to represent the severity of the ice jam. As discussed in Chapter 3 and seen below in Figure 4.2, water level does not relate exactly to ice jam severity, and thus are not interchangeable; even so, water level modelling is the best available option for modelling methods that rely on continuous values. To determine if any of the parameters correlated with ice jamming the coefficient of determination (R^2) value was analysed using the below formula:

$$R^2 = \left(\frac{n\,(\sum xy) - (\sum x)(\sum y)}{\sqrt{\left[n \sum x^2 - (\sum x)^2\right]\left[n \sum y^2 - (\sum y)^2\right]}} \right)^2 \qquad (4.1)$$

Where: n is the number of observations;

x is the independent variable; and

y is the dependant variable.

The R^2 value ranges from 0 – 1 and gives the decimal of the variability in the dependant variable that is explained by the independent variable. A low R^2 value indicates a weak correlation between variables, where a large value indicates a strong correlation.

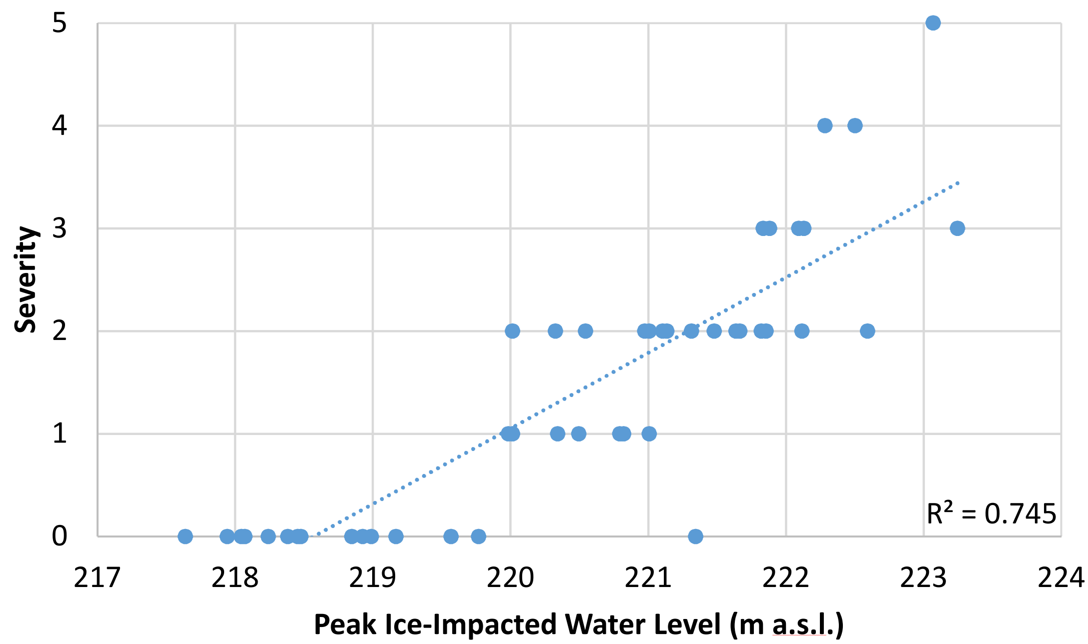

Figure 4.2: Peak ice-impacted water level and the resulting ice jam severity.

Due to ice jamming's complex physical process and from review of past modelling studies, it was expected that most individual parameters would have little correlation with ice jamming severity. Only the river flow at or near the time of breakup had a relatively strong correlation to ice jamming, as the river flow is the main driving force on the ice. We would expect that, if a direct measurement of the resisting force (ice thickness or strength) were available at breakup, it would be highly correlated as well. Unfortunately, parameters that indicate the driving or resisting force of the ice cover with any lead-time up to breakup did not have a strong correlation, enforcing the difficulty of predicting future ice jam events with certainty. The type of ice jam parameters examined are explained in the following sections.

4.3.1 Flow parameters

High flows are often associated with ice jamming, as they provide a large driving force that can break up and transport ice downstream. They can also cause ice jams to thicken, as flow can push ice floes underneath the juxtaposed ice cover, resulting in more severe jams. It can be challenging to use flow data to predict ice jams, as it provides little lead-time between high flow values and ice jamming. As a result, parameters that predict high flows are often used, including snowfall amounts, snow height on ground, and forecasted spring precipitation. Still, understanding the relationship between flows and ice jamming is important and can be especially useful if the flows for a given spring period can be forecasted.

Average daily flow values at the Lockport, Selkirk, Ste. Agathe, Emerson, and Headingley Stations were examined (see Section 4.1.1). The Lockport Station was moved to Selkirk in 2008, so their flow records are treated as one. The flows at the breakup date were compared to both the peak ice-impacted water level at the Selkirk GS and the severity of jam each year. Surprisingly, the Ste. Agathe flow had the highest correlation to the high water levels observed at the Selkirk GS, despite being further away than the Lockport/Selkirk Station, which had a comparatively poor correlation. The Headingley flow has a smaller impact because the Assiniboine River contributes much less flow to the Lower Red River. Results were similar when comparing the severity of the ice event to flow, with the Ste. Agathe station having the best correlation between high flows and the severity of events. The Ste. Agathe flow data can be seen in Figures 4.3 and 4.4.

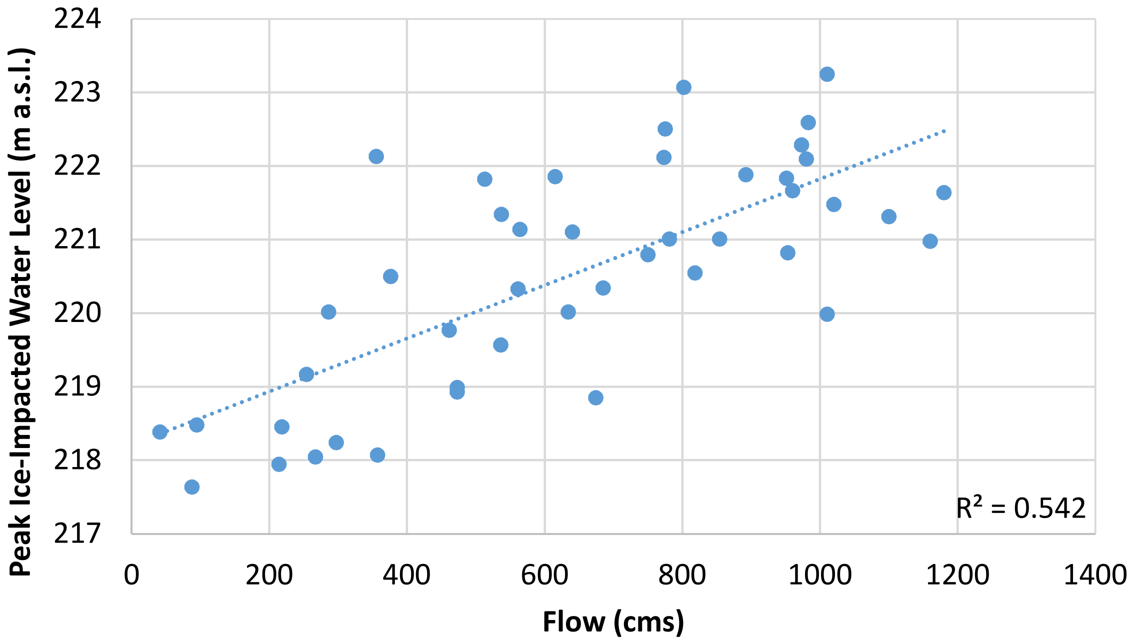

Figure 4.3: Relationship between the flow at the Ste. Agathe station and Selkirk GS peak ice-impacted water level.

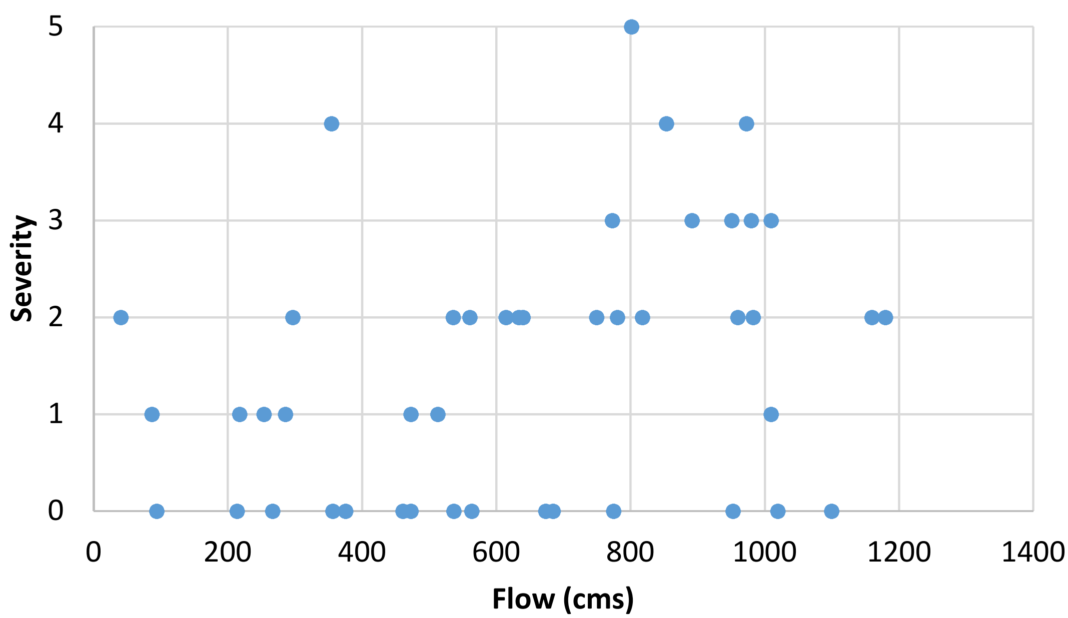

Figure 4.4: Relationship between the flow at the Ste. Agathe station and ice jam severity.

In addition to daily flow values, the change in flow was also considered at the different stations being examined. The highest change in flow between March 1st and the breakup date, over several temporal periods ranging from a one-day change to a seven-day change, were calculated. The correlation between change of flow and peak ice-impacted water level increased as the time period decreased. This resulted in the one-day change of flows having the highest R^2 value for all stations on the Red River. The Headingley Station exhibited a much smaller relationship between change in flow and water level, but displayed a different trend from the other stations, with the R^2 values increasing as the time period increased. When comparing change of flow to both the peak ice-impacted water level and severity of ice jam, the Ste. Agathe station one-day change in flow was the most highly correlated with a R^2 of 0.288.

4.3.2 Precipitation and Soil Moisture

Rainfall data was taken from the Winnipeg Richardson International Airport from 1961 to 2007, and then from Stony Mountain from 2007 until 2017. There is a Selkirk weather station with data from 1963 to 2008, however, the rainfall data is infrequent so the weather station at the Winnipeg airport was used instead. For exact locations, please see Figure 4.1.

Soil moisture conditions in the spring affect the quantity and timing of snowmelt reaching the river (Mahabir et al., 2006). Higher soil moisture levels in the fall result in frozen spring soil. Water freezes within the pores of the soil, reducing its permeability; in spring when the snow melts, the underlying soil is still frozen. Frozen soils admit less infiltration, and a larger amount of snowmelt becomes runoff. This can indirectly lead to ice jamming as runoff increases river flow.

Chapter 4: Ice Jam Parameters

Direct soil moisture data was not available for the study area; therefore, an antecedent precipitation index (API) was used as an index of the fall soil moisture levels. The API equation used for the study was developed by the Province of Manitoba, and is used in spring flood forecasting. The API calculated for a given year is based on the rain precipitation that fell in the previous year, as seen in equation 4.2:

$$API = 0.07PT_{May} + 0.08PT_{June} + 0.12PT_{July} + 0.18PT_{Aug} + 0.25PT_{Sept} + 0.30PT_{Oct,Nov} \quad (4.2)$$

Where: API is in mm; and

PT_{Month} is the precipitation in mm for a given month.

Figures 4.5 and 4.6 shows the calculated API compared to ice jam severity and peak ice-impacted water levels. The API has a weak negative correlation with the water levels and no correlation with the severity of ice jamming.

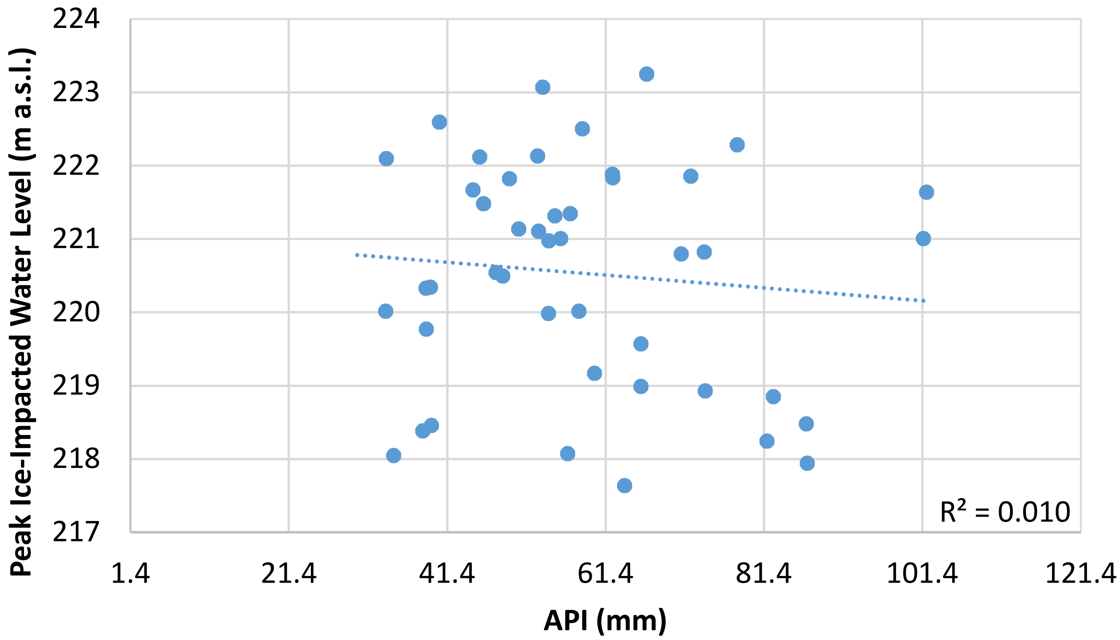

Figure 4.5: Relationship between the calculated API and Selkirk GS peak ice-impacted water level.

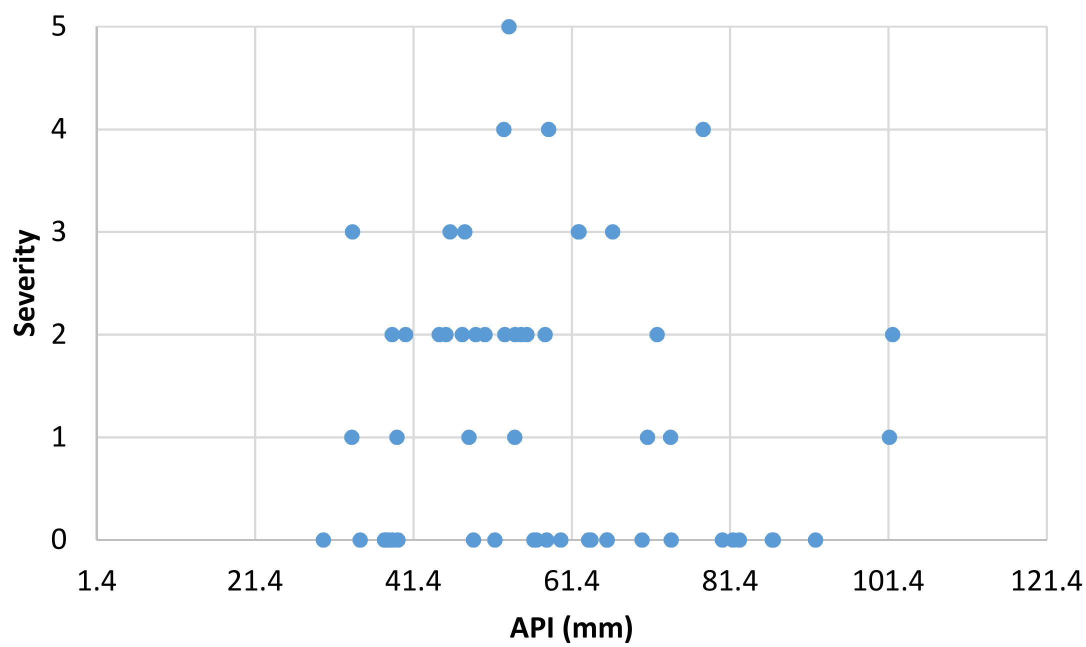

Figure 4.6: Relationship between the calculated API and ice jam severity.

Chapter 4: Ice Jam Parameters

Precipitation in spring, especially rain on snow events, can lead to the rapid melting of snow and generation of runoff (Beltaos, 2008). Many different timeframes for spring rain or combined spring precipitation were examined for significance relating to ice jamming. Three parameters had a notable positive correlation with ice jamming. The total amount of rain up to three days prior to breakup, seen in Figures 4.7 and 4.8, had the strongest relation to the ice jam severity indicators. The other parameters with positive correlation to ice jamming were total precipitation from March 15th until breakup (R^2 of 0.108) and total precipitation from March 1st until breakup (R^2 of 0.082).

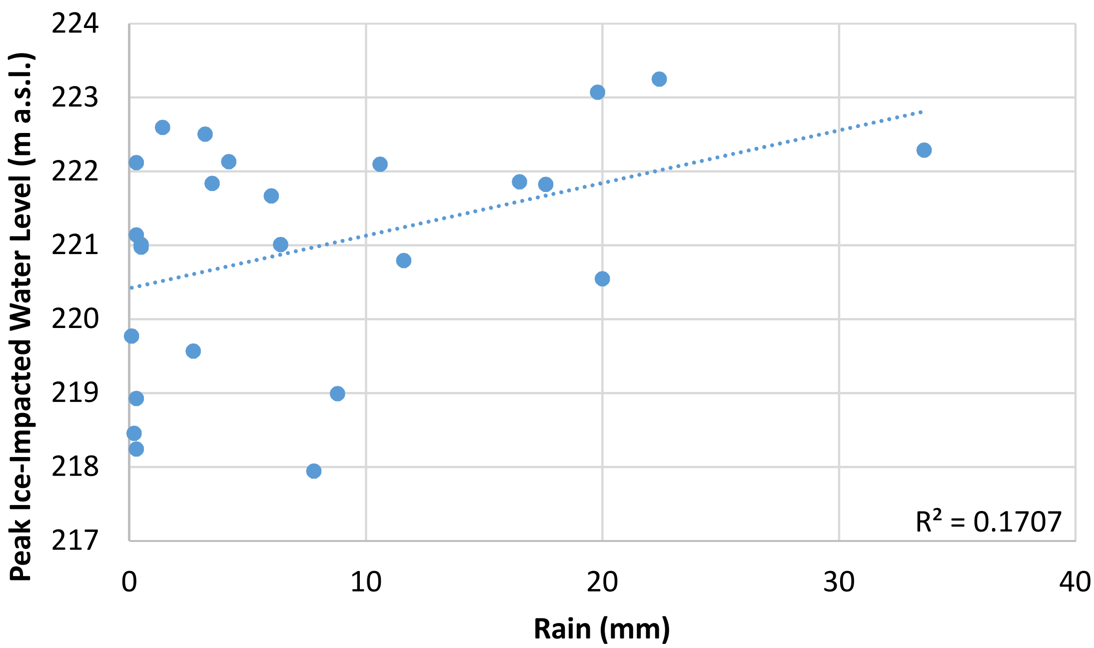

Figure 4.7: Relationship between total amount of rain up to three days prior to breakup and Selkirk GS peak ice-impacted water level.

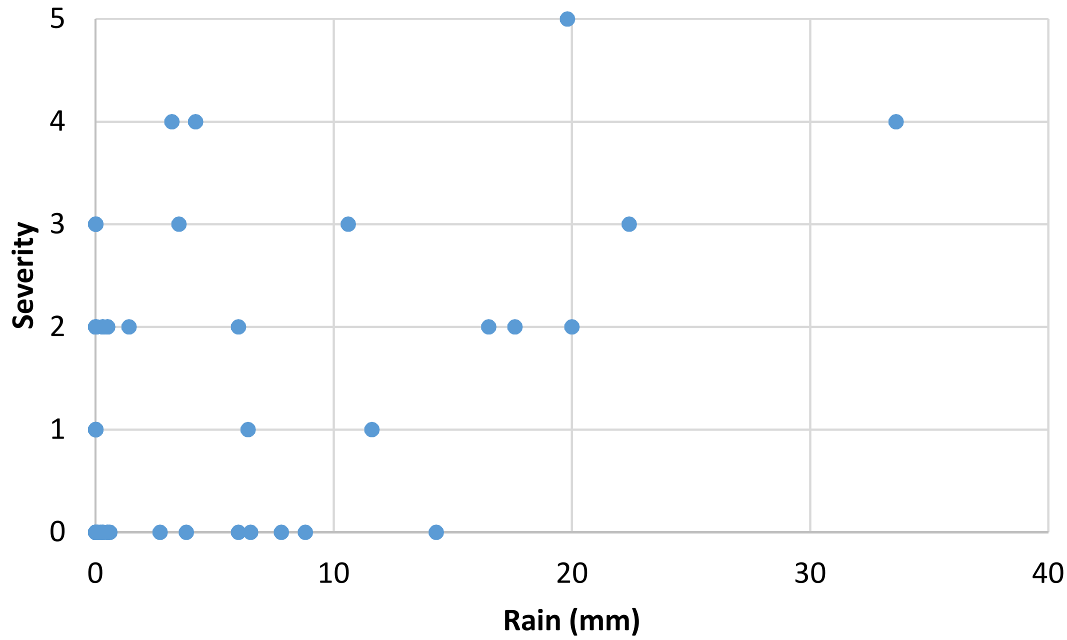

Figure 4.8: Relationship between total amount of rain up to three days prior to breakup and ice jam severity.

4.3.3 Snow

The relationship between snowfall and ice jamming is a complicated one. The melting snowpack contributes greatly to spring runoff, with large amounts of snow increasing the likelihood of a dynamic breakup. Alternatively, snow insulates the ice cover and reduces the amount of thermal growth throughout winter, especially earlier in the season, resulting in thinner ice. In the spring, the snow insulates the ice from warmer temperatures and reduces the amount of solar radiation penetration, reducing the rate of top melt and prolonging the integrity of the ice cover (Mahabir et al., 2006).

Both total winter snowfall and snow on ground readings were examined. The snow precipitation data was taken from the same stations listed in the precipitation section. Over winter, snowfall amounts started to accumulate after five consecutive days of temperatures below 0°C in the fall, and continued until the breakup date (Beltaos, 2008). Figures 4.9 and 4.10 displays a weak positive correlation between snowfall and ice jamming. This weak correlation could be the result of the contradicting role snow has in ice jamming, especially without the temporal aspects of when the snowfall occurred.

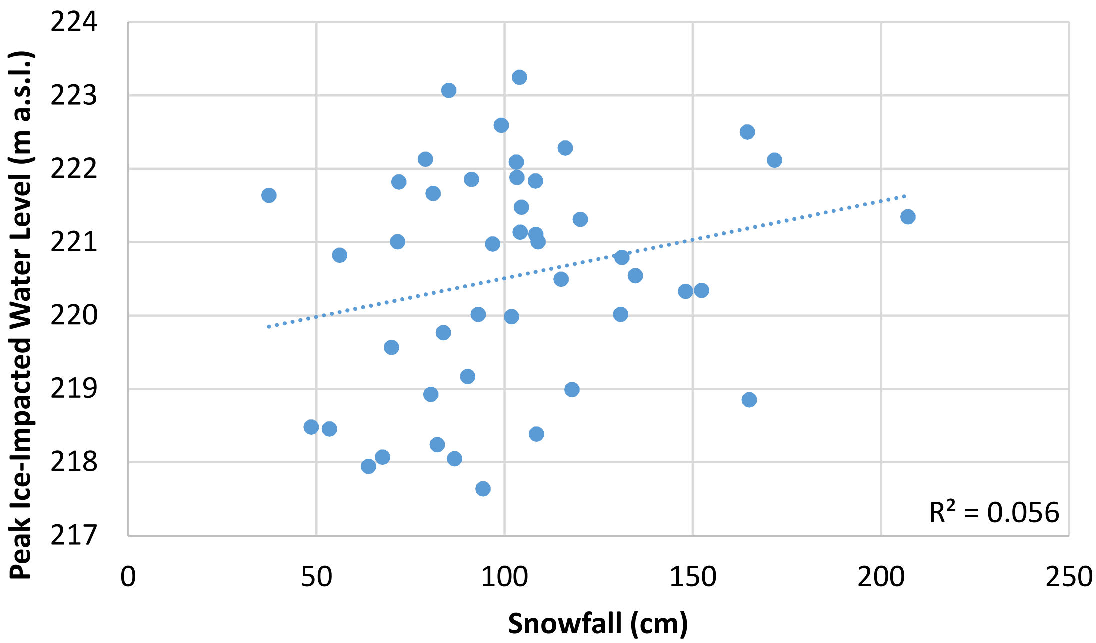

Figure 4.9: Relationship between over winter snowfall and Selkirk GS peak ice-impacted water level.

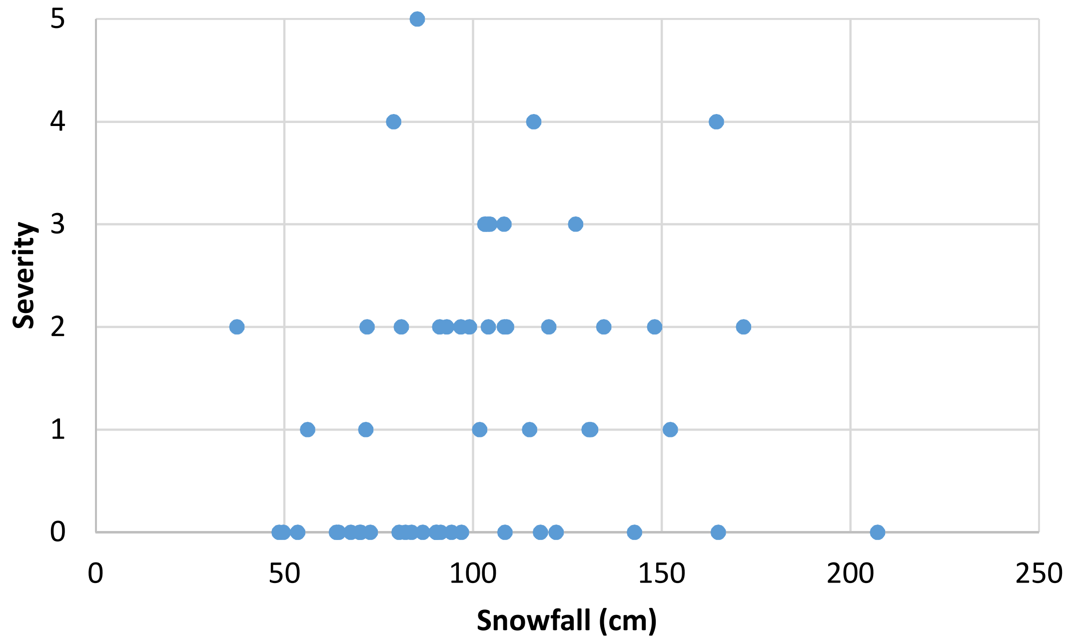

Figure 4.10: Relationship between over winter snowfall and ice jam severity.

Snow on ground readings are scarcer, and a daily value was only available from the Winnipeg Richardson International Airport weather station until 1989, when readings from Oakbank weather station became available. Many dates of snow on ground readings were compared to the ice jam severity indicators, with the best results coming from readings 21 days before breakup. Figures 4.11 and 4.12 shows that late season snow on ground amounts seem to have more of a correlation with ice jamming than the total snowfall amounts. The amount of snow on ground is directly related to spring runoff generation; therefore, higher levels of snow can result in more dynamic spring breakups.

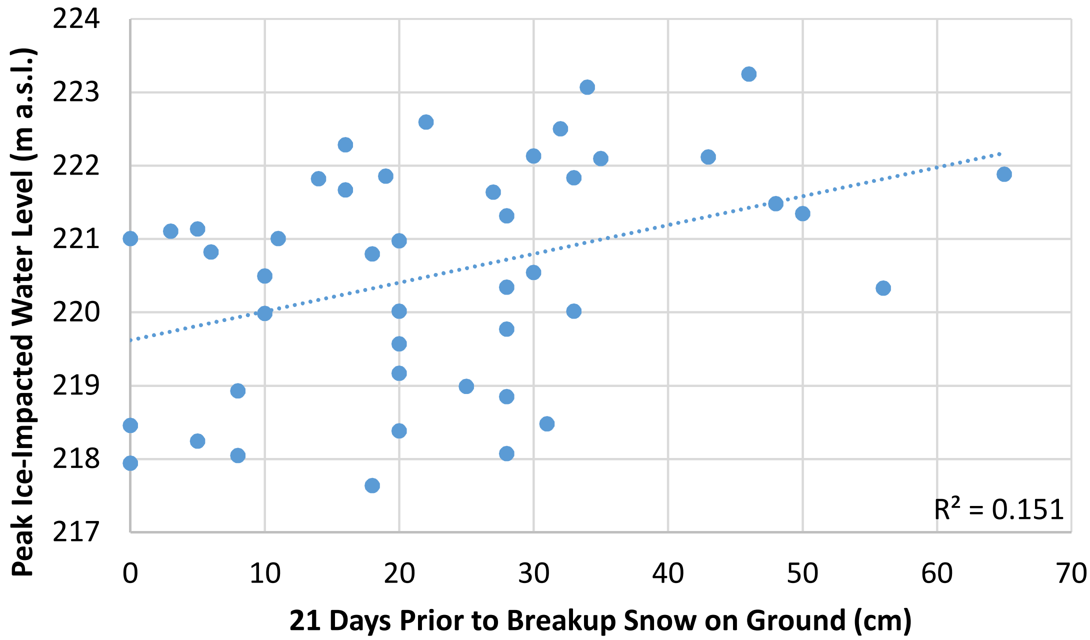

Figure 4.11: Relationship between snow on ground 21 days prior to breakup and Selkirk GS peak ice-impacted water level.

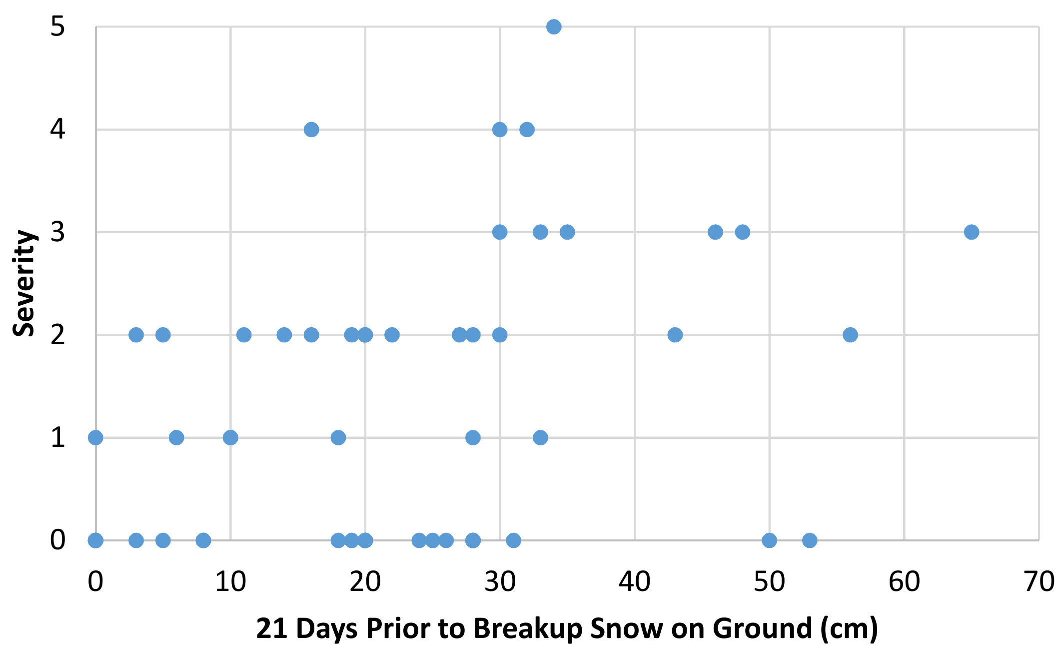

Figure 4.12: Relationship between snow on ground 21 days prior to breakup and ice jam severity.

4.3.4 Solar Radiation

As outlined in Chapter 2, solar radiation in spring deteriorates the ice cover and reduces its integrity. Solar radiation data is often viewed as more informative to the ice cover than temperature data, as colder – but sunny – days in spring can melt the ice cover more than warmer, cloudy days (Hicks et al., 1995; Beltaos 2008). The incident solar radiation (i.e. the radiation at the edge of the earth's atmosphere) can be calculated for a given location based on latitude, longitude, and local date and time. Solar insolation, the solar radiation that reaches the earth's surface, is dependant on the amount of scatter or reflection that occurs when traveling through the earth's atmosphere, as well as the cloud cover. An empirical equation for calculating the solar insolation is given by Gray (1970) as:

$$sc = so(a_2 + b_2 \frac{n}{N}) \tag{4.3}$$

Where: sc is the solar insolation [Wm^{-2}];

so is the incident solar radiation [m];

a_2 and b_2 are the location dependant empirical constants; and

$\frac{n}{N}$ is the ratio of bright sunshine hours to total daylight hours.

The empirical constants for a given location change depending on the time of year. Driedger (1969) determined the empirical constants for Winnipeg through calibrating solar radiation and direct sunlight data at the Winnipeg International Airport. The equations developed by Driedger to determine constants a_2 and b_2 were used in this study.

Once the solar radiation reaches a surface, its albedo will determine how much of the solar radiation is reflected or absorbed. This process is given by Equation 4.4:

$$E_{si} = (1 - \alpha_1)sc \tag{4.4}$$

Where: E_{si} is the flux of solar radiation that penetrates a surface [Wm^{-2}]; and

α_1 is the albedo value for that surface [m].

The albedo value for river ice depends on the presence of snow cover, as well as its condition (new snow differs from ripened snow). As the snow cover on the ice or the ice itself melts, the albedo decreases; as a result, the albedo value is very dynamic in the spring. For the purpose of this study, the solar insolation was used as an index for the amount of solar radiation absorbed by the ice cover. It was assumed that the solar insolation would directly correlate with the amount of radiation absorbed.

The solar insolation (henceforth referred to as the solar radiation for simplicity) was calculated for multiple periods before the breakup date. The best result was from the total cumulative solar radiation during the seven-day period before breakup, as seen in Figures 4.13 and 4.14. Results show almost no correlation between solar radiation and the ice jam indicators.

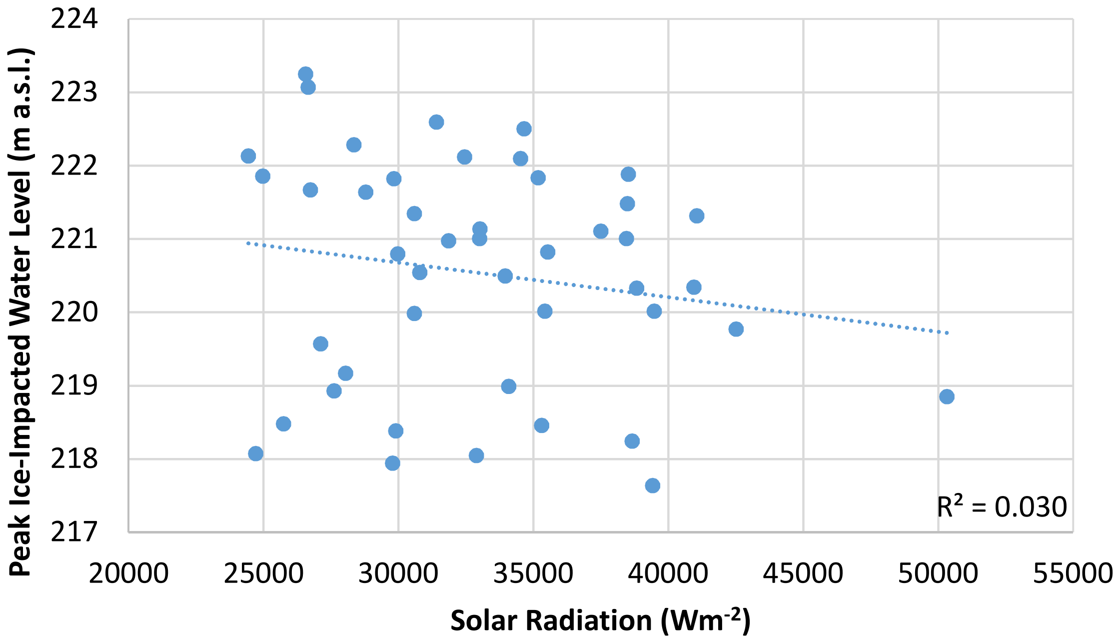

Figure 4.13: Relationship between solar radiation and Selkirk GS peak ice-impacted water level.

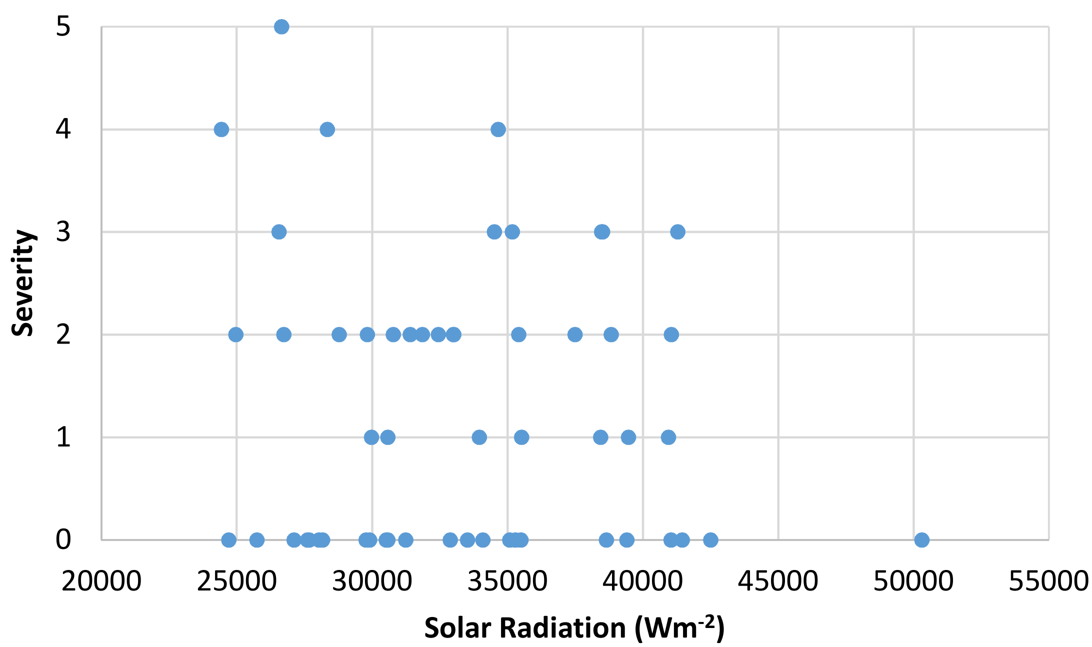

Figure 4.14: Relationship between solar radiation and ice jam severity.

4.3.5 Temperature

The degree-day approach is commonly used when relating temperature to ice processes and ice jamming. Chapter 2 goes into detail as to how accumulated degree days of freezing (ADDF) and accumulated degree days of thawing (ADDT) are used in estimating ice thickness. These two parameters are also used when referring to ice jamming, however they are not used for explicit calculation, but rather as indices for the severity of winter (ADDF) and spring (ADDT). High ADDF values usually indicate a thick ice cover, and result in a higher risk for severe ice jamming. Oppositely, high ADDT values at breakup indicate a slow melt and thermally-weakened ice.

The ADDF values were summed from the first five consecutive days of 0°C (or colder) weather in the fall, until the breakup dates. The ADDF values in Figures 4.15 and 4.16 show a much weaker positive relationship with ice jamming variables. The ADDT values were summed when temperatures were above -5°C from March 1st until the breakup date for every year. Figures 4.17 and 4.18 show that the higher ADDT values are negatively associated with severe ice jamming. Again, these high ADDT values can indicate a slow melt with a gentle rise in water levels and thinned ice.

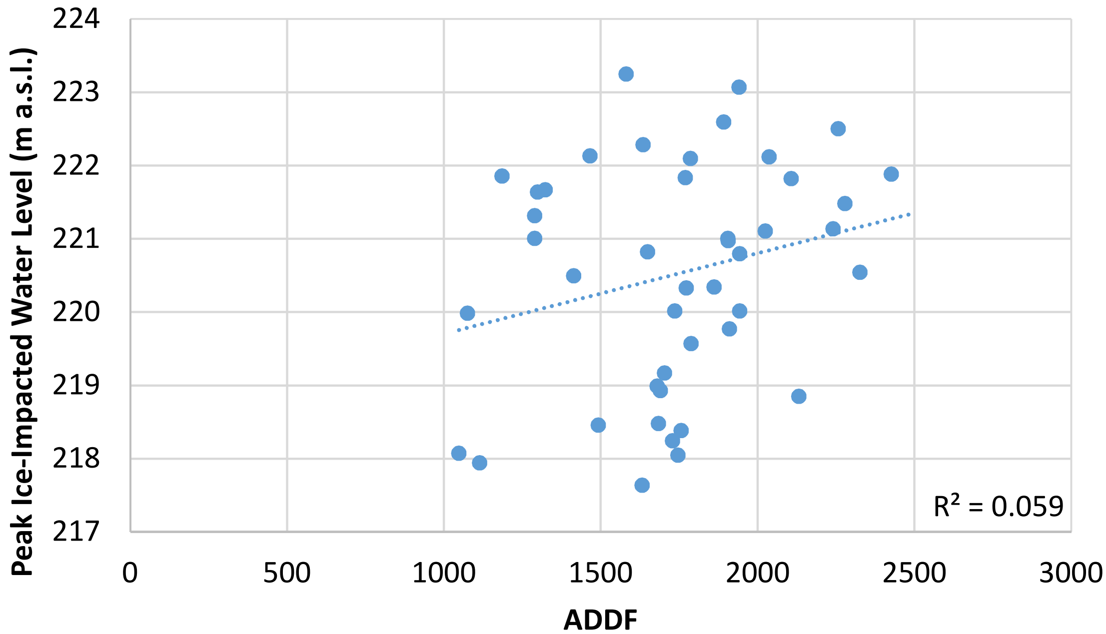

Figure 4.15: Relationship between ADDF and Selkirk GS peak ice-impacted water level.

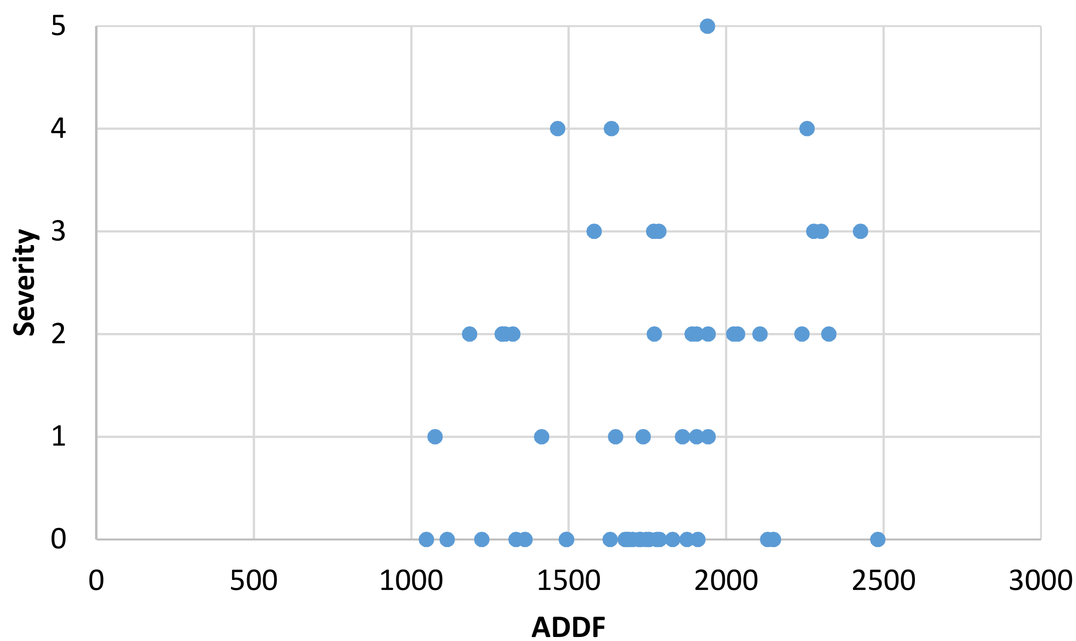

Figure 4.16: Relationship between ADDF and ice jam severity.

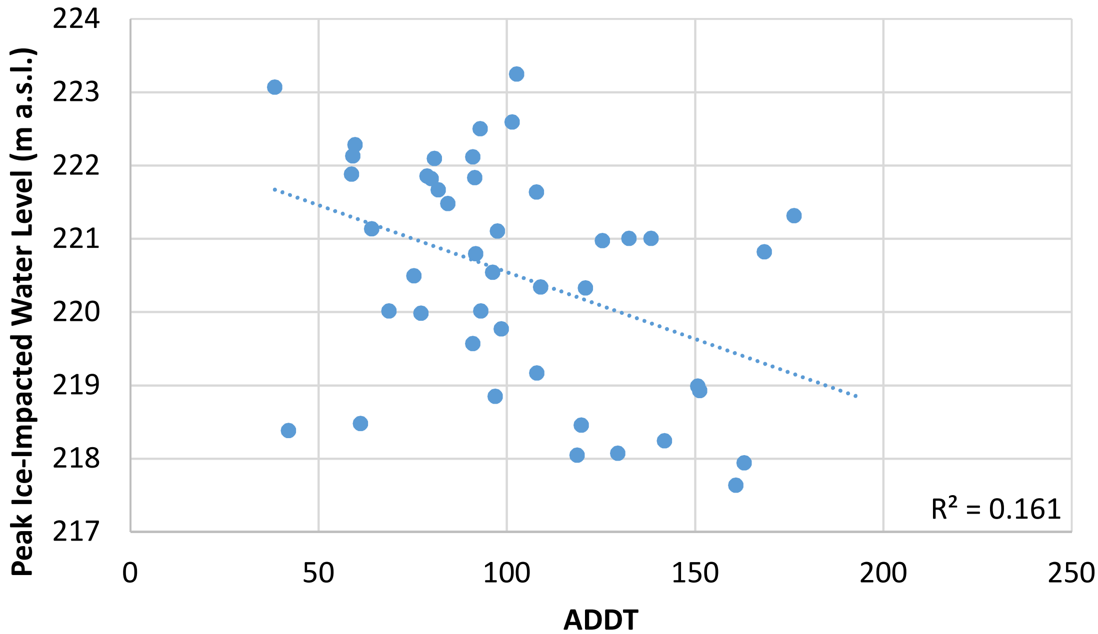

Figure 4.17: Relationship between ADDT and Selkirk GS peak ice-impacted water level.

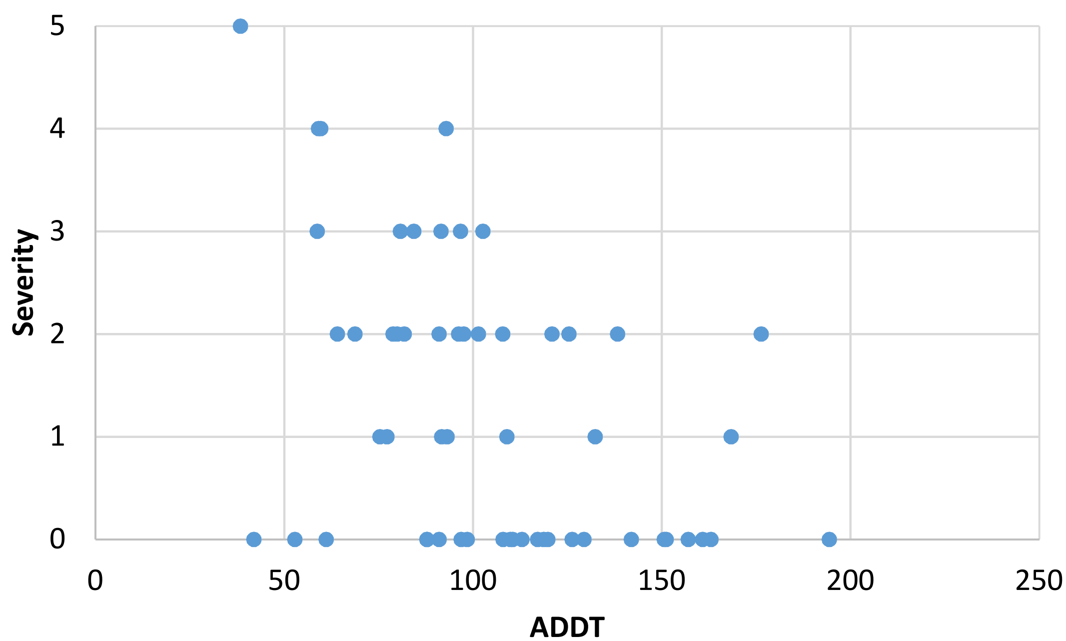

Figure 4.18: Relationship between ADDT and ice jam severity.

4.3.6 Freeze-up Water Level

A low freeze-up water level usually results in dynamic breakups, as it is likely that only a small increase in discharge is needed to break up the ice cover. However, the severity of an ice jam is greatly reduced when the flows are low. High freeze-up levels from wet fall conditions require higher flows to cause a dynamic breakup; therefore, high freeze-up water levels paired with large runoff can result in severe ice jams (F. Hicks, 2016). As freeze-up on the Red River usually occurs in late November or early December, the freeze-up water level was recorded as the average late December level. Figures 4.19 and 4.20 show that the freeze-up stage of the Red River at the Selkirk GS has a positive correlation to both ice jam severity and peak spring ice-impacted water level.

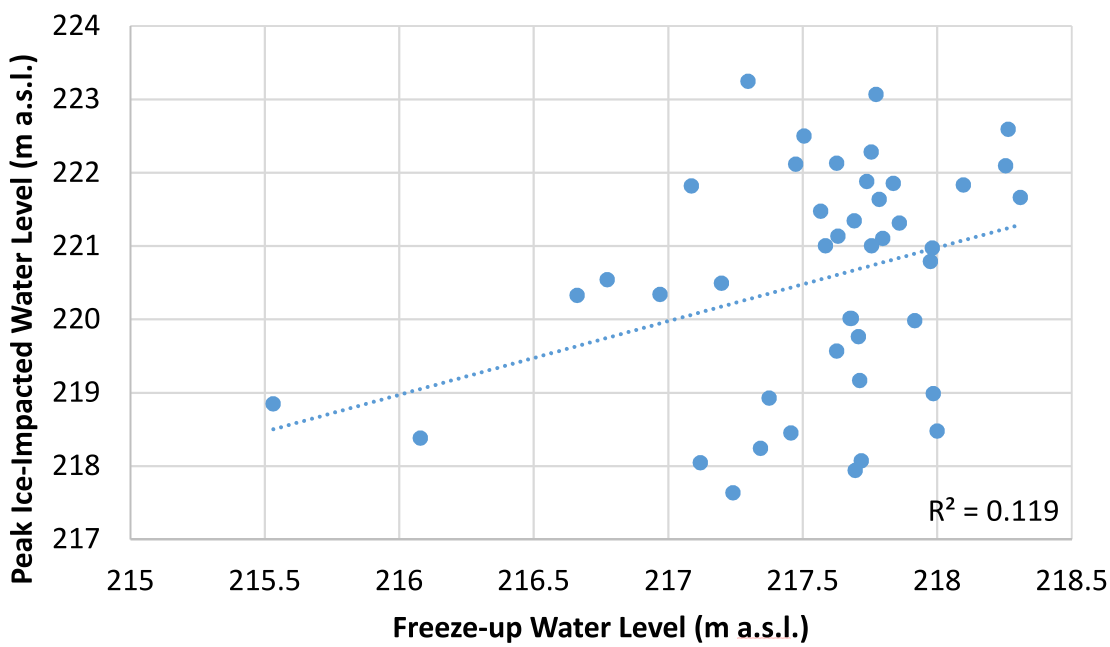

Figure 4.19: Relationship between the freeze-up water level and Selkirk GS peak ice-impacted water level.

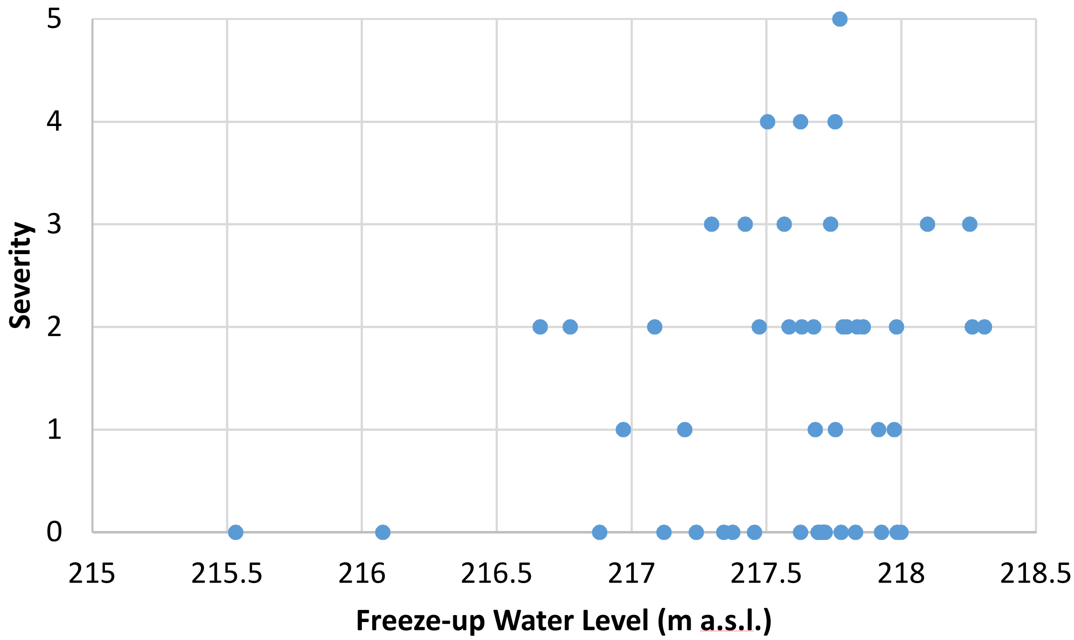

Figure 4.20: Relationship between the freeze-up water level and ice jam severity.

4.4 Ice Thickness

Since late season ice thickness is indicative of ice strength and the resisting force of the ice, understanding the relationship between ice thickness and severe ice jamming on the Lower Red River may be very insightful. Although the ice thickness near the time of breakup would be most informative, collection of ice thickness data becomes impossible due to the dangers of a melting ice cover. Peak ice thickness, before melting and loss of structural integrity occurs, can also be related to ice jamming. This study modelled peak ice thickness for this purpose and although it was decided to not use the modelled ice thickness as an ice jam parameter due to multicollinearity with ADDF, the results may be useful and are included in this thesis.

4.4.1 Ice Thickness Data Collection

Ice thickness data along the Lower Red River was made available by the Province of Manitoba, dating back to 1998. From 1998 to 2008 intermittent auger readings were taken at eight locations (2-3 holes drilled at each location) from Netley Lake to the City of Selkirk. The eight locations can be seen in Figure 4.21. Starting in the 2008-2009 ice season, the Province of Manitoba implemented its ice jam mitigation program and now takes ice thickness readings using Ground Penetrating Radar (GPR). The GPR is used to record ice thicknesses from Lake Winnipeg to Selkirk, however exact extents range each year due to ice conditions. From 2009-2017 the GPR data was used to extract ice thickness data at the eight primary locations.

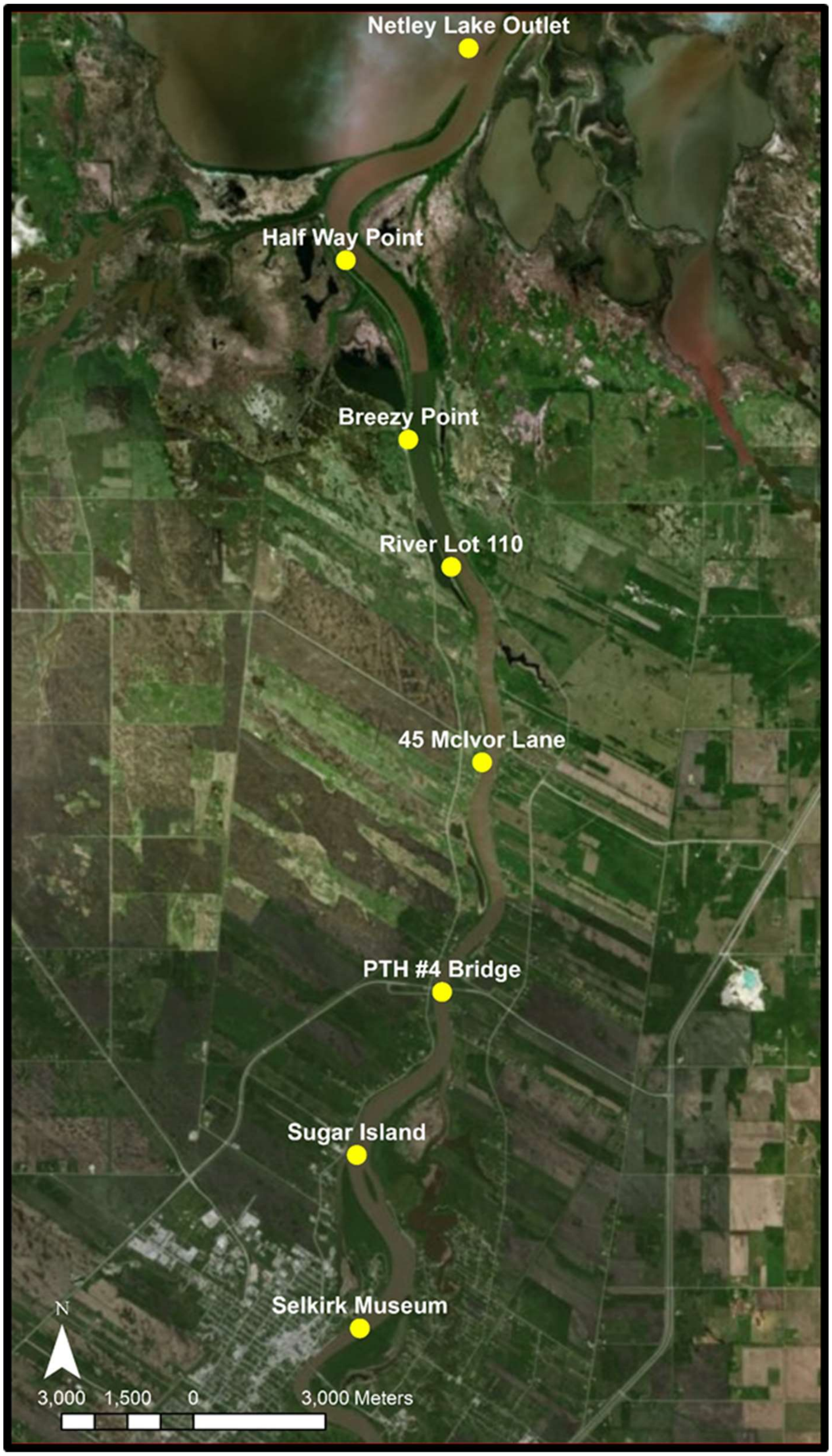

Figure 4.21: Ice thickness data collection locations along the Lower Red River.

Since GPR provides thousands of data points in a small area, average ice thicknesses were taken from the GPR data. A large and small area of the river, spanning 300 m and 150 m along the river respectively, was used at each location to see if average ice thickness at each location was affected by the size of the area used. The average amount of readings in each size were 4600 (large) and 2300 (small). It was found that there was little variation between the large and small areas, therefore the averages were taken from the larger areas since there are more data points.

4.4.2 Ice Thickness Modelling

In order to model ice thickness both the Stephan Equation and multiple regression were used. The Stephan Equation, detailed in Section 2.1.3, requires only ADDF which was calculated using Equation 2.4. Temperature data was taken from the Selkirk weather station, when available, and supplemented from surrounding stations when not available (see Table 4.1). ADDF starts accruing in the fall when temperatures are below 0°C for five consecutive days. The α value for each of the eight sites was calibrated and is shown in Table 4.2. Comparing to α values that are available in the literature (Table 2.1), the α values for the Lower Red River are in the range of an average lake with snow. This could be due to the slow-moving nature of the Red River and possibly the backwater effects from Lake Winnipeg in its most downstream section.

Table 4.2: Ice thickness modelling results using both the Stephan Equation and multiple regression.

	Stefan Equation		Regression		
	α	RSE	$\boldsymbol{a}$	$\boldsymbol{b_n}$	RSE
Netley Lake Outlet	0.020	0.08	-2.86	0.35	0.08
Half Way Point	0.018	0.12	-2.40	0.27	0.11
Breezy Point	0.019	0.12	-3.50	0.44	0.12
River Lot 110	0.018	0.10	-3.86	0.48	0.10
45 McIvor Lane	0.019	0.10	-3.94	0.49	0.10
PTH #4 Bridge	0.019	0.12	-4.18	0.53	0.12
Sugar Island	0.020	0.12	-4.27	0.55	0.12
Selkirk Museum	0.017	0.11	-3.78	0.46	0.11

The parameters that were initially considered for the regression model were ADDF, average over winter flow, and snowfall. The average over winter flow was taken from either the Lockport or Selkirk hydrometric stations. Two simple regression models were used, a standard linear regression and a power regression, which are identical except that the power regression uses the natural log of the observed data and model parameter values. Equations 4.5 and 4.6 represent linear and power regression models:

$$y = a + b_n x_n \tag{4.5}$$

$$ln\, y = ln\, a + b_n ln\, x_n \tag{4.6}$$

Where: y is the estimated dependant variable;

x_n is the value of the nth parameter;

a is the intercept; and

b_n is the coefficient of the nth parameter.

At every location only the ADDF was statistically significant with a p-value of less than 0.05. Additionally, at every location the power regression outperformed the linear regression. The results of the power regression can be seen in Table 4.2. The residual standard error (RSE) was used as a goodness-of-fit measurement for both the regression modelling and the Stephan Equation. The RSE tells you on average what the residual – the difference between an observed and estimated value – is for the model. RSE is calculated using equation 4.7 (James et al., 2013):

$$RSE = \sqrt{\frac{\sum(y_{ob} - y)^2}{n-2}} \tag{4.7}$$

Where: y is the estimated dependant variable;

n is the number of observations; and

y_{ob} is the estimated value of the dependant variable.

The power regression performs slightly better than the Stephan Equation, but the differences are minimal. An example of the power regression results can be seen in Figure 4.22.

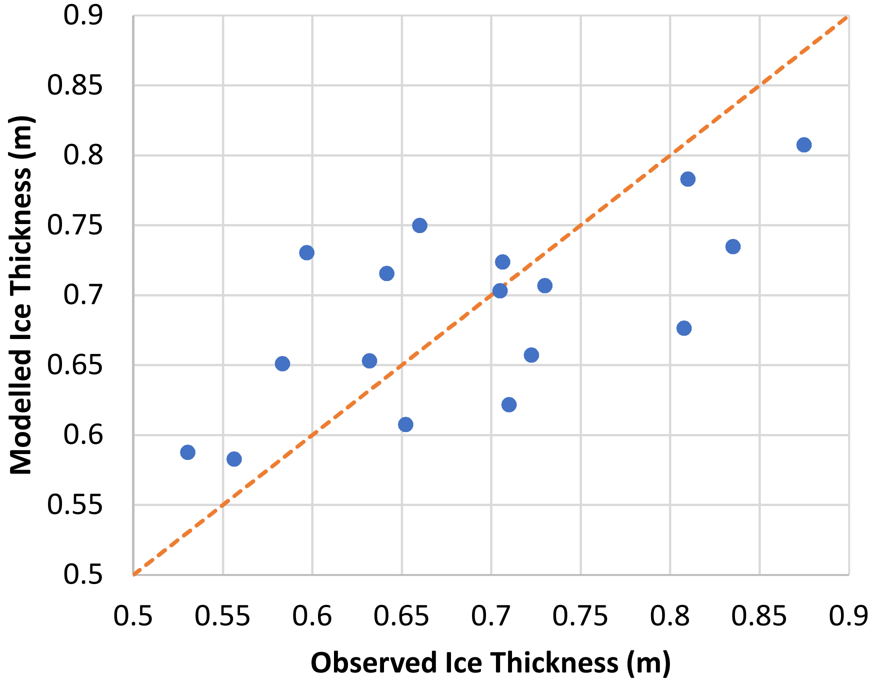

Figure 4.22: Modelled and observed ice thicknesses for the Netley Lake Outlet. The dashed line represents where modelled values would equal observed values. The resulting R^2 and RSE are 0.447 and 0.08 respectively.

Unfortunately, using a modelled ice thickness as a parameter that is based only on ADDF as well as using ADDF as a separate parameter would cause multicollinearity issues. Multicollinearity can result in models becoming unstable and make it difficult to distinguish the significance of parameters independently, therefore only one of ADDF and modelled ice thickness can be used. The best option is to use the ADDF parameter over the modelled ice thickness since the modelled value of ice thickness has an associated error. Using parameters that are estimated and include errors would compound the error of the ice jam model results, which is undesirable.

4.5 Parameter Trends

The individual parameter relationships are only weakly related to ice jamming and its severity; again, this is due to the complexity and interaction of multiple physical processes. Looking at all the parameters and their possible interactions for a given year may better illustrate how ice jamming occurs on the Lower Red River, compared to the analysis of individual parameters. All parameters for the most severe ice jam years (Severity 3 and above) were compared to two non-jam years with high flows. As previously identified, flow has a stronger correlation with ice jamming compared to other parameters; therefore, the non-jam years were chosen for their potential for ice jamming based on breakup flow (2006 and 1979 were the only years that ice-impacted flow was above 1900 cms but no ice jam occurred). Table 4.3 gives a summary of the parameter values for these years.

Table 4.3: Risk categories for ice jam predictor variables for Severity 3 and above ice jam years as well as non-jam years with ice-impacted flows greater than 1900 cms. Square colours indicate high risk (red), medium risk (yellow), and low risk (green).

	Year	2009	2004	1996	1995	2014	2011	2007	2005	1974	1967	2006	1979
	Severity	5	4	4	4	3	3	3	3	3	3	0	0
Flow	Peak ice-impacted												
Snow	Snow on ground 21 days prior to breakup												
	Snow on ground Feb 1st												
	Total snowfall at breakup												
Rain	API												
	Rain 3 days prior to breakup												
	Rain equivalent March 1st to breakup												
Solar Radiation	Solar radiation 7 days prior to breakup												
Water Level	Freeze-up												
Temperature	ADDF after March 1 until breakup												
	ADDF at breakup												
	ADDF at Feb 15th												
	ADDT March 1st until breakup												

In Table 4.3, the coloured squares represent the rank of the parameter value and its relation to ice jamming. The percentile value of each parameter was categorized in three ranges:

- Range 1: 0 – 33 percentile;
- Range 2: 33-66 percentile; and
- Range 3: 66 percentile and above.

Then, based on the parameter, each range was given a colour code dependent on if the parameter was positively or negatively correlated with ice jamming. The colours represent the relative risk to ice jamming, with red as high risk, yellow as medium, and green as low risk. For example, ADDF values are positively correlated with ice jamming, so values in Range 1 are green, Range 2 are yellow, and Range 3 are red. Contrarily, ADDT is negatively correlated with ice jamming, so the colour scheme and associated risk are reversed. The table is sorted from highest severity to lowest, and gives a visual of how high risk parameter values diminish as the severity decreases.

From Table 4.3, spring ADDT values are low or moderate, and at least one of the snow parameters reflects high values for all years with ice jamming. Solar radiation shows no trend between jam and non-jam years, and does not seem to influence jamming. Most jam years are the result of cool spring temperatures, paired with high snowpack, spring precipitation, and high freeze-up levels; however, the latter two conditions did not occur every jam year.

Table 4.3 is useful in determining why years with high flows did not result in ice jamming. In 2006, high flows paired with low ADDT values occurred, which could be expected to lead to ice jamming. The winter that year was very warm (ADDF in the 9th percentile), however, a warm winter paired with high levels of snowfall can result in a thinner ice cover, and thus a smaller likelihood of ice jamming. Average modelled March 15th ice thickness for the Lower Red River had a cumulative frequency of less than 5% in 2006, meaning that 95% of other years result in thicker ice modelled. In 1979, high flows combined with spring rain and a cold winter occurred, but a warm spring (ADDT in the 77th percentile) indicated ice strength could have been greatly deteriorated leading up to the breakup date.

Table 4.3 was used for preliminary analysis to understand the parameters' impact on ice jamming. The common trend of the non-jam years is having at least one extremely mild parameter value that could hinder ice jamming. This result is not necessarily shown in Table 4.3, as the table separates the parameter values evenly into three ranges, each 33 percentiles wide. These results indicate that a threshold method (where parameters need to reach a certain value to be considered a risk) could be useful in determining jam and non-jam years.

Chapter 5: Ice Jam Prediction Model

Many different methods exist for predicting breakup ice jam formation. Due to the complex processes that occur during ice breakup and jam formation, most models are empirically based rather than physically based. These models rely on local parameter data, including antecedent conditions, such as fall or over-winter parameters, or even early breakup meteorological and hydrometric data. As ice jams are considered a local phenomenon, these models are also highly site-specific and are not easily transferrable to other locations (Mahabir et al., 2007; White, 2003).

White (2003) describes a useful prediction tool as one that is able to provide a qualitative probability of the ice jam occurrence and the magnitude of flooding based on easily forecasted or measured parameters. As ice jams occur rapidly, one main goal of an ice jam model should be to predict ice jams with enough lead-time that proactive measures can be taken, such as evacuations. The occurrence of false positives – and especially false negatives – should be kept to a minimum.

5.1 Threshold Models

Threshold models have been used to some success in predicting the occurrence of ice jams. Threshold models are built from parameters that have clear limits such that, depending on the parameter, ice jams either always occur or never occur once the threshold limit is crossed. In some studies, a single parameter can be used to develop a prediction tool; however, due to the complexity of ice jamming, usually more than one parameter is needed. A simplistic threshold model was developed by Shuliakovskii (1963) for the Yenesei River in Russia. This model only used historical freeze-up stage data, as it gave clear threshold limits: if the freeze-up stage was over 300 cm, an ice jam has always occurred; if the freeze-up stage was between 185 cm and 300 cm, ice jams have occurred, with the frequency increasing as the stage approaches 300 cm (White, 2003).

Most threshold models are not as simplistic, and require multiple variables that can be difficult to collect or calculate. Galbraith (1981) used a combination of thawing degree days, a snowmelt index, and the rate of heat transfer to predict ice jamming. To calculate heat transfer, one needs an extensive amount of data such as incident solar radiation, cloud cover, incoming and outgoing longwave radiation, surface temperatures, and wind properties (White, 2003). Wuebben (1995) was able to hindcast and forecast ice jam events using a weighted threshold model with variables all related to stage, ice thickness, and ice strength. Both models were developed from first studying the historic breakup and ice jam trends for the desired locations, and are very site-specific, so there is no guarantee that similar models along different river reaches would produce comparable results (White, 2003).

Recently, Shaw et al. (2013) developed an ice jam forecasting tool for the Kashechewan First Nations community on the North Albany River. The tool was developed as a threshold model with the ability to indicate high risk of ice jam-related flooding at least 10 days in advance, which is the length of time needed to evacuate local residents. The model used current and forecasted meteorological and hydrometric data to provide the risk of an ice jam occurring based off two criteria: early warning and late warning. The early warning criteria looked at the accumulated daily rainfall and daily snow melt, as well as whether the amount crosses a date-based threshold.

The late warning criteria had three factors: the three-day change in flow threshold, a total flow threshold, and a calendar date of April 28th (no ice jams have occurred after this date).

Shaw et al. (2013) documented the use of the tool from its development in 2008 to 2013. Of the six years documented, the tool produced two false positive predictions and four correct negative predictions. One of the false positive predictions resulted in thresholds being only slightly exceeded; however, the second resulted from large recorded flow values. It was later determined that the high flow values were likely due to ice jamming near the gauge, not a large increase in flow. No flood event happened during the study years, however the tool was shown to properly hindcast the 2006 flood event, which was the most severe event for the community. The study did not indicate if the tool was able to hindcast all other previous flood events, or just the event in 2006.

5.2 Statistical Models

Statistical models have also been used to predict ice jamming, using methods such as multiple regression, logistic regression, and discriminate function analysis (White, 2003). Advantages of using these methods include the selection of variables based on statistical significance, as well as quantitative values of false-positive or false-negative results.

Logistic regression models are well-liked as a predictive tool for their binomial results of either a "jam" or "no jam" event. White (1996) used logistic regression to predict ice jamming on the Platte River in Nebraska. Statistically significant variables were selected using a stepwise regression method. Once the relationships were developed, forecasted variable data could be used to track ice jam probability through the winter season. The model performed moderately well and produced a false negative rate of nearly 4% and a false positive rate of nearly 27%.

In 2006, Mahabir et al. applied multiple linear regression to a comprehensive database of both meteorological and hydrological data, consisting of 106 different variables from the period of 1972 to 2004, to model maximum water level during spring breakup. The study site of the Athabasca River has frequent ice jams, and the highest water levels observed were ice-induced. Due to multicollinearity of the data, the dataset had to first be reduced in order to be suitable for multiple linear regression. The optimal solution – consisting of eight variables from fall, winter, and spring conditions – had an R^2 value of 0.84 and a RSE of 0.7 m. This model performed well in respect to other ice jamming models developed for the location. The authors noted, despite the fact that some of the variables used did not have data for the entire timespan being studied, that the 32 years of data was a limitation to the model, which had far more available data than most locations (Mahabir et al., 2006).

Discriminant function analysis (DFA), similar to logistic regression modelling, uses a combination of parameters to discriminate between different outcomes such as jam or no-jam events. Depending on the number of outcomes required, the model will develop discriminate functions that separate each outcome. For example a two-outcome linear DFA would produce a linear discriminate function similar to a linear regression equation, however the purpose of the function is to separate the jam and non jam years so a linear boundary can be drawn between them. An example to illustrate DFA results is shown in Figure 5.1. Similarly, quadratic DFA produces quadratic discriminate functions and quadratic boundaries between outcomes. The discriminate function can then be used to predict the outcomes of future years.

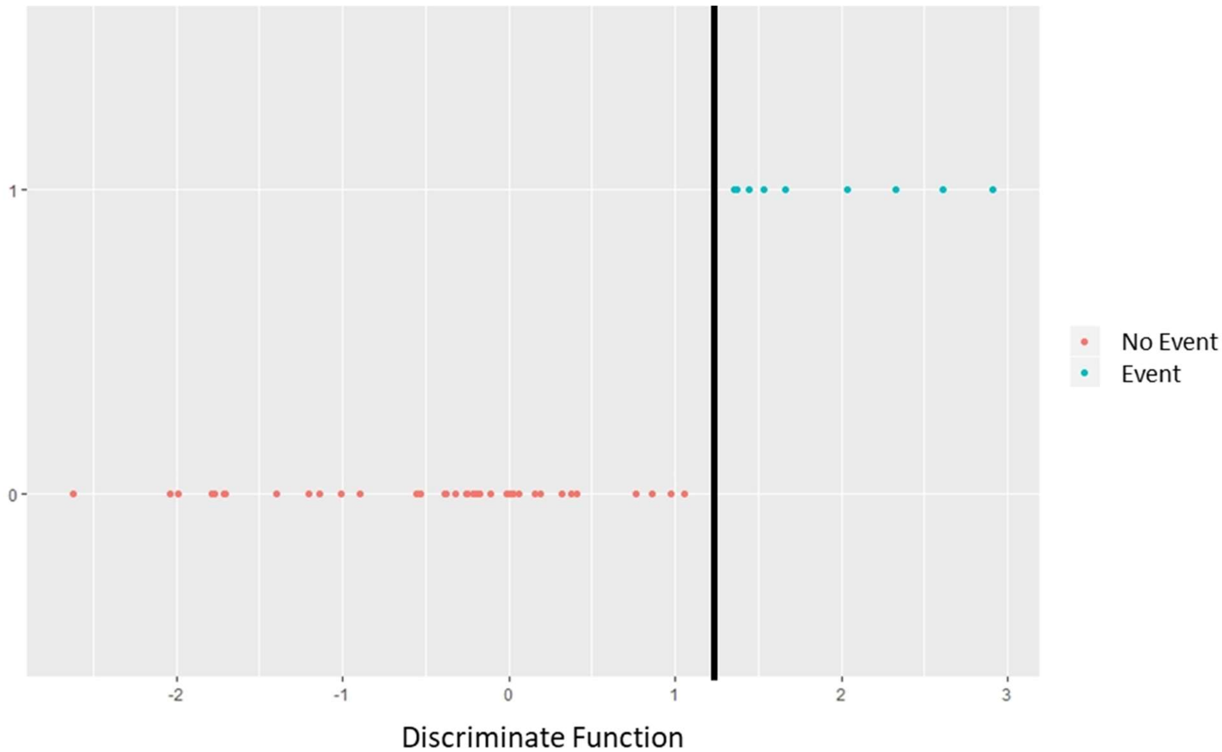

Figure 5.1: Example results of a two-outcome discriminate function analysis.

There are two documented studies of DFA being used to predict ice jamming. Zachrisson (1990) had a three-outcome model (low, medium, and high risk) for the Tornealven River that runs along the shared border of Finland and Sweden. The parameters used in the model are a five-day change in discharge, accumulated degree day of thaw (ADDT) index, over-winter precipitation, and April precipitation. In the two years of documented use, the model had one correct negative result and one false negative (White, 2003). White and Daly (2002) also used DFA for a two-outcome (jam or no jam) prediction model at Oil City, Pennsylvania. The model, which used a combination of air temperature indices and flow parameters, resulted in a false negative rate of 12% and a false positive rate of 40% (White, 2003).

5.3 Lower Red River Ice Jam Prediction Modelling

This study examined the three most widely used modeling approaches for ice jam prediction to determine their suitability to the study area, they include:

- Threshold modelling;
- Regression; and
- Discriminate function analysis.

The study years for this project ranged from 1962 – 2017, however – depending on the modelling technique – some years had to be excluded due to lack of data. It should be noted that the year 1982 was omitted universally because no breakup initiation date could be determined from media sources or hydrologic records.

Consideration was given to the effects that the ice jam mitigation program would have on modelling results. The program, beginning in 2006, involves pre-breaking the ice on the Lower Red River so it can more freely move come spring breakup, ostensibly reducing the risk of an ice jam. One consideration was for the study years to be divided into two datasets, pre- and post-2006, and modelled separately. This approach considered all other conditions to be the same, with the only difference being the ice mitigation program. This is not the case in reality, however, as hydrometric and meteorological conditions differ from year to year. Breaking up the dataset would exclude years with extreme parameter values and would negatively affect the quality of model results. For this reason, each modelling method considered all year's meeting the data requirements, regardless of the commencement of the ice jam mitigation program.

Ice jamming on the Lower Red River can cause devastating flooding and occurs frequently, but the most common jams are Severity 1 or 2, as seen in Figure 5.2. Severity 1 jams result in no flooding whatsoever, and Severity 2 jams see only minor flooding. The most common scenario is the Selkirk Park flooding, causing the Selkirk Bridge to be closed due to access issues. Thus, due to the wide range of flooding scenarios that could occur, merely modeling whether a jam will or will not occur has little benefit. Due to the low frequency of events, the individual severity categories cannot be modelled; instead, jams in Severity 3 and above were grouped together as "severe jams", as these were years resulting in evacuations, and would be of interest for emergency preparedness planning. For modelling purposes, an event year is considered to be one with a severe jam, while Severity 2 and below ("minor jams") as well as no ice jamming ("no jam") years are considered non-events.

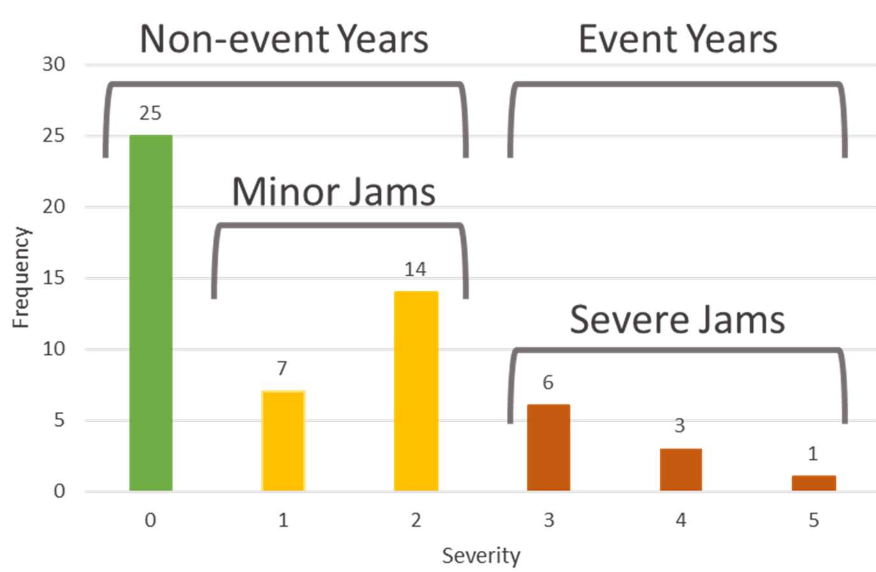

Figure 5.2: Frequency of each ice jam severity rating.

Chapter 5: Ice Jam Modelling

The Province of Manitoba's Hydrological Forecasting Centre can forecast the timing and magnitude of the spring hydrograph. To predict the spring hydrograph, data such as winter precipitation, antecedent soil moisture conditions, snow water equivalence, and future meteorological forecasts are used alongside hydraulic routing of the spring peak moving upstream. If the models are developed with the peak spring flow as a parameter, then the predicted peak spring flow in future years can be used to forecast ice jam severity. This can be very beneficial as, relative to other parameters, peak spring flow has a stronger correlation with severe jamming. Although the accuracy of the spring hydrograph prediction is outside the scope of this project, many of the modeling methods were conducted with and without the peak spring flow to provide the option of including or excluding it at a later date.

5.3.1 Threshold Modelling

Parameters were examined for their applicability to a threshold model to identify severe jam years. Figure 5.3 gives an example of parameters that can and cannot be used in this type of model. Figure 5.3(a) considers the depth of snow on ground at February 1st. For this parameter, the lowest value seen for a severe jam was ~30 cm; this value can then be used to exclude non-event years: values lower than the dashed line would be excluded from the model. Figure 5.3(b) shows pre-breakup rain for each year. In this case, the lowest value of a Severity 3 (or higher) event would not exclude any years being considered; therefore, this parameter cannot be used in a threshold model.

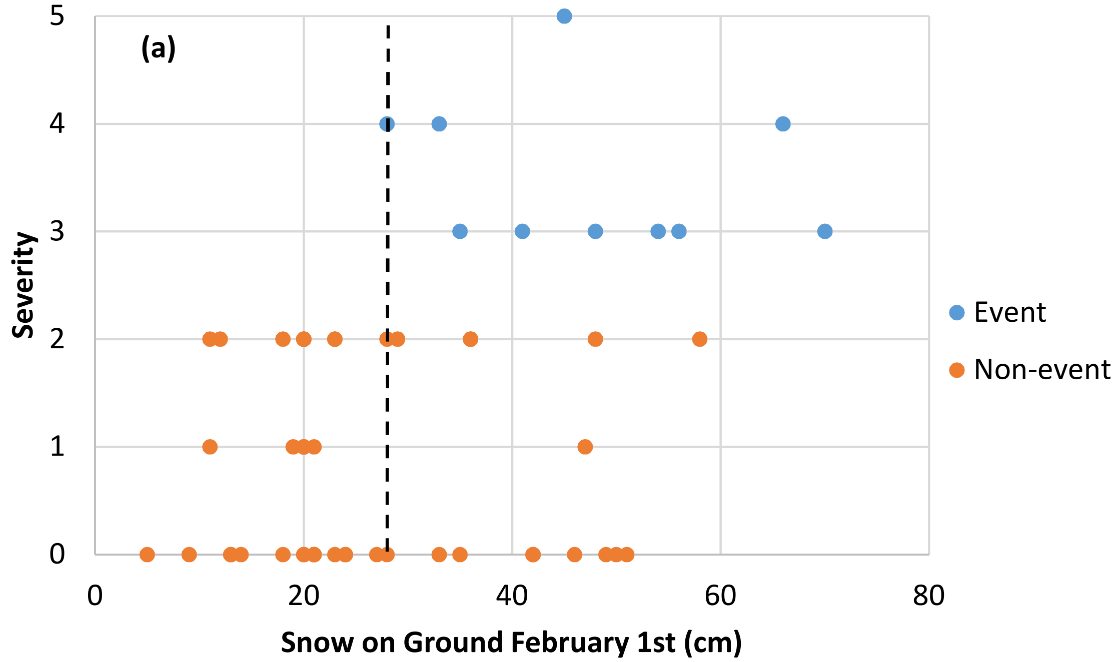

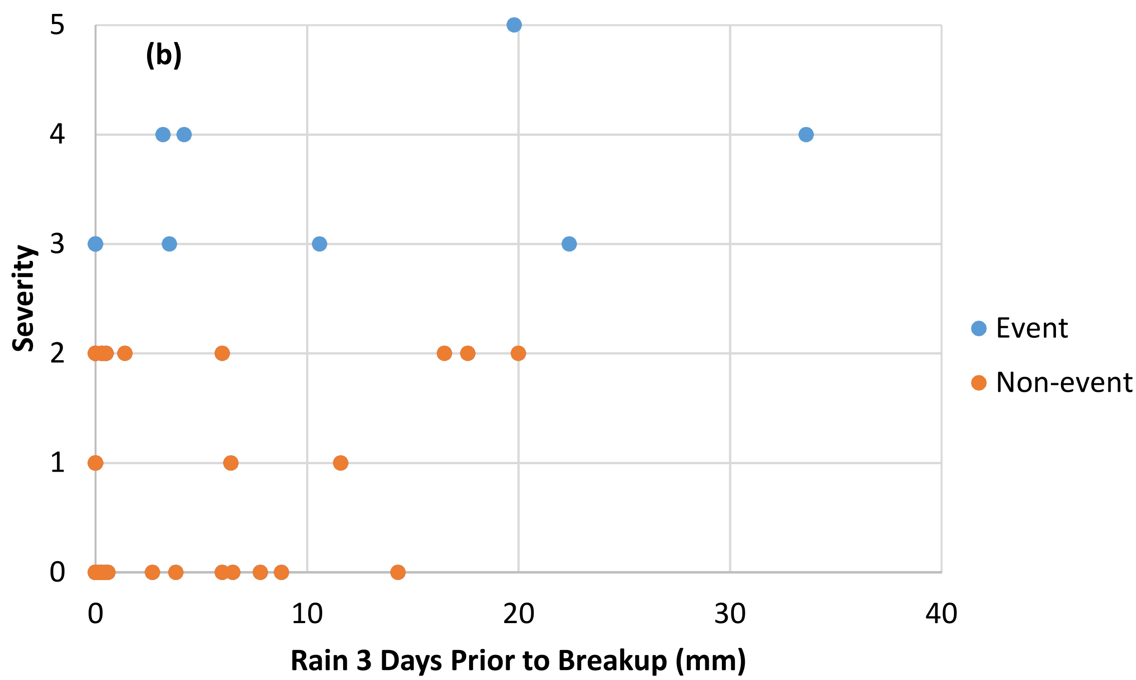

Figure 5.3: (a) An example of a threshold parameter with the lowest value of an event year shown by the black line. (b) An example of a parameter not suitable for threshold modeling.

Chapter 5: Ice Jam Modelling

Through this evaluation, a threshold model was developed with six parameters, including:

- ADDT from March 1^{st} to breakup;
- Rain equivalence from March 1^{st} to breakup;
- Freeze-up water level at Selkirk GS;
- Snow on ground on February 1^{st}; and
- ADDF on February 15^{th}.

The two over-winter parameters, snow on ground and ADDF, were initially measured at breakup but then adjusted to determine if a longer lead time could be used. Values were adjusted by roughly 15-day intervals (15^{th} and last day of every month) from the breakup date. This analysis found that the lead time for snow on ground could be reduced to February 1st – and ADDT to February 15^{th} – and achieve the same results as found using the breakup value of these parameters. The final model parameters and their threshold values can be found in Table 5.1 and are shown in Figure 5.4. All parameter values need to exceed the indicated threshold criteria for a jam to occur, except for the ADDT in which the value needs to stay below the threshold criteria.

Table 5.1: Threshold model parameters and threshold values.

Parameter	Threshold
Freeze-up water level	> 217.25 m
Snow on ground - February 1st	> 27.9 cm
ADDF - February 15th	> 1116.5
Rain equivalence – breakup	> 2.55 mm
ADDT - breakup	< 102.7
Peak spring flow	> 1519 cms

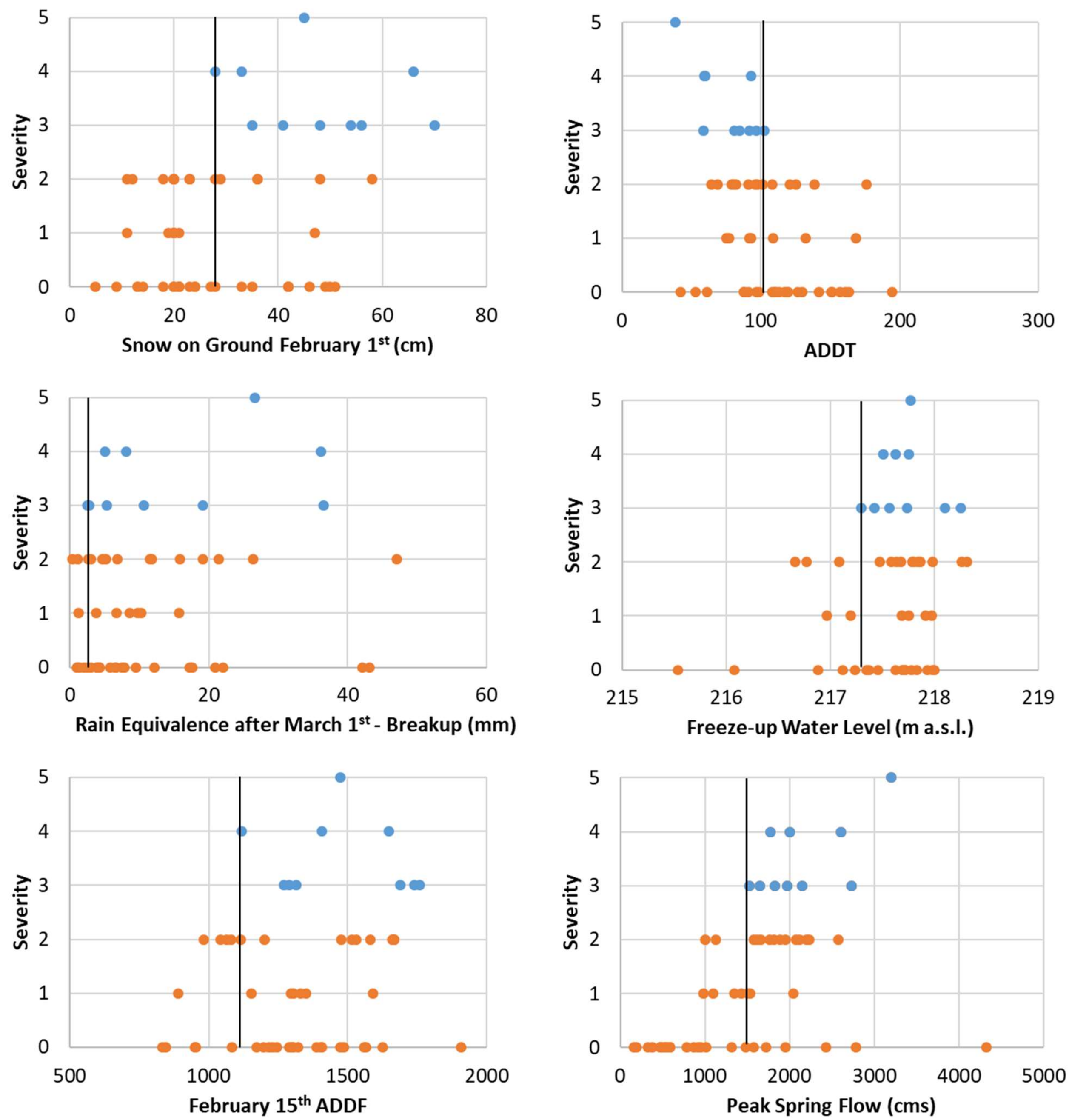

Figure 5.4: Threshold model parameters displaying where the threshold value is located. Values in blue are event years and the values in orange are non-event years.

In Table 5.1 and Figure 5.4, the peak spring flow is also listed as a model parameter. All years that meet the spring peak threshold also met the other five parameters' criteria. The addition or subtraction of the peak spring flow parameter does not, therefore, affect the results of this model. The peak spring flow parameter can, however, be used in parallel with the model to provide the user an additional check of the model results.

The model was developed based on 55 years of data, including 10 severe events. Freeze-up water level values were missing in some years; in those years, however, other parameters did not meet their threshold criteria, allowing the years in question to be classified as non-event years. Through eliminating years that failed to meet any one parameter's threshold criteria, the model can correctly predict 44 years as non-events and 11 years as severe jams, including one false positive year, 1966. Very little was found regarding the ice jam of 1966 other than that the jam caused minor flooding in the Breezy Point area, putting it as a Severity 2 jam. It is possible that there was less development in the area at the time or this jam was more severe but wasn't captured in the available information, as is usually a concern for older events as less information is available.

This threshold model can be used as a prediction tool following a two-step process similar to the tool developed by Shaw et al. (2013). On February 15th, three of the five parameters can be evaluated: freeze-up water level, ADDF, and snow on ground. If all three thresholds are not exceeded, then that year can be viewed as a low risk year as, historically, severe ice jams have never occurred under those conditions. If these thresholds are exceeded, however, then severe ice jamming has, historically, occurred 53% of the time. Additionally, if the peak spring flow forecast meets the threshold criteria, severe jamming has occurred 71% of the time historically. In this situation, monitoring is required for the spring parameters, namely ADDT and rain equivalence.

Chapter 5: Ice Jam Modelling

By monitoring the spring parameter data, ice jam risk can be determined based on risk zones – as seen in Figure 5.5 – which are:

- **High Risk:** If breakup occurs in this zone, severe ice jams have always occurred.
- **Moderate Risk:** Severe ice jams have not historically occurred; if breakup has not occurred, however, there is still a risk that jam conditions form.
- **Low Risk:** If breakup occurs in this zone, severe ice jams have never occurred.

It should be noted that the risk factors are based on consequences (Severity) and historical probability. Figure 5.5 can be used starting March 1st, and both observed and forecasted values can be plotted. If rain equivalence amount exceeds the threshold, then there is a high risk of severe ice jamming when the ice breaks up. If the spring melt is prolonged and the ADDT threshold is exceeded, then that risk is reduced back down to a low risk.

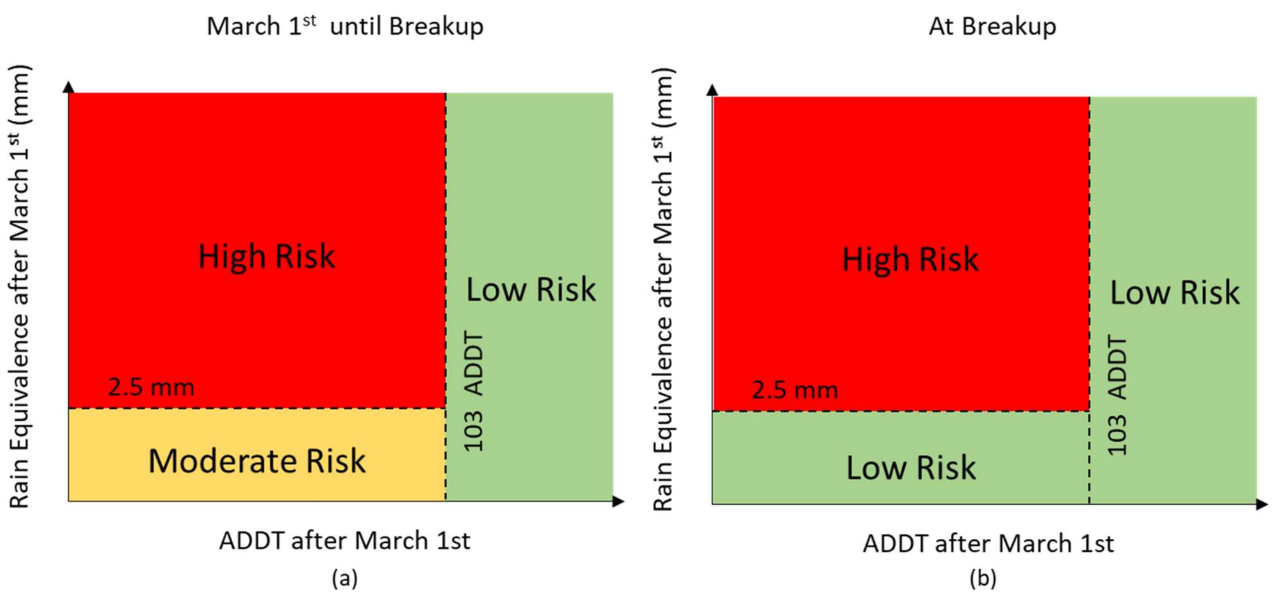

Figure 5.5: (a) Risk zones from March 1st until breakup. (b) Risk zones at breakup.

A drawback to this model is that the risk level is dependent on when breakup occurs. Figure 5.6 shows example data where the current conditions are in the red (high-risk) zone, however they are forecasted to cross into the green (low risk) zone within the 10-day forecast. The date of the spring breakup is now very important but, unfortunately, the spring breakup date is challenging to predict and close monitoring of the river ice and discharge will be crucial. Early indicators of breakup include a rise in the river discharge above stable winter levels; advanced indicators include longitudinal and transverse cracking. The forecasted spring hydrograph can also give insight to breakup timing: breakup occurs, on average, 9 days before the peak spring flow, with a standard deviation of 7.5 days. Therefore, 66% of breakups have historically occurred within a 15-day range (1.5 to 16.5 days before the peak spring flow).

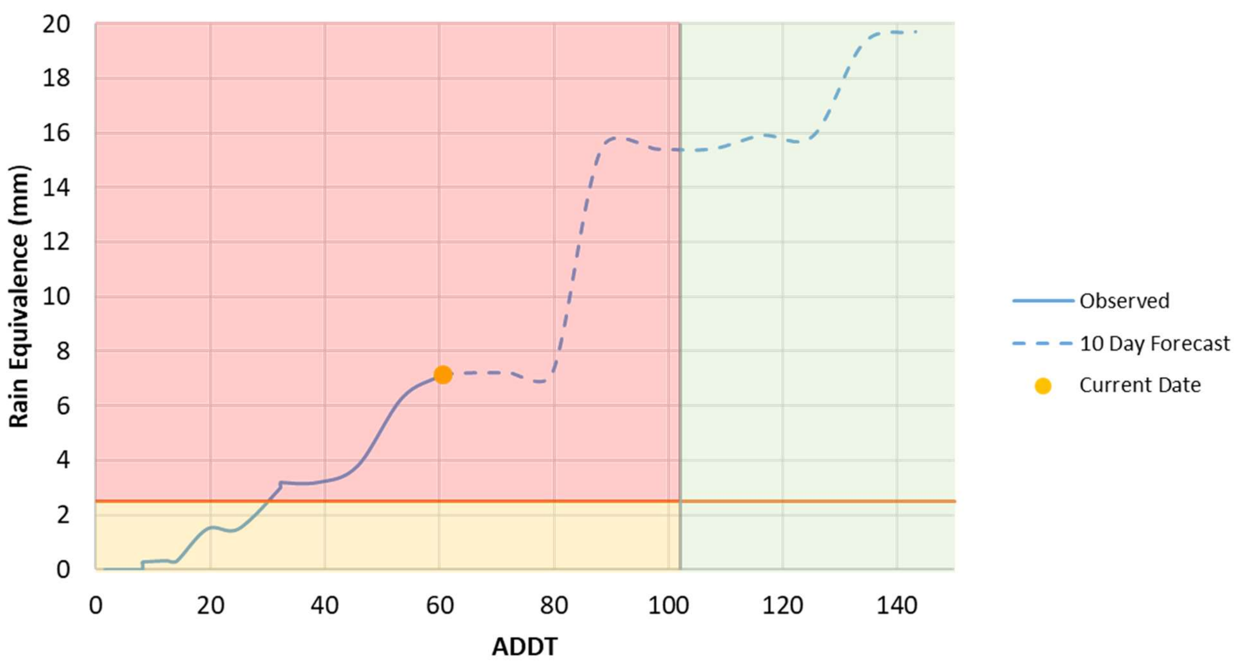

Figure 5.6: Threshold model forecasting tool showing both observed and forecasted conditions.

Due to the nature of threshold models, risk zones and threshold limits are based solely on past events. Future events can change the threshold values, especially with changing climate norms.

The most recent event year to impact the threshold values was 2007, where the freeze-up water level threshold was reduced from 217.4 m to 217.25 m and the ADDT was increased from 97 to 102.7. Another concern is the firm boundary between low risk and high risk. It is possible that one year could see all other threshold criteria met, only to have an ice jam occur at 108 ADDT, in which case the model would have reported this event as low risk (0% historical occurrences). In reality, it could be assumed that the risk more gradually decreases from 100% to 0%, or vice versa. For the above listed reasons, caution should be used when parameters are near the threshold values.

It may also be concerning that, for years where the winter parameters' threshold criteria are not met, the spring forecasting tool cannot be used as it assumes a 0% chance of ice jamming based on historical events. It should be emphasised, however, that the winter threshold has historically only been met 35% of the time, and severe ice jams have never occurred the other 65% of years.

The threshold model's ability to predict severe ice jamming on the Lower Red River performs well when compared to other existing threshold models. Although there are drawbacks and considerations with the model – the biggest being that future events may not fit the criteria developed from past events – some error for this can be mitigated by incorporating a buffer zone around the threshold values. Even with these limitations, the threshold model is a useful tool for severe ice jam forecasting.

5.3.2 Regression Modelling

To examine the efficiency of linear regression in predicting severe ice jams on the Lower Red River, a two-step approach was required. First, linear regression was used to model the peak ice-impacted water level at Selkirk GS, as only this method can be used on continuous data. Second, a logistic regression was used to predict the likelihood of a severe jam based on the water level. Initially a multivariate logistic regression was attempted, which would bypass the first step of this regression analysis, however, suitable results could not be modelled. All regression modelling was done with the assumptions of homoscedasticity, independence, and normality and was completed using RStudio open source software.

Since water level readings are required, only 43 of 56 years could be modelled, with 7 of 10 severe events included. The excluded years are 1974, 1977, 1979-1984, 2002-2003, 2005-2006, and 2008. Two types of linear regression were modelled: a standard linear regression and a power regression (which is identical to standard linear regression except the natural logs of the observed data and model parameter values are used). Modelling was carried out similarly to the ice thickness modelling in Section 4.4 using Equations 4.5 and 4.6. The models were evaluated using the RSE (discussed in Section 4.4) and the adjusted R^2 value. As R^2 increases when multiple variables are used in a regression model, regardless of whether the additional variables are significant, the adjusted R^2 corrects for this inflation using Equation 5.1 (James et al., 2013):

$$Adjusted\ R^2 = 1 - \left[\frac{(1-R^2)(n-1)}{n-k-1}\right] \tag{5.1}$$

Where: R^2 is the coefficient of determination (See Section 4.3);

n is the number of observations; and

k is the number of parameters in the model.

Both regressions were run using winter parameters (i.e. data known by March 1st) and all parameters included peak spring flow, but not every parameter in each set was used. Parameter selection for each regression was based on statistical significance and reducing multicollinearity. In each parameter set, the parameters were checked for statistical significance, and only parameters with a p-value of below 0.1 were actually used in the model. Parameters with p-values above 0.1 are not significant and can decrease the efficiency of the model.

To check for multicollinearity the variance inflation factor – which indicates the amount of multicollinearity in each parameter – was used. Parameters with a variance inflation factor of 5 or more were considered to be problematic and additional steps were taken. For example, highly correlated parameters, such as the breakup flow at Ste. Agathe and Lockport, would have to be analyzed separately. In cases where both parameters met the significance requirement, then the one with the most significance was used.

Results of the model runs can be seen in Table 5.2. The power regression outperforms the linear regression using winter parameters and both preform similarly using all parameters. Even with the better results, the model with all parameters still had significant error. For example the power regression using all parameters had a RSE of 0.81 m. This means, on average, that the observed water levels deviate 0.81 m from the regression line, as seen in Figure 5.7. Again, this is only the average error; Figure 5.8 shows the modelled outcome with 95% confidence intervals and, for many years, the observed values do not fall within the associated confidence intervals.

Table 5.2: Results of the linear and power regression models using both winter parameters and all parameters.

	Linear Regression		Power Regression	
	RSE	Adjusted R^2	RSE	Adjusted R^2
Winter Parameters	1.13 m	0.48	1.00 m	0.65
All Parameters	0.79 m	0.75	0.80 m	0.81

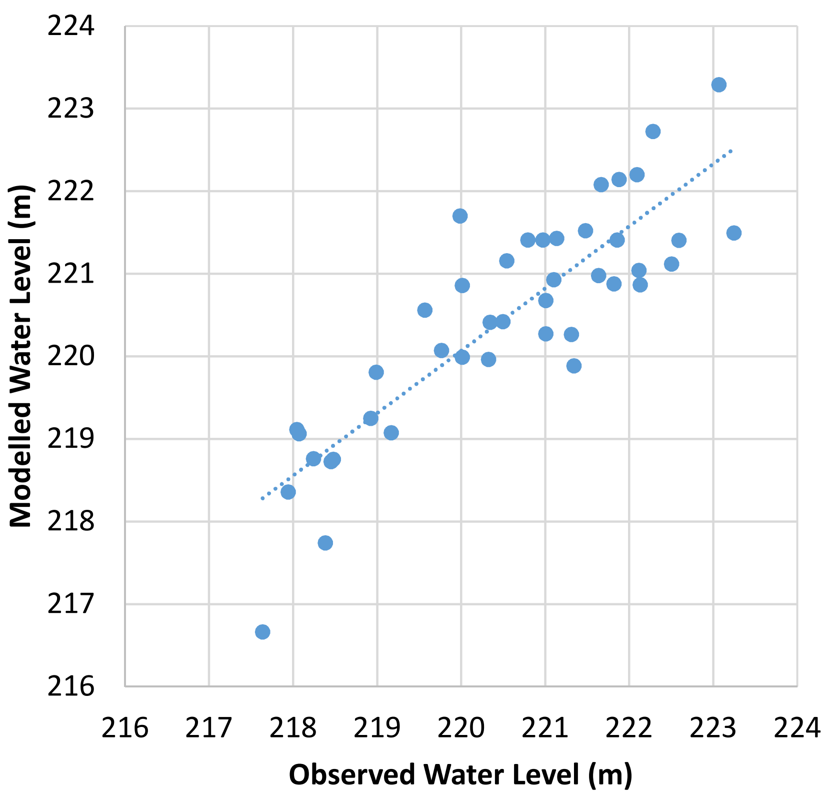

Figure 5.7: Observed and modelled water levels for the Selkirk GS. Water Levels were modelled using a power regression with winter and spring parameters.

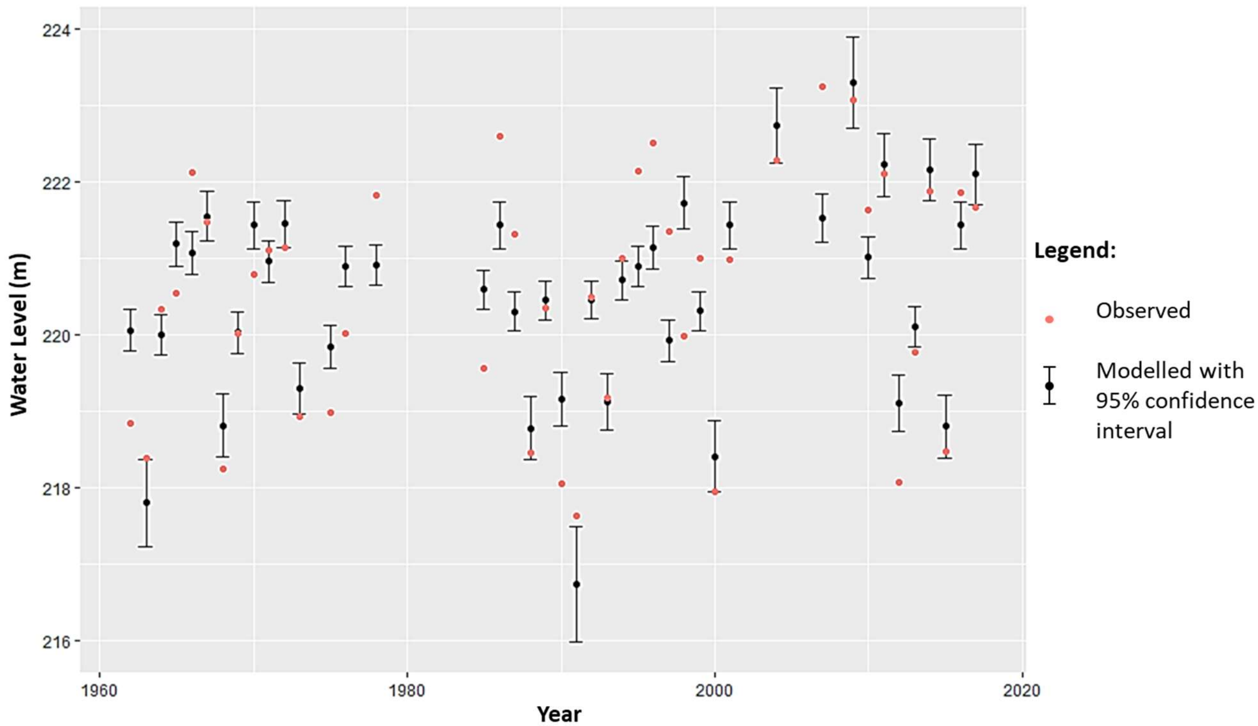

Figure 5.8: Observed and modelled water levels by year for the Selkirk GS. Water Levels were modelled using a power regression with winter and spring parameters.

The second step then requires a logistic regression model, developed from the relationship between the peak ice-impacted Selkirk GS water level and severe ice jams. The logistic regression model then gives the probability of a severe jam based on water level; the model can be seen in Figure 5.9. The 95% confidence interval of the regression is depicted as the dark grey area, and shows more uncertainty for larger water levels. When the error associated with the water level regression model is considered, the 95% confidence intervals become larger. For example, a water level of 222.5 m has a 95% confidence interval that spans from a 0.25 to 0.83 probability, depicted by the purple dots in Figure 5.9. Additionally, if the error from the power regression model is introduced (RSE of 0.81 m), that interval grows to a probability range of 0.10 to 0.97, depicted by the red dots.

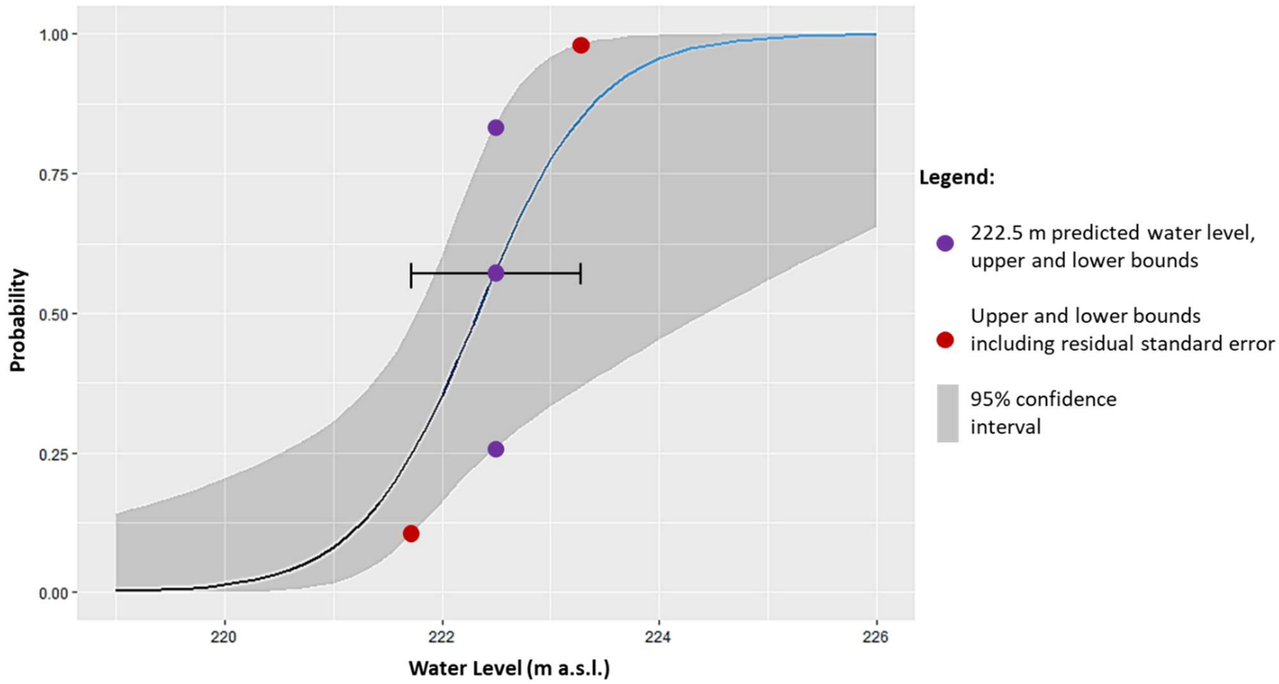

Figure 5.9: Logistic regression model for the probability of a severe jam event occurring based on peak ice-impacted water level at the Selkirk GS.

With the compounding error of needing two separate models to develop a prediction tool, the regression modelling results in more errors than the other two modelling methods, and is not recommended as a predictive tool. Table 5.3 shows the power regression using spring and winter parameters as a confusion matrix. The diagonal green boxes are modelled events that matched observed events. The yellow boxes are false positive results and the red boxes are false negatives. The results show only two severe event correctly identified and five false negatives. The water level regression model could be a useful tool for mitigation measures, such as diking and sandbagging requirements, provided the residual errors are manageable. More work could be done to develop the water level regression model as a predictive tool for this purpose.

Table 5.3: Results of the two-step regression model using the power regression with winter and spring parameters. Green squares represent correctly identified events, yellow squares are false positives, and red squares are false negatives.

	Modelled	
Observed	Non-event	Severe Jam
Non-event	36	0
Severe Jam	5	2

5.3.3 Discriminate Function Analysis

The same parameters that were used in the threshold modelling were used to develop a discriminate function analysis (DFA) model using RStudio open source software. The DFA uses the same assumptions as regression modelling with the addition that all outcomes are mutually exclusive, meaning a year can only be labelled as one type of event (non-event or severe jam) (James et al., 2013). The DFA was performed with 48 events (excluding years 1980-1984, 2002, 2003, and 2005), as years with any missing data could not be used. The DFA was conducted using both linear and quadratic methods to predict whether years would result in a severe jam or non-event; the results are shown in Table 5.4.

Table 5.4: Results of the linear, quadratic with flow, and quadratic without flow for two-outcome DFA models. Green squares represent correctly identified events, yellow squares are false positives, and red squares are false negatives.

DFA Method		**Modelled**		
	Observed	**Non-event**	**Severe Jam**	**% Correct**
Linear DFA	Non-event	36	2	85
	Severe Jam	5	5	
Quadratic DFA - With flow	Non-event	36	2	92
	Severe Jam	2	8	
Quadratic DFA - Without Flow	Non-event	36	2	92
	Severe Jam	2	8	

There is no relevant statistic to measure error for DFA other than the percent correct value, in which the correctly modelled observations are divided by the total observations. When considering the danger and damage associated with severe ice jamming, the amount of false negative predictions are also an important metric, as these can lead to under preparedness to manage these events. The results shown in Table 5.4 indicate that the quadratic method performed better, therefore it is the model of choice and it was developed both with and without peak spring flow. The quadratic model with flow out performed the without flow model.

Focusing on the results of the quadratic DFA with flow, the two years that were incorrectly identified are shown in Table 5.5. The percentages indicate the modelled likelihood that the year results in a non-event or severe jam, with the red boxes showing the predicted incorrect outcome. The results for all years can be seen in Appendix D. The 1995 event shows a 75% chance of a non-event occurring when in fact a severe jam occurred that year. The 1969 event shows an 82% chance of a severe event when there was none. One solution could be to have confidence only in a result with at least an 83% likelihood of occurring, and identify all others as undecided. In this case, 42 of the 48 events would have a confident prediction and six years – including the two years in Table 5.5 – would be undecided. This model (i.e. the DFA model with the best results) does not perform as well as the threshold model, as the threshold model has just one false positive (also 1969) and zero false negatives.

Table 5.5: Incorrectly predicted years for the quadratic DFA model with flow. The red squares indicate the incorrect event.

Year	Non-event	Severe Jam	Observed
1995	75%	25%	Severe Jam
1969	18%	82%	Non-event

DFA was also used to create a three-outcome model where each year could be predicted as a no jam, minor jam (Severity 1-2), or severe jam (Severity 3-5), and results can be seen in Table 5.6. The results show the models did not perform as well as the previous DFA models, which can be expected with additional complexity such as an added outcome. Again, focusing on the results of the quadratic DFA with flow (best result), the three years where a severe jam was improperly identified are shown in Table 5.7.

Table 5.6: Results of the linear, quadratic with flow, and quadratic without flow for three-outcome DFA models. Green squares represent correctly identified events, yellow squares are false positives, and red squares are false negatives.

DFA Method	Observed	Modelled			% Correct
		No Jam	Minor Jam	Severe Jam	
Linear DFA	No Jam	15	6	0	69
	Minor Jam	3	15	2	
	Severe Jam	0	4	5	
Quadratic DFA - With flow	No Jam	15	3	1	83
	Minor Jam	2	17	1	
	Severe Jam	0	1	8	
Quadratic DFA - Without Flow	No Jam	10	8	1	65
	Minor Jam	4	14	2	
	Severe Jam	0	2	7	

Table 5.7: Years with incorrect predictions related to severe jamming for the three-outcome quadratic DFA model with flow. The red squares indicate the predictions of interest.

Year	No Jam	Minor Jam	Severe Jam	Observed
1995	14%	70%	15%	Severe Jam
1990	45%	0%	55%	Minor Jam
1969	3%	31%	66%	Minor Jam

All the years that resulted in either a minor jam or non-event year being misclassified were not included in Table 5.7. Due to how common these events are and the low severity associated with them, these misclassifications are not as concerning. The years 1995 predicted a minor jam when a severe jam occurred. Years 1990 and 1969 were predicted as severe events when only a minor event occurred; both the threshold model and two-outcome DFA also predicted 1969 as a severe event. Labelling results as uncertain below a likelihood threshold, as suggested in the two-outcome model, is not as easily implemented in the three-outcome model. For example, using a 71% likelihood (one more than the largest incorrect value in Table 5.7), would result in 39 of the 48 years being undecided.

The two-outcome DFA models do not perform as well as the threshold model, and provide no additional value. The three-outcome DFA models, although not as accurate as the threshold model, can distinguish minor jams from the non-event years. The false positives and false negatives associated with severe jamming are concerning, however they would have been correctly predicted through the threshold model. Using the three-outcome DFA in a predictive framework alongside the threshold model would result in more reliable severe and minor jam predictions.

Use of the DFA model to predict future outcomes, similar to the threshold model, relies on forecasted values of the peak spring flow, spring precipitation, and ADDT. DFA models, unlike the threshold model, do not allow a user to visually determine how close a parameter is to the threshold values and therefore how sensitive a change in that parameter would be on the predicted outcome. Instead, a sensitivity analysis is needed.

A sensitivity analysis assesses how the uncertainty in the input parameters affects the estimation of the dependant variable, which in this case is the occurrence of ice jamming. There are two types of sensitivity analysis: local and global. Local sensitivity analysis looks at how small changes in an input parameter impacts the dependant variable. A global sensitivity analysis provides a more broad assessment of sensitivity and, in addition to the dependant variable, measures the sensitivity that changes in parameters have on each other (Saltelli & Annoni, 2011).

In this study, a local sensitivity analysis was performed using a one at a time approach where only the impacts from one parameter are assessed during a model run (Saltelli & Annoni, 2011). The quadratic DFA with flow model was used to predict the results when one of the three spring parameters had a 20% change in value and all other values were kept the same. This process was repeated for each of the estimated spring values since these parameters are forecasted, therefore, there is some error associated with the forecasted value. The results of the sensitivity analysis can be seen in Table 5.8. Due to the positive correlation with severe jamming, both peak spring flow and spring rain equivalency were run with a 20% decrease in value, whereas the ADDT was run with a 20% increase. This would insure that the sensitivity analysis was capturing an underestimation in severe jam risk.

Table 5.8: Results of a 20% sensitivity analysis for the quadratic DFA model with peak spring flow.

Sensitivity	Observed	Modelled			% Correct
		No Jam	Minor Jam	Severe Jam	
20% decreases in flow	No Jam	16 (+1)	1 (-2)	2 (+2)	81 (-3)
	Minor Jam	4 (+2)	15 (-2)	1	
	Severe Jam	0	1	8	
20% decrease in spring precipitation	No Jam	16 (+1)	3	0 (-1)	83
	Minor Jam	2	17	1	
	Severe Jam	0	2 (+1)	7 (-1)	
20% increase in ADDT	No Jam	17 (+2)	2 (-1)	0 (-1)	81 (-3)
	Minor Jam	4 (+2)	16 (-1)	0 (-1)	
	Severe Jam	1 (+1)	2 (+1)	6 (-2)	

The sensitivity analysis found that the three forecasted parameters were not very sensitive to a 20% change in value. The most sensitive parameters are the peak spring flow – which is expected since flow is the single most correlated parameter to ice jamming – and ADDT. All parameters saw better results for the no jam prediction, this would be expected as the adjustments made to the parameter values are trying to simulate a underestimation of severe jam risk.

Chapter 6: Conclusion

6.1 Project Summary

To gain a better understanding of ice jamming along the Lower Red River, a database of ice jam events was developed from a historical review of both media sources and water level records. The database included basic spatial and temporal data about each event and a summary of the event. The historical jam events were also given a severity rating from 1-5, based on the resulting flooding that occurred. The severity rating was developed specifically for this study to reflect the types of impacts that ice jam floods cause in this area, such as damage to property and evacuation requirements.

Once the timings of ice jams were collected, meteorological and hydrometric parameter data for both jam and non-jam years could be compared to determine parameter suitability for an ice jam prediction tool. Parameters relating to flow, water level, snow, rain, heat transfer, and temperature were analysed to determine if they correlated to ice jam severity or the peak ice-impacted water level. As expected, individual parameters had little correlation with ice jamming, with the most correlated parameter being flow. The interactions between parameters were also investigated and, generally, severe jams occurred with higher risk values in each parameter category, whereas non-jam years had at least one extremely mild parameter value. Ice thickness models were also developed to estimate late season ice thickness. It was determined, however, that using estimated ice thickness as a parameter would negatively affect the ice jam prediction tool.

Three different ice jam prediction models were examined to determine their suitability for the study area including threshold modelling, regression modelling, and discriminate function analysis. For modelling purposes, ice jam events were grouped together. Ice jams with Severity 1-2 are considered minor jams (these years and no jam years are considered non-events) and Severity 3-5 ice jams are considered severe jams (these years are considered event years). All models were run with the ability to include a predicted spring peak flow value.

6.2 Key Findings

The key findings in this research related to ice jamming trends on the Lower Red River are:

- From 1962-2017, there were 31 years with ice jams and 54 total ice jam events. The most common locations of ice jam events were found to be Sugar Island, Selkirk Bridge, and the Netley Creek Confluence, with at least 10 events at each location.
- All ice jam events classified as severe occurred north of Selkirk, with the highest frequency occurring at the Netley Creek Confluence, which saw five severe events.
- The amount of reported ice jams are increasing, but the number of years with events is staying stable. The increase in reported events can most likely be attributed to the increase in media outlets capturing small events.
- All ice jam events occurred when the peak spring flow exceeded 1000 cms, with the most severe events occurring with peak flows above 1500 cms. When peak flows exceed 1000 cms for a given year it is more likely that an ice jam will occur than not occur.

The key findings in this research related to threshold modelling are:

- Of the models that were assessed in this research, the threshold model is the best tool to predict the occurrence of severe ice jams.

Chapter 5: Ice Jam Modelling

- The developed threshold model uses the threshold criteria listed below, and can correctly hindcast event and non-event years resulting in only one false positive prediction:
    - Freeze-up water level at the Selkirk Generating Station > 217.25 m;
    - Snow on ground on February 1st > 27.9 cm;
    - ADDF on February 15th > 1116.5;
    - Rain equivalence at breakup > 2.55 mm;
    - ADDT at breakup < 103; and
    - Peak spring flow > 1519 cms (optional).
- The developed threshold model can also be used to predict if the upcoming year will result in either a severe event or non-event, following a two-step process:
    - Step one: On February 15th, three of the five parameters can be evaluated; if all three are exceeded, severe ice jamming has occurred 53% of the time and step two can be followed. Additionally, if there is confidence that the peak spring flow will exceed the threshold from the spring forecast, severe ice jams have occurred 71% of the time historically. If any one threshold criterion is not exceeded, then ice jamming has never occurred.
    - Step two: Starting March 1st, observed and forecasted ADDT and rain equivalence can be monitored and, based on the parameter values in relation to the threshold criteria, ice jam risk can be identified as high, moderate, or low.

The key findings in this research related to discriminate function analysis (DFA) are:

- The quadratic DFA with the spring flow provided the best prediction results for both the two-outcome and three-outcome DFA models. Neither the best two-outcome nor three-outcome DFA models performed as well as the threshold model. The three-outcome quadratic DFA resulted in three false negative and five false positives, the two-outcome DFA resulted in one false negatives and one false positive.
- The three-category DFA was not as accurate as the two-outcome DFA, but the three-outcome DFA provides the additional benefit of being able to distinguish between minor jam and no jam years. For predicting ice jams, this study recommends using the three-outcome DFA alongside the threshold model, as the threshold model is more robust in terms of predicting severe jams, while the DFA provides insight to minor jam formation.

The key findings in this research related to regression modelling are:

- The power regression model was not as effective as the threshold model or DFA in predicting ice jamming. Using winter parameters (known by March 1st) the regression results in the identification of only two of seven incorporated severe events.
- Although regression modelling is not recommended for use in ice jam prediction, it provides a means to estimate peak spring water level. Modelled peak spring water levels using winter parameters resulted a RSE of 0.79 m and an adjusted R-squared value of 0.75. This could be a useful tool for mitigation measures, such as diking and sandbagging requirements, provided the residual error is manageable.

6.3 Limitations and Future Work

Due to the large study area and only one consistent location of recorded water level, this study uses an ice jam severity rating instead of the peak ice-impacted spring water level, to determine ice jam severity. A limitation to this approach is that the severity is dependent on development in the area; as development increases (or decreases), ice-impacted water levels may have more (or less) severe impacts. The addition of the Breezy Point station in 2000 gives the opportunity to divide the study area into two reaches, each with a water level gauge, once that water level record is sufficiently long enough. Since a majority of jams occur in close proximity to either the Selkirk Generating Station or the Breezy Point Station, it could be possible to use the water level alone to determine the severity of the ice jams at either location.

A drawback to using the threshold model as a predictive tool is that the risk level depends on when breakup occurs. The spring breakup date is challenging to predict, and close monitoring of river ice and discharge is critical. As the timing of the spring hydrograph can be forecasted, this study did a preliminary analysis on when breakup occurs in relation to peak spring flow. This resulted in identifying a 15-day window where 66% of the breakups have historically occurred. It is recommended that further study be done to better understand the timing of breakup on the Lower Red River, which can enhance the use of the threshold model as a prediction tool.

Due to the nature of threshold modelling, the threshold criteria are based solely off past events and, therefore, threshold criteria can change with future events. Thus, having firm criteria limits can be problematic – risk would likely change more gradually from 0% to 100 – as it is unlikely that the criteria would change considerably. A buffer zone for each threshold could be implemented, where the zone would include the values that are just shy of meeting the threshold for a severe jam, and values in the buffer would be considered as meeting the threshold. The trade-off would be an increase in false positive predictions and some consideration is needed regarding what a suitable buffer would be.

With only 56 years of data – less depending on the modelling method – each additional year of data can give more insight to ice jamming trends in the study area. New ice jam events as previously discussed may slightly change the threshold criteria or introduce extreme parameter values not before seen. Continuing to develop the ice jam database with new events as well as updating each model with yearly parameter values will allow for the continued confidence in these prediction tools.

References

Acres. (2004). *Manitoba Floodway Expansion Authority—Floodway Expansion Project—Project Definition and Environmental Assessment, Preliminary Engineering Report Appendix L: Environmental Baseline Studies—Water Regime Effects, Final Report,*. Winnipeg.

Ashton, G. (1986). *River and Lake Ice Engineering*. Highlands Ranch, Colorado: Water Resources Publications.

Beltaos (Ed.). (2008). *River Ice Breakup*. Water Resource Publications, LLC.

Beltaos, S, Gerard, R., Petryk, S., & Prowse, T. D. (1990). Working group on river ice jams. *Field Studies and Research Needs. National Hydrology Research Institute Science Report*, *2*, 35–42.

Beltaos, Spros. (2008). *River ice breakup*. Water Resources Publications, LLC.

Bilello, M. A. (1980). *Maximum thickness and subsequent decay of lake , river and fast sea ice in Canada and Alaska*. https://doi.org/Report 80-6

Bulatov, S. N. (1970). Calculating the strength of thawing ice cover and the beginning of wind activated ice drift, Trudy Vypysk, 74, Gidrometeorologisheskoye Izdatei'stvo, Leningrad. *Translation by US Army CRREL, IR*, *799*, 120.

Carr, M. L., Gaughan, S. P., George, C. R., & Mason, J. G. (2015). *CRREL ' s Ice Jam Database : Improvements and Updates*.

de Rham, L., Dibike, Y., Prowse, T., & Beltaos, S. (2019). Overview of a Canadian River Ice Database Derived from Water Survey of Canada Hydrometric Archives. *Proceedings of the 20th*

Workshop on the Hydraulics of Ice Covered Rivers, (1990), 19.

Driedger, H. L. (1969). *An analysis of the relationship between total daily solar radiation receipt and total daily duration of sunshine at Winnipeg, 1950 to 1967*. University of Manitoba.

Galbraith, P. W. (1981). *On estimating the likelihood of ice jams on the Saint John River using meteorological parameters*. Atmospheric Environment Service.

Government of Manitoba. (2015). *Flood Fighting in Manitoba A History*. Retrieved from https://www.gov.mb.ca/asset_library/en/spring_outlook/flood_fighting_2015.pdf

Gray, D. M. (1970). *Handbook on the Principles of Hydrology: with special emphasis directed to Canadian conditions in the discussions, applications and presentation of data*. Secretariat, Canadian National Committee for the International Hydrological ….

Hicks, F. (2016). *An Introduction to River Ice Engineering: For Civil Engineers and Geoscientists*. CreateSpace Independent Publishing Platform.

Hicks, F., Chen, X., & Andres, D. (1995). Effects of ice on the hydraulics of Mackenzie River at the outlet of Great Slave Lake, NWT: a case study. *Canadian Journal of Civil Engineering*, *22*(1), 43–54.

Hicks, F. E., Cui, W., & Andres, D. D. (1995). *Forecasting breakup on the Mackenzie River at the Ft. Providence Ferry Crossing* (Water Reso). Depatment of Civil Engineer, University of Alberta.

Hoye, B. (2019, March 30). Manitoba Amphibex program ' had to write the book ' on odd art of ice-breaking. *CBC*, pp. 1–11. Retrieved from https://www.cbc.ca/news/canada/manitoba/amphibex-ice-breaker-manitoba-flood-1.5072933

IJC. (1997). *Red River flooding: Short term measures*. Interim report of the International Red River Basin Task Force to the ….

James, G., Witten, D., Hastie, T., & Tibshirani, R. (2013). *An Introduction to Statistical Learning with Applications in R*. https://doi.org/10.1007/978-1-4614-7138-7_8

KGS, Acres, & UMA. (2004). *Manitoba Floodway Expansion Authority—Floodway Expansion Project—Project Definition and Environmental Assessment, Preliminary Engineering Report*.

Kowal, P. (2019). *A historical analysis of the changes in connectivity and plant cover in Netley-Libau Marsh, Manitoba, Canada: Distinguishing the effects of Lake Winnipeg and Red River hydrology on coastal marsh emergent macrophyte areal extent*. University of Manitoba.

Lindenschmidt, K. E. (2012). Ice Jam Modelling of the Lower Red River. *Journal of Water Resource and Protection*, *04*(01), 1–11. https://doi.org/10.4236/jwarp.2012.41001

Lindenschmidt, K., Syrenne, G., & Harrison, R. (2010). *Measuring Ice Thicknesses along the Red River in Canada Using RADARSAT-2 Satellite Imagery*. *2010*(August), 923–933. https://doi.org/10.4236/jwarp.2010.211110

Mahabir, C., Hicks, F. E., & Fayek, A. R. (2007). Transferability of a neuro-fuzzy river ice jam flood forecasting model. *Cold Regions Science and Technology*, *48*(3), 188–201. https://doi.org/10.1016/j.coldregions.2006.12.004

Mahabir, C., Hicks, F. E., Robichaud, C., & Fayek, A. R. (2006). Forecasting breakup water levels at

Fort McMurray, Alberta, using multiple linear regression. *Canadian Journal of Civil Engineering*, *33*(9), 1227–1238. https://doi.org/10.1139/L06-067

Michel, B. (1971). *Winter Regime of rivers and lakes*. https://doi.org/Monograpg III-B1a

Northwest Hydraulics. (2005). *Evaluation of the Effects of the Expansion of the Winnipeg Floodway on Ice-related Water Levels Downstream of Floodway Outlet.pdf*.

Rannie, W. (2016). The 1997 flood event in the Red River Basin : Causes , assessment and damages. *Canadian Water Resources Journal / Revue Canadienne Des Ressources Hydriques*, *41*(1–2), 65–73. https://doi.org/10.1080/07011784.2015.1008048

Saltelli, A., & Annoni, P. (2011). Sensitivity Analysis. In M. Lovric (Ed.), *International Encyclopedia of Statistical Science* (pp. 1298–1301). https://doi.org/10.1007/978-3-642-04898-2_509

Schroeder, A. J., Gourley, J. J., Hardy, J., Henderson, J. J., Parhi, P., Rahmani, V., … Taraldsen, M. J. (2016). The development of a flash flood severity index. *Journal of Hydrology*, *541*, 523–532. https://doi.org/10.1016/j.jhydrol.2016.04.005

Shaw, J. K. E., Lavender, S. T., Stephen, D., & Jamieson, K. (2013). Ice Jam Flood Risk Forecasting at the Kashechewan FN Community on the North Albany River. *17th Workshop on River Ice - CGU HS Committee on River Ice Processes and the Environment*. Retrieved from http://cripe.ca/docs/proceedings/17/Shaw-et-al-2013.pdf

Shuliakovskii, L. G. (Editor). (1963). *Manual for forcasting iceformation for rivers and inland lake*.

Wazney, L., & Clark, S. P. (2016). The 2009 flood event in the Red River Basin: Causes, assessment and damages. *Canadian Water Resources Journal*, *41*(1–2), 56–64.

https://doi.org/10.1080/07011784.2015.1009949

White, K. D. (1996a). A NEW ICE JAM DATABASE. *JAWRA Journal of the American Water Resources Association*, *32*(2), 341–348.

White, K. D. (1996b). Predicting breakup ice jams using logistic regression. *Journal of Cold Regions Engineering*, *10*(4), 178–189.

White, K. D. (2003). *Review of prediction methods for breakup ice jams*. *100*, 89–100. https://doi.org/10.1139/L02-047

White, K. D., & Daly, S. F. (2002). Predicting ice jams with discriminant function analysis. *ASME 2002 21st International Conference on Offshore Mechanics and Arctic Engineering*, 683–690. American Society of Mechanical Engineers.

Wuebben, J. L., Gagnon, J. J., & Deck, D. S. (1995). Ice jamming near the confluence of the Missouri and Yellowstone Rivers: characterization and mitigation. *USA CRREL Report SR*, *95*, 19.

Zachrisson, G. (1990). Severe break-ups in the River Tornealven: measures to mitigate damages from ice jamming. *Proceedings International Association of Hydraulic Research Ice Symposium (August 20–23) Espoo, Finland*, *2*, 845–857.

Appendix A: Ice Jam Database for the Lower Red River

Table A.1: Ice Jam Database for the Lower Red River.

Year	Start Date	End Date	Location	UTM East	UTM North	Severity
2017	31-Mar	03-Apr	Netley Creek Confluence	652212.17 m E	5573464.11 m N	1
2017	30-Mar	31-Mar	Sugar Island	653114.00 m E	5558834.00 m N	2
2016	21-Mar	24-Mar	McIvor Lane	654632.50 m E	5565507.09 m N	1
2016	19-Mar	20-Mar	Sugar Island	653114.00 m E	5558834.00 m N	2
2014	23-Apr	23-Apr	Netley Creek Confluence	652212.17 m E	5573464.11 m N	3
2014	22-Apr	23-Apr	McIvor Lane	654632.50 m E	5565507.09 m N	1
2014	21-Apr	22-Apr	Father Turney Road	653963.34 m E	5561030.34 m N	2
2014	18-Apr	20-Apr	St. Clement Drive	650676.94 m E	5554549.11 m N	1
2011	09-Apr	11-Apr	Netley Creek Confluence	652212.17 m E	5573464.11 m N	3
2011	07-Apr	09-Apr	McIvor Lane	654632.50 m E	5565507.09 m N	3
2011	05-Apr	07-Apr	Selkirk Bridge	652239.64 m E	5556513.03 m N	1
2010	29-Mar	29-Mar	Netley Creek Confluence	652212.17 m E	5573464.11 m N	2

Appendix B: Yearly Hydrographs at the Selkirk Generating Station

2010	24-Mar	24-Mar	Sugar Island	653114.00 m E	5558834.00 m N	2
2009	12-Apr	13-Apr	Breezy point	653390.00 m E	5570837.00 m N	5
2009	11-Apr	12-Apr	Sugar Island	653114.00 m E	5558834.00 m N	2
2009	06-Apr	10-Apr	South of Selkirk Generating	653187.00mE	5554983.00mN	2
2009	27-Mar	03-Apr	Lower Fort Garry	648039.00 m E	5553053.00 m N	1
2007	04-Apr	11-Apr	PTH 4 Bridge	653991.74 m E	5562031.38 m N	3
2007	31-Mar	01-Apr	Sugar Island	653114.00 m E	5558834.00 m N	2
2005	05-Apr	05-Apr	Breezy point	653390.00 m E	5570837.00 m N	3
2005	04-Apr	05-Apr	Sugar Island	653114.00 m E	5558834.00 m N	2
2004	03-Apr	04-Apr	Netley Creek Confluence	652212.17 m E	5573464.11 m N	4
2004	02-Apr	03-Apr	McIvor Lane	654632.50 m E	5565507.09 m N	3
2004	02-Apr	02-Apr	PTH 4 Bridge	653991.74 m E	5562031.38 m N	2
2004	31-Mar	02-Apr	Selkirk Bridge	652239.64 m E	5556513.03 m N	2
2001	09-Apr	11-Apr	Netley Creek Confluence	652212.17 m E	5573464.11 m N	2
1999	02-Apr	06-Apr	Netley Creek Confluence	652212.17 m E	5573464.11 m N	2

Appendix B: Yearly Hydrographs at the Selkirk Generating Station

1998	29-Mar	30-Mar	Selkirk Bridge	652239.64 m E	5556513.03 m N	1
1996	20-Apr	21-Apr	Netley Creek Confluence	652212.17 m E	5573464.11 m N	4
1996	19-Apr	19-Apr	PTH 4 Bridge	653991.74 m E	5562031.38 m N	2
1996	18-Apr	18-Apr	Selkirk Bridge	652239.64 m E	5556513.03 m N	2
1996	18-Apr	19-Apr	Sugar Island	653114.00 m E	5558834.00 m N	3
1995	26-Mar	31-Mar	Breezy point	653390.00 m E	5570837.00 m N	4
1994	09-Apr	10-Apr	Selkirk Bridge (assumed)	652239.64 m E	5556513.03 m N	1
1992	03-Apr	04-Apr	Selkirk Bridge (assumed)	652239.64 m E	5556513.03 m N	1
1989	19-Apr	22-Apr	Selkirk Bridge (assumed)	652239.64 m E	5556513.03 m N	1
1987	06-Apr	08-Apr	Sugar Island	653114.00 m E	5558834.00 m N	2
1986	02-Apr	03-Apr	Netley Creek Confluence	652212.17 m E	5573464.11 m N	2
1986	31-Mar	02-Apr	Selkirk Bridge	652239.64 m E	5556513.03 m N	2
1984	07-Apr	08-Apr	Selkirk Bridge (assumed)	652239.64 m E	5556513.03 m N	1
1978	11-Apr	11-Apr	Sugar Island	653114.00 m E	5558834.00 m N	2
1976	06-Apr	09-Apr	Selkirk Bridge	652239.64 m E	5556513.03 m N	1

Appendix B: Yearly Hydrographs at the Selkirk Generating Station

1974	21-Apr		Netley Creek Confluence	652212.17 m E	5573464.11 m N	3
1972	15-Apr	16-Apr	Sugar Island	653114.00 m E	5558834.00 m N	2
1971	11-Apr	13-Apr	Sugar Island	653114.00 m E	5558834.00 m N	2
1970	17-Apr	19-Apr	Selkirk Bridge	652239.64 m E	5556513.03 m N	1
1969	13-Apr	13-Apr	McIvor Lane	654632.50 m E	5565507.09 m N	2
1969	12-Apr	12-Apr	Sugar Island	653114.00 m E	5558834.00 m N	1
1967	11-Apr	11-Apr	Father Turney Road	653963.34 m E	5561030.34 m N	2
1967	11-Apr	14-Apr	McIvor Lane	654632.50 m E	5565507.09 m N	3
1967	08-Apr	11-Apr	Selkirk Bridge	652239.64 m E	5556513.03 m N	2
1966	08-Apr	09-Apr	McIvor Lane	654632.50 m E	5565507.09 m N	2
1965	14-Apr	15-Apr	Sugar Island	653114.00 m E	5558834.00 m N	2
1964	16-Apr	18-Apr	PTH 4 Bridge location	654721.78 m E	5563153.67 m N	2

Appendix B: Yearly Hydrographs at Selkirk Generating Station

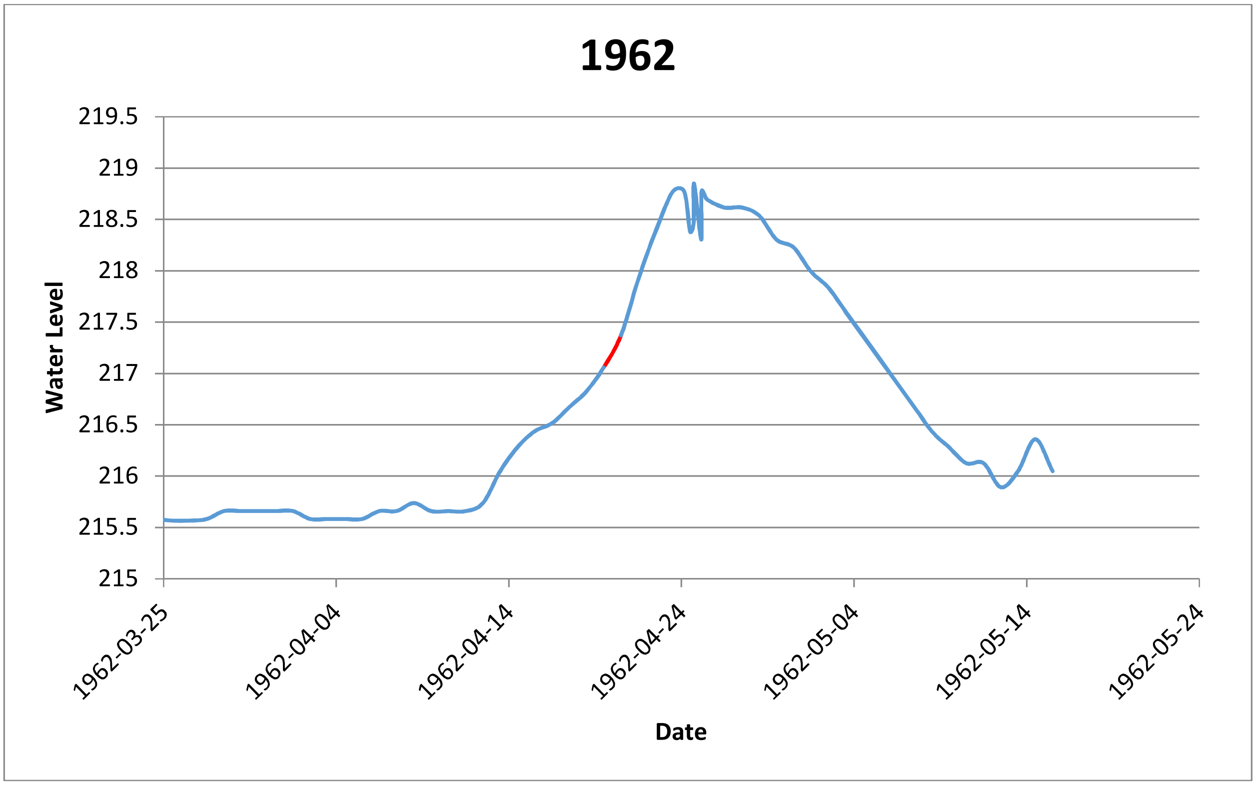

Figure B.1: Spring hydrograph for the Selkirk Generating Station in 1962.The red section of the line is the assumed time of breakup.

Appendix B: Yearly Hydrographs at the Selkirk Generating Station

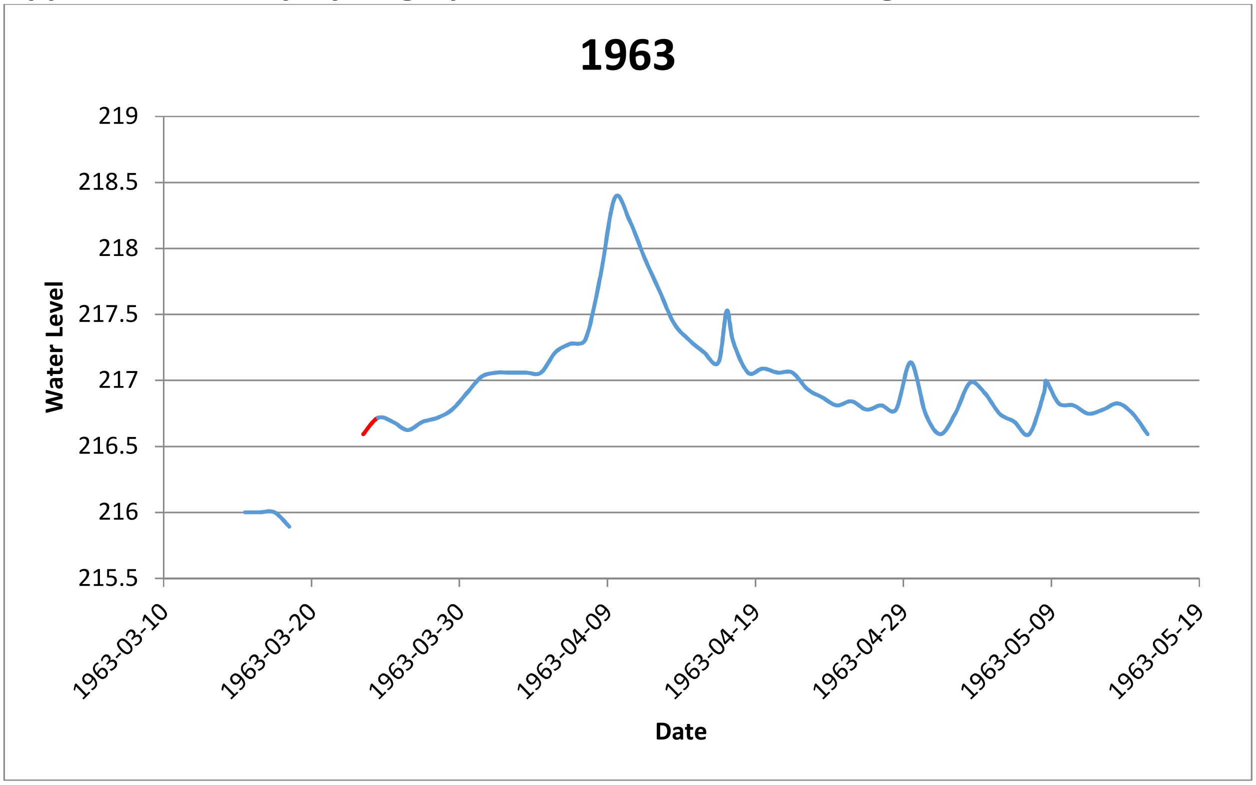

Figure B.2: Spring hydrograph for the Selkirk Generating Station in 1963. The red section of the line is the assumed time of breakup.

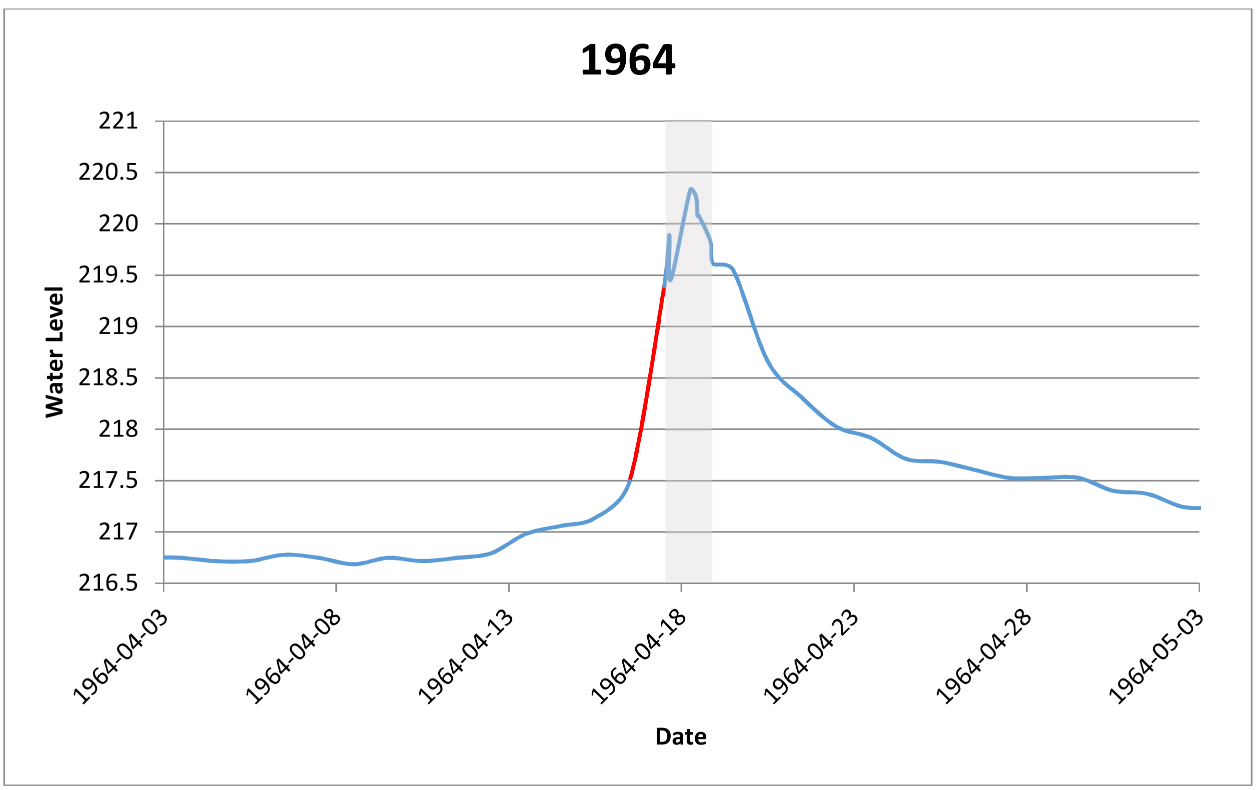

Figure B.3: Spring hydrograph for the Selkirk Generating Station in 1964. The red section of the line is the assumed time of breakup. The grey section of the graph indicates when an ice jam occurred.

Appendix B: Yearly Hydrographs at the Selkirk Generating Station

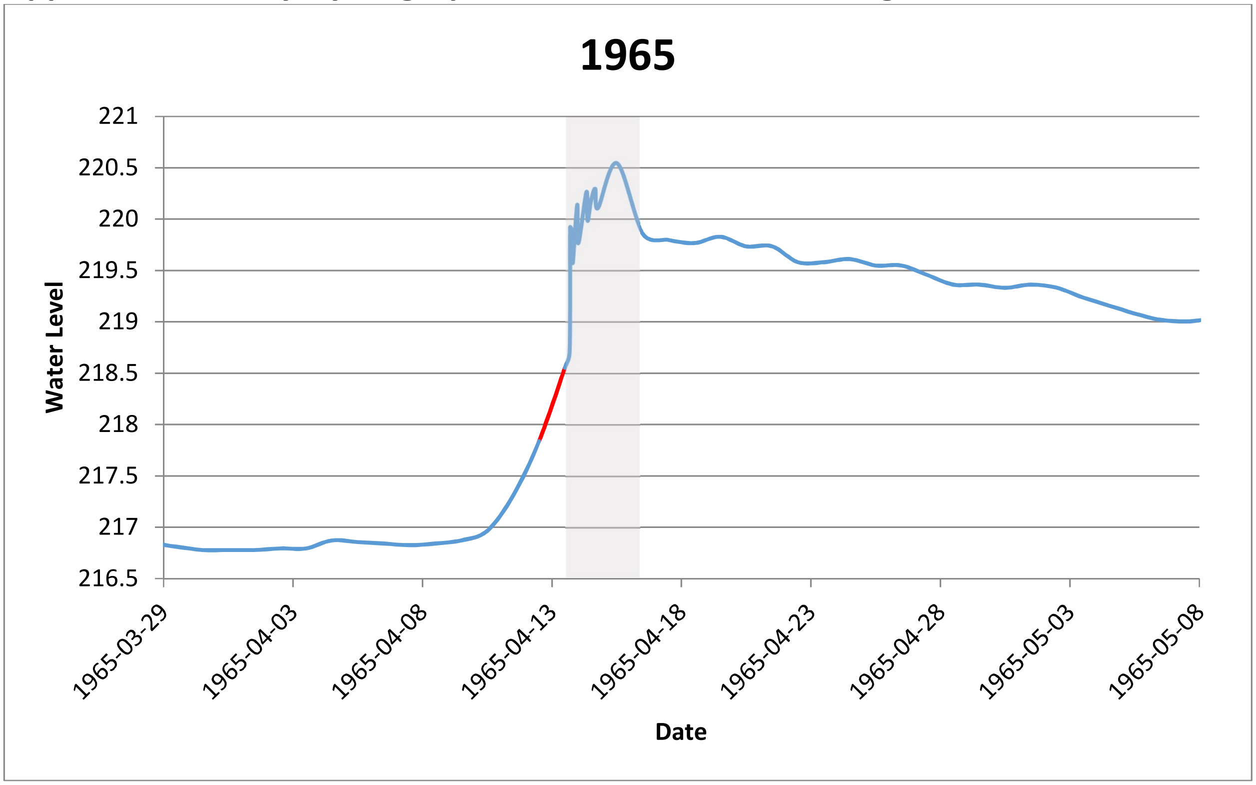

Figure B.4: Spring hydrograph for the Selkirk Generating Station in 1965. The red section of the line is the assumed time of breakup. The grey section of the graph indicates when an ice jam occurred.

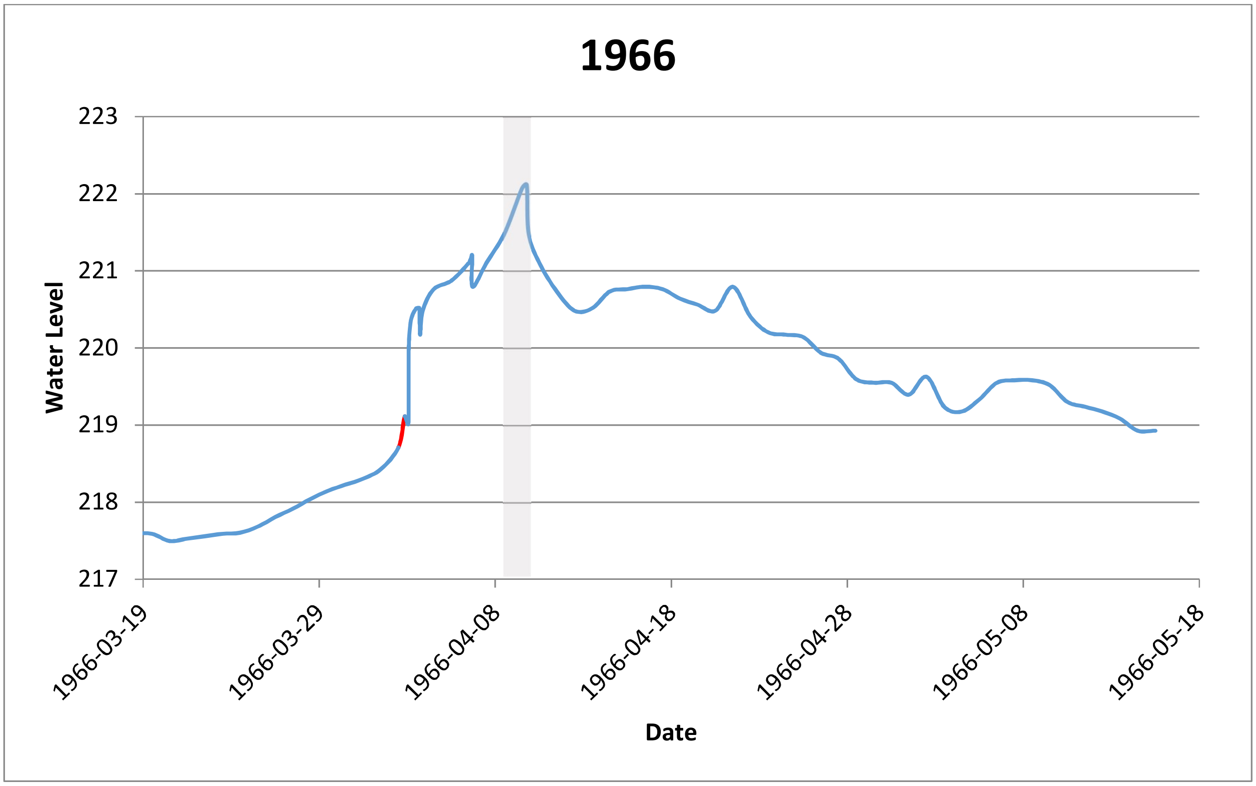

Figure B.5: Spring hydrograph for the Selkirk Generating Station in 1966. The red section of the line is the assumed time of breakup. The grey section of the graph indicates when an ice jam occurred.

Appendix B: Yearly Hydrographs at the Selkirk Generating Station

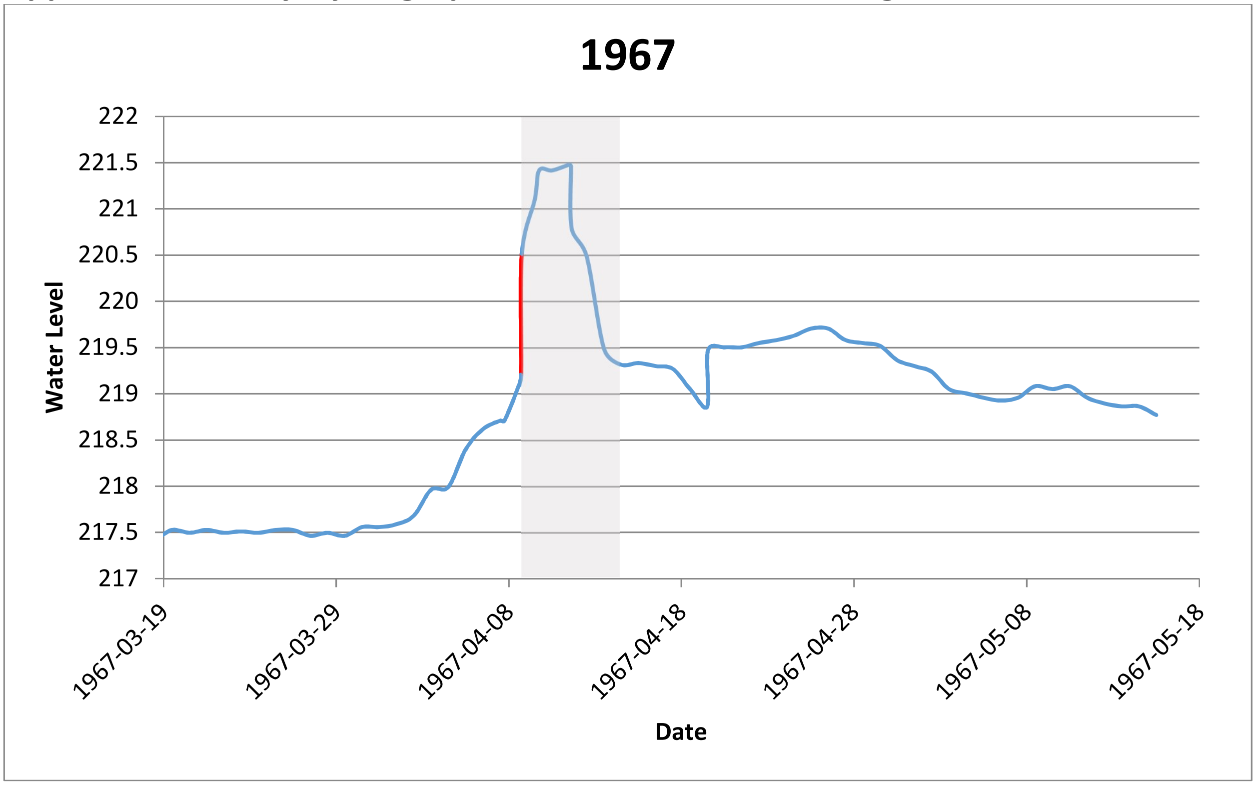

Figure B.6: Spring hydrograph for the Selkirk Generating Station in 1967. The red section of the line is the assumed time of breakup. The grey section of the graph indicates when an ice jam occurred.

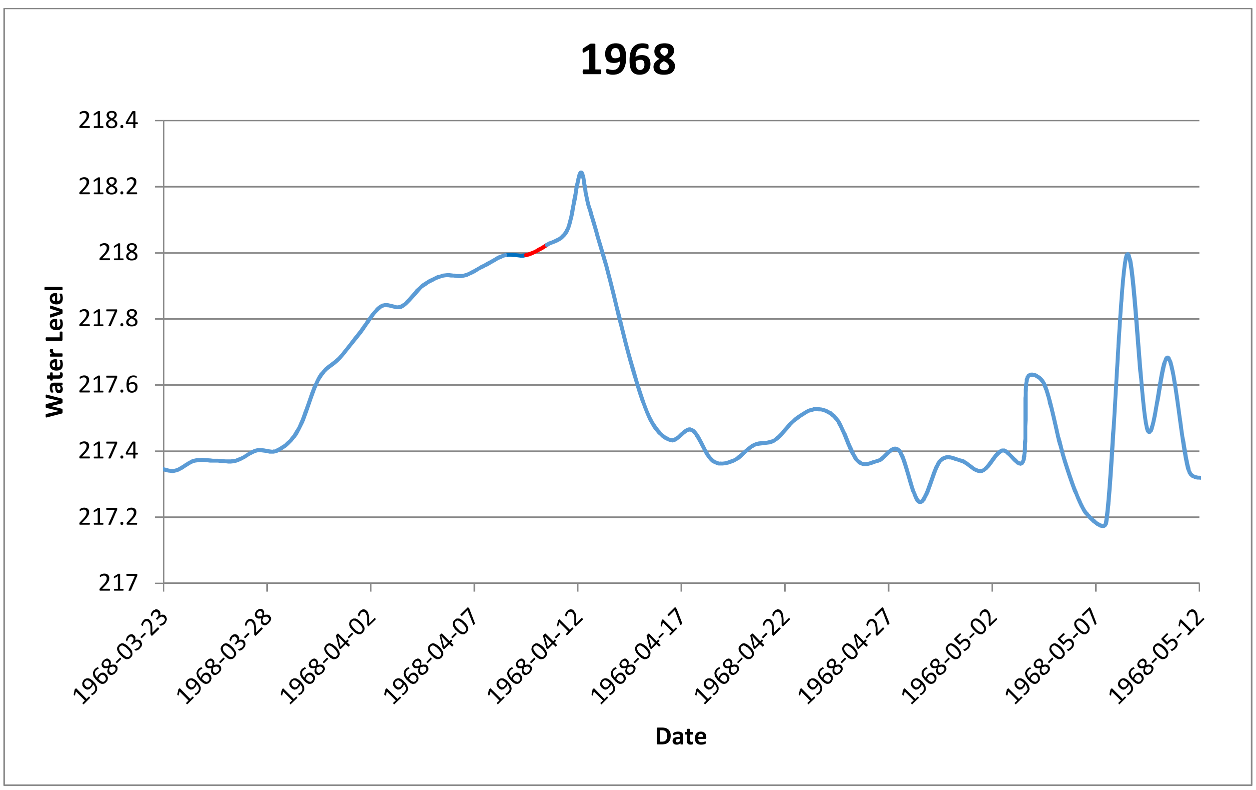

Figure B.7: Spring hydrograph for the Selkirk Generating Station in 1968.The red section of the line is the assumed time of breakup.

Appendix B: Yearly Hydrographs at the Selkirk Generating Station

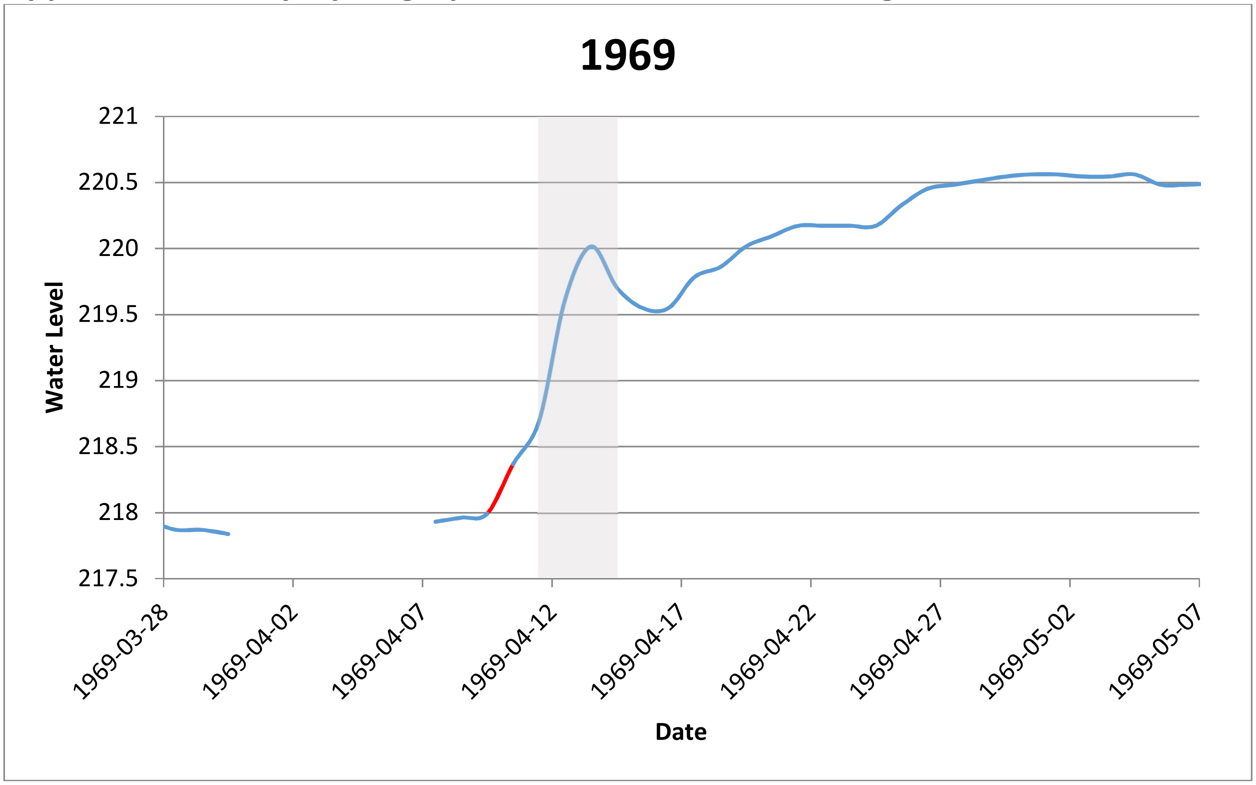

Figure B.8: Spring hydrograph for the Selkirk Generating Station in 1969.The red section of the line is the assumed time of breakup. The grey section of the graph indicates when an ice jam occurred.

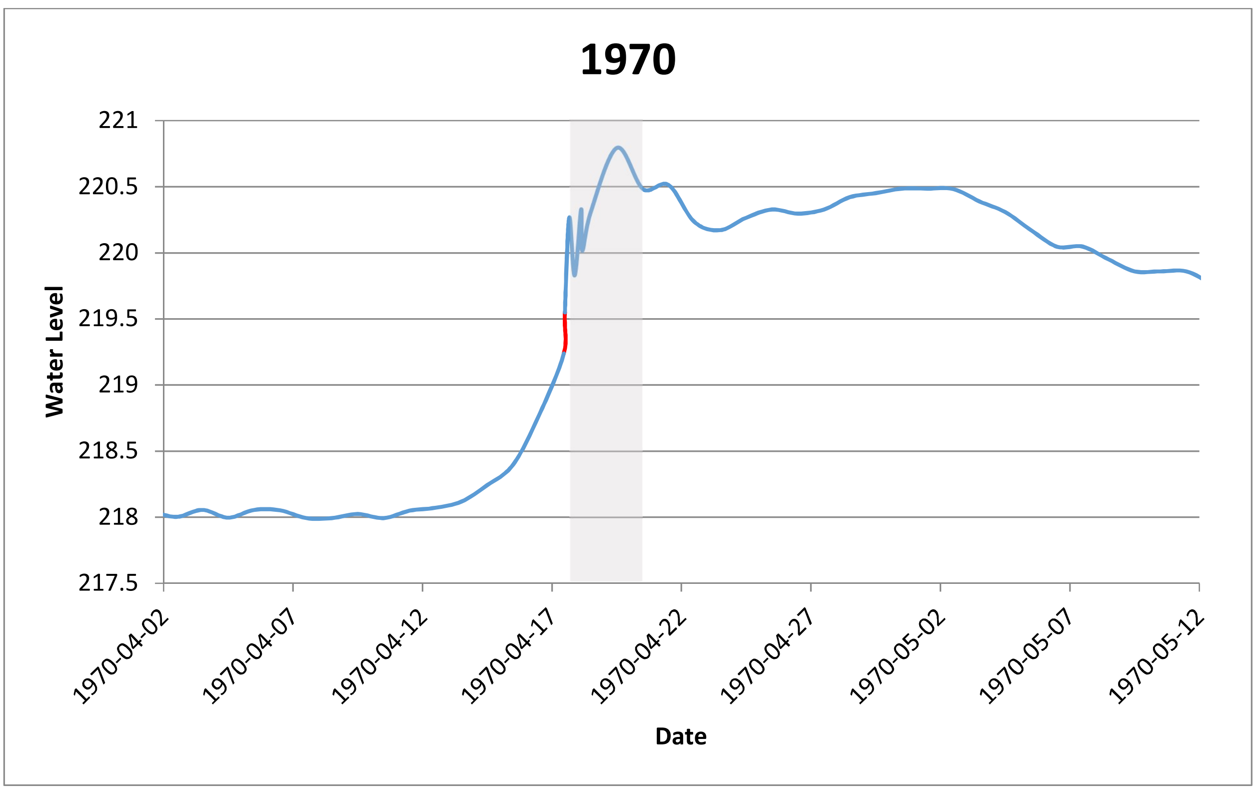

Figure B.9: Spring hydrograph for the Selkirk Generating Station in 1970.The red section of the line is the assumed time of breakup. The grey section of the graph indicates when an ice jam occurred.

Appendix B: Yearly Hydrographs at the Selkirk Generating Station

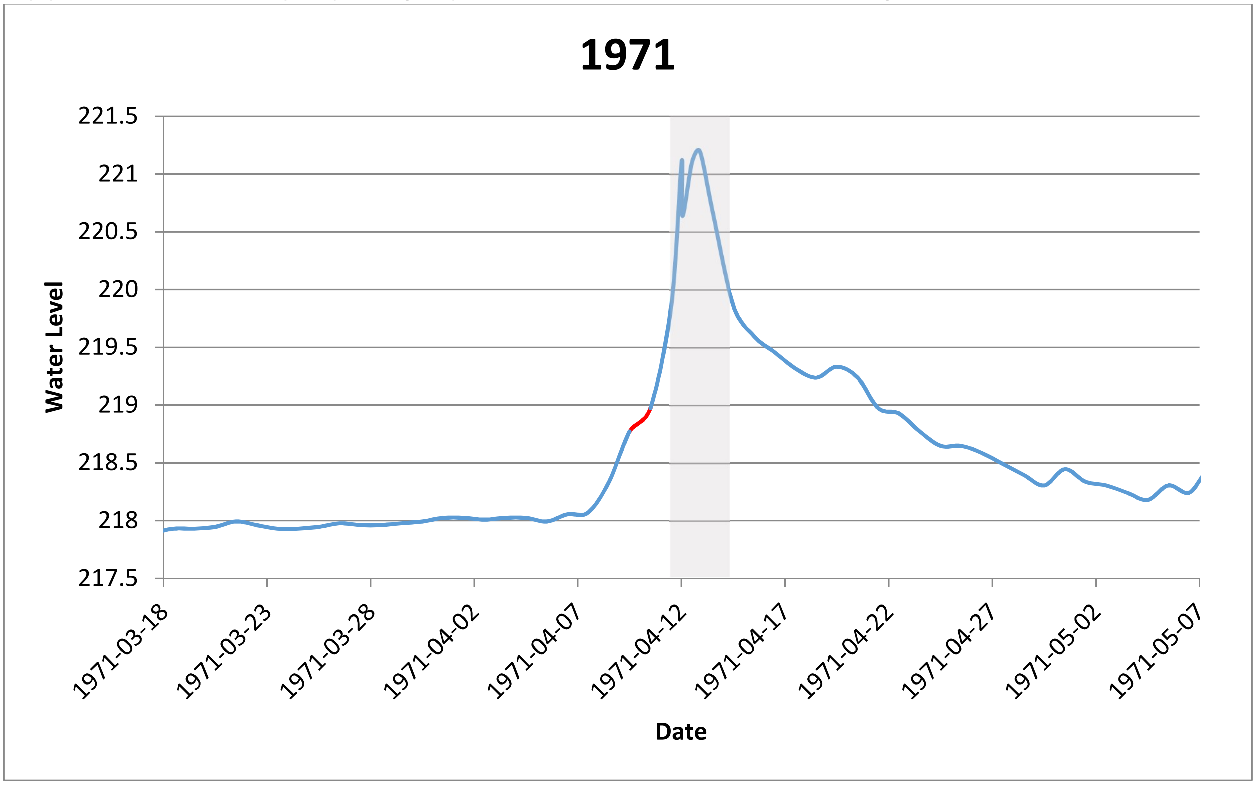

Figure B.10: Spring hydrograph for the Selkirk Generating Station in 1971.The red section of the line is the assumed time of breakup. The grey section of the graph indicates when an ice jam occurred.

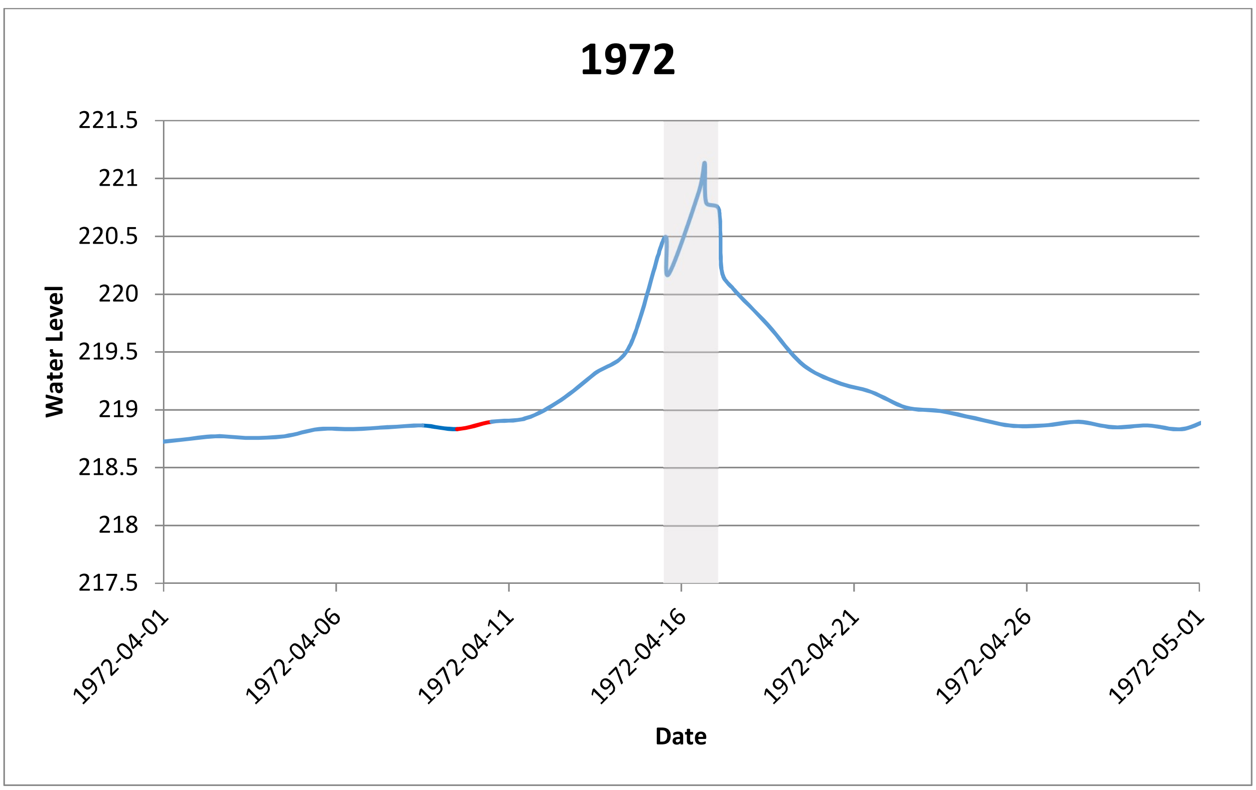

Figure B.11: Spring hydrograph for the Selkirk Generating Station in 1972.The red section of the line is the assumed time of breakup. The grey section of the graph indicates when an ice jam occurred.

Appendix B: Yearly Hydrographs at the Selkirk Generating Station

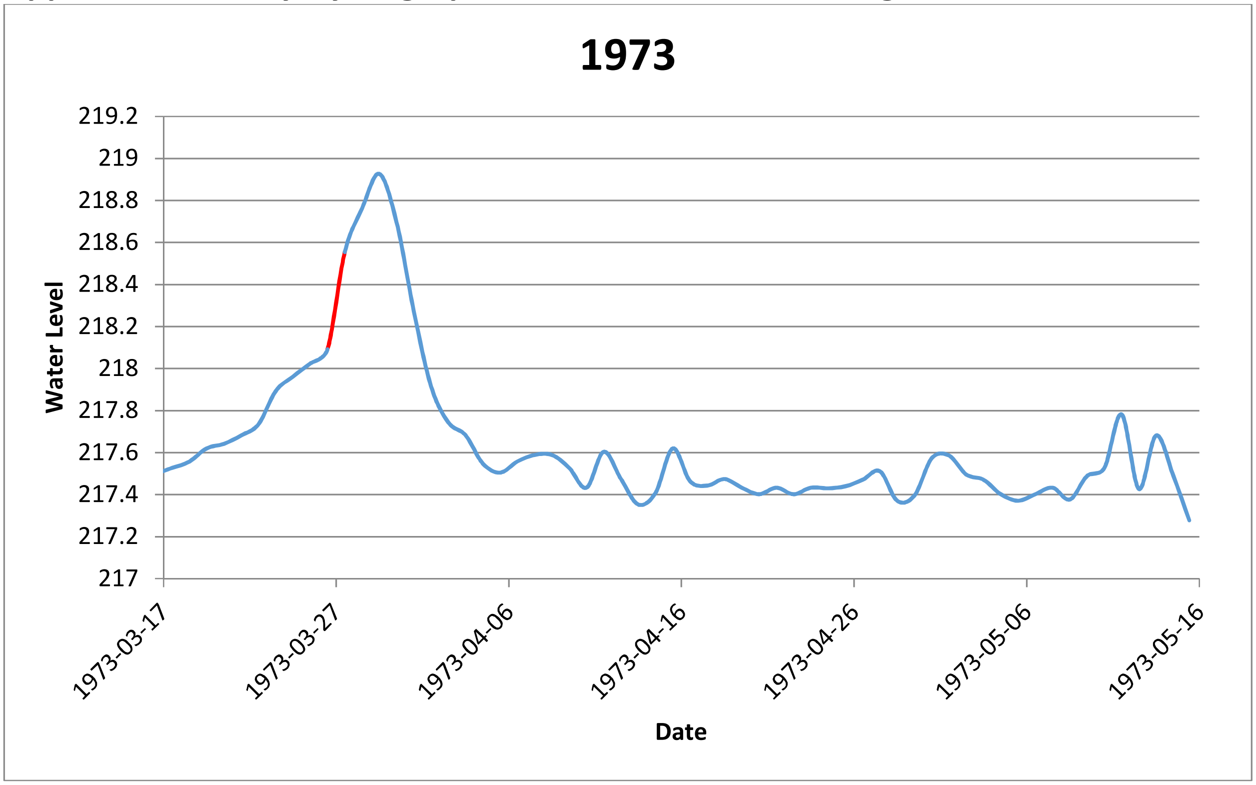

Figure B.12: Spring hydrograph for the Selkirk Generating Station in 1973.The red section of the line is the assumed time of breakup.

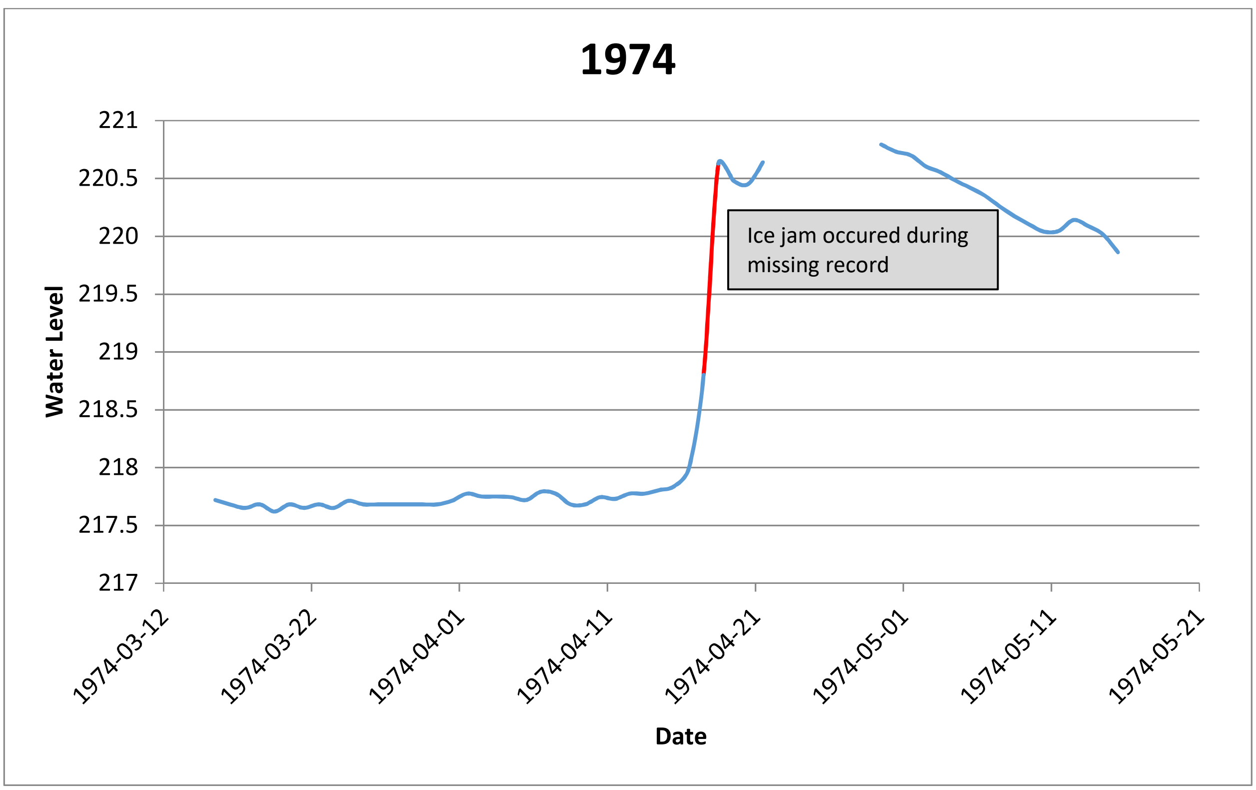

Figure B.13: Spring hydrograph for the Selkirk Generating Station in 1974.The red section of the line is the assumed time of breakup.

Appendix B: Yearly Hydrographs at the Selkirk Generating Station

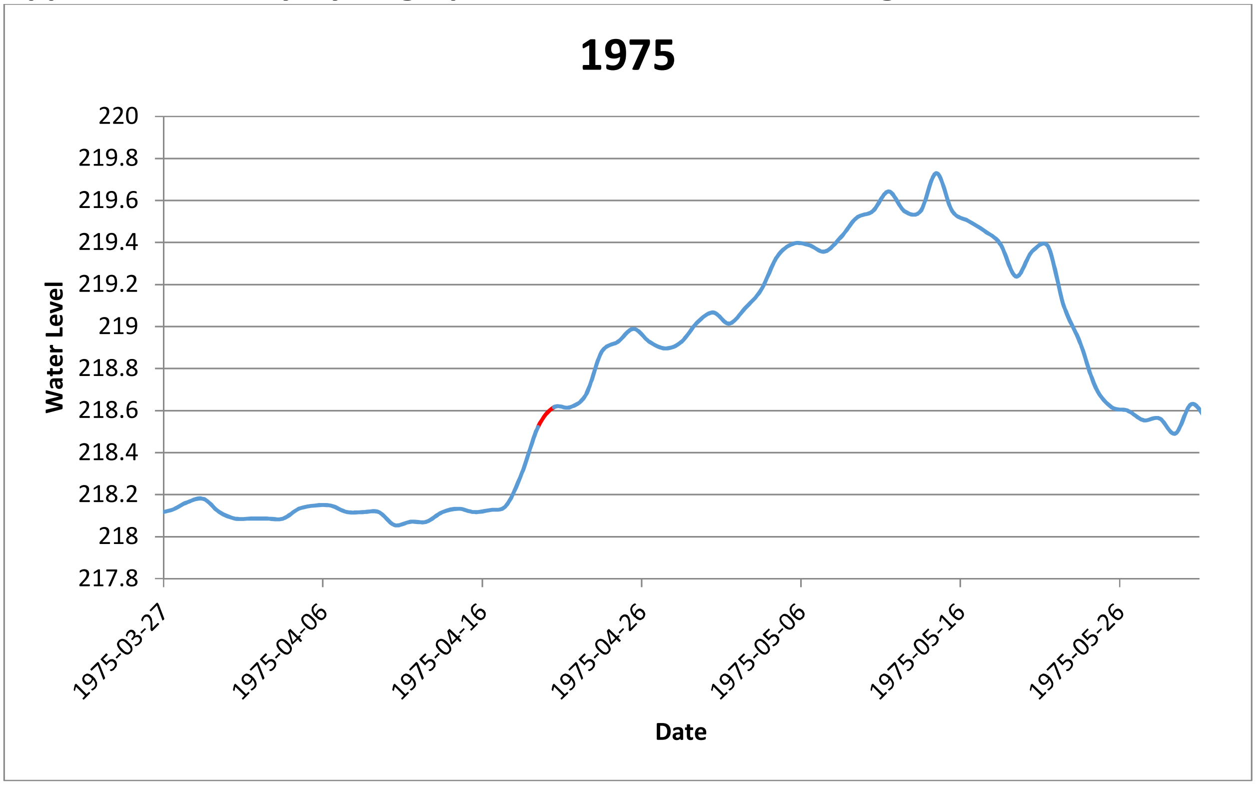

Figure B.14: Spring hydrograph for the Selkirk Generating Station in 1975.The red section of the line is the assumed time of breakup.

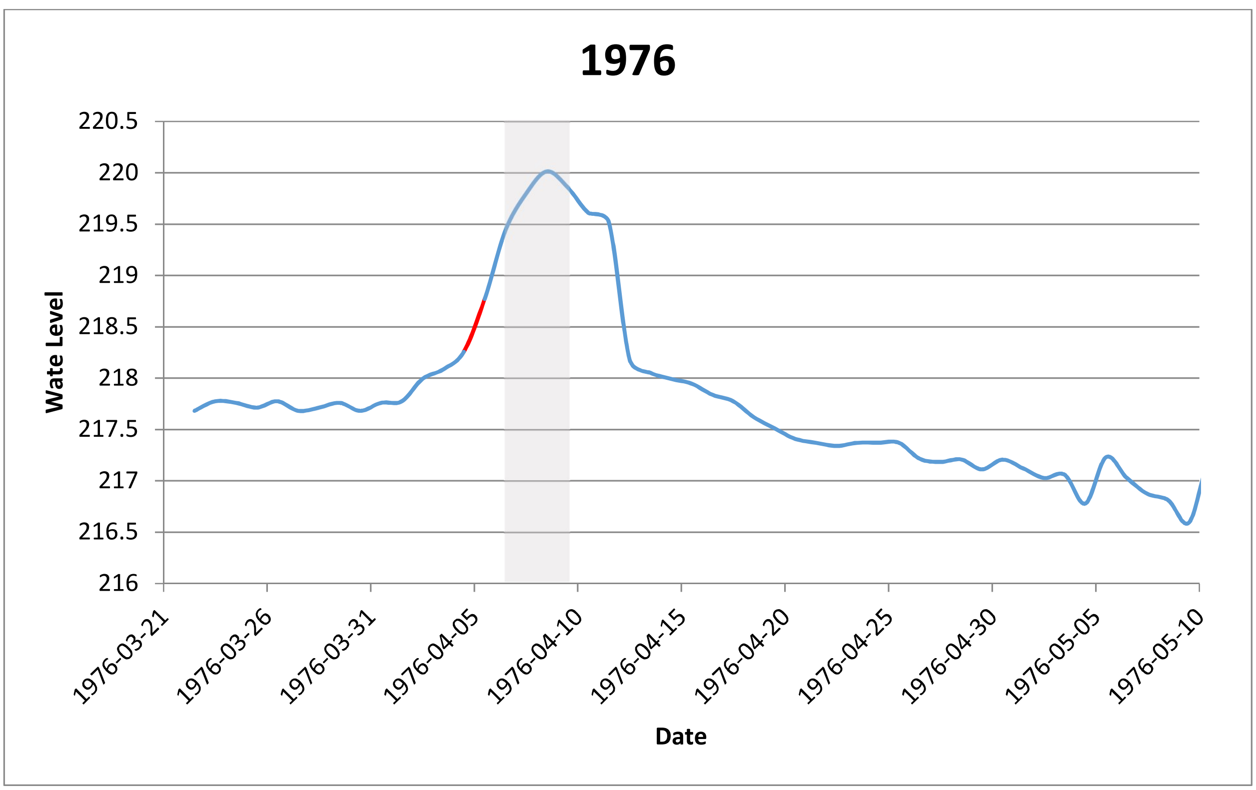

Figure B.15: Spring hydrograph for the Selkirk Generating Station in 1976. The red section of the line is the assumed time of breakup. The grey section of the graph indicates when an ice jam occurred.

Appendix B: Yearly Hydrographs at the Selkirk Generating Station

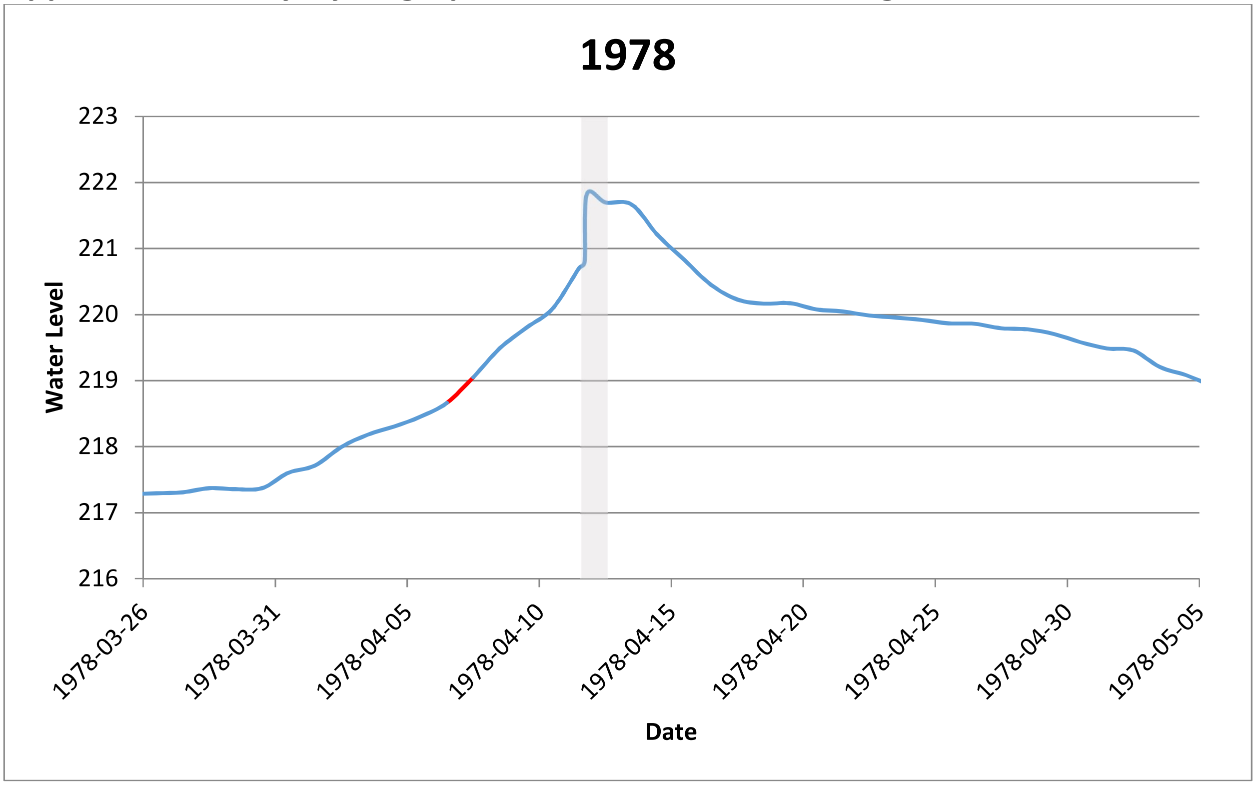

Figure B.16: Spring hydrograph for the Selkirk Generating Station in 1978. The red section of the line is the assumed time of breakup. The grey section of the graph indicates when an ice jam occurred.

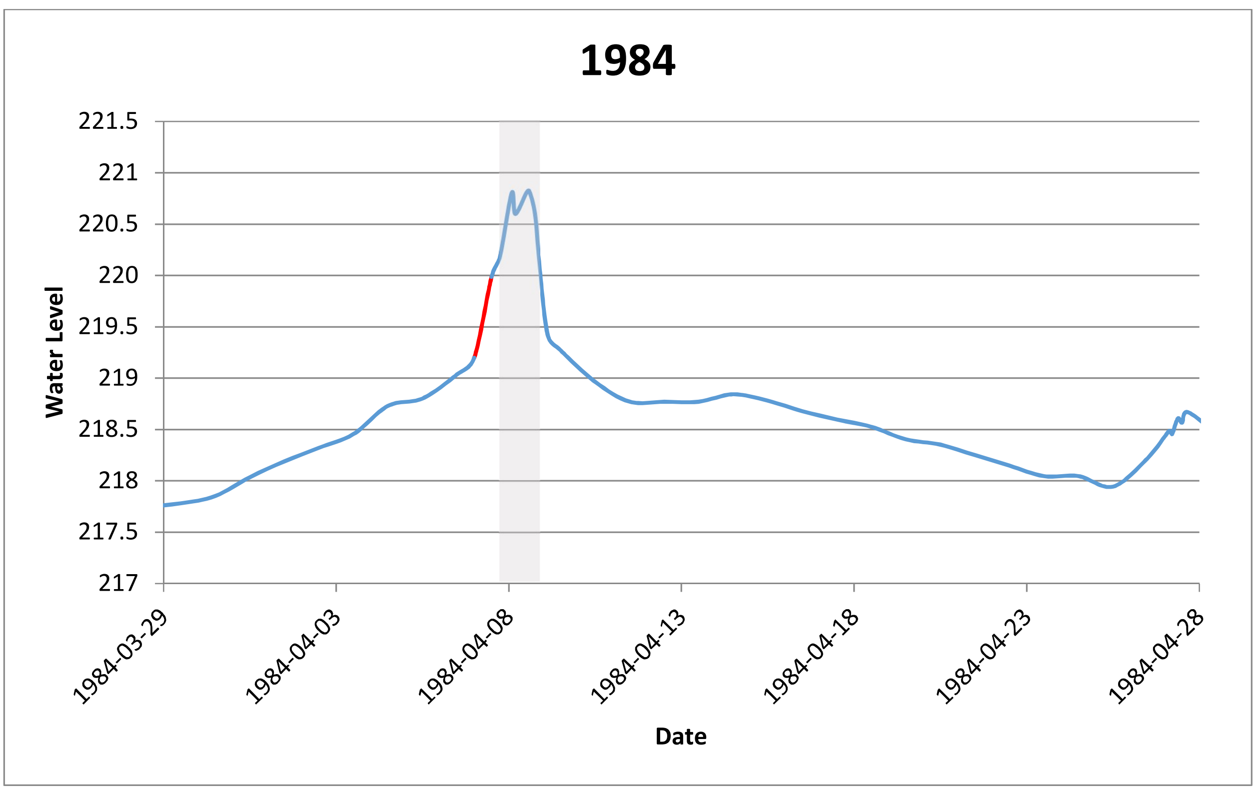

Figure B.17: Spring hydrograph for the Selkirk Generating Station in 1984. The red section of the line is the assumed time of breakup. The grey section of the graph indicates when an ice jam occurred.

Appendix B: Yearly Hydrographs at the Selkirk Generating Station

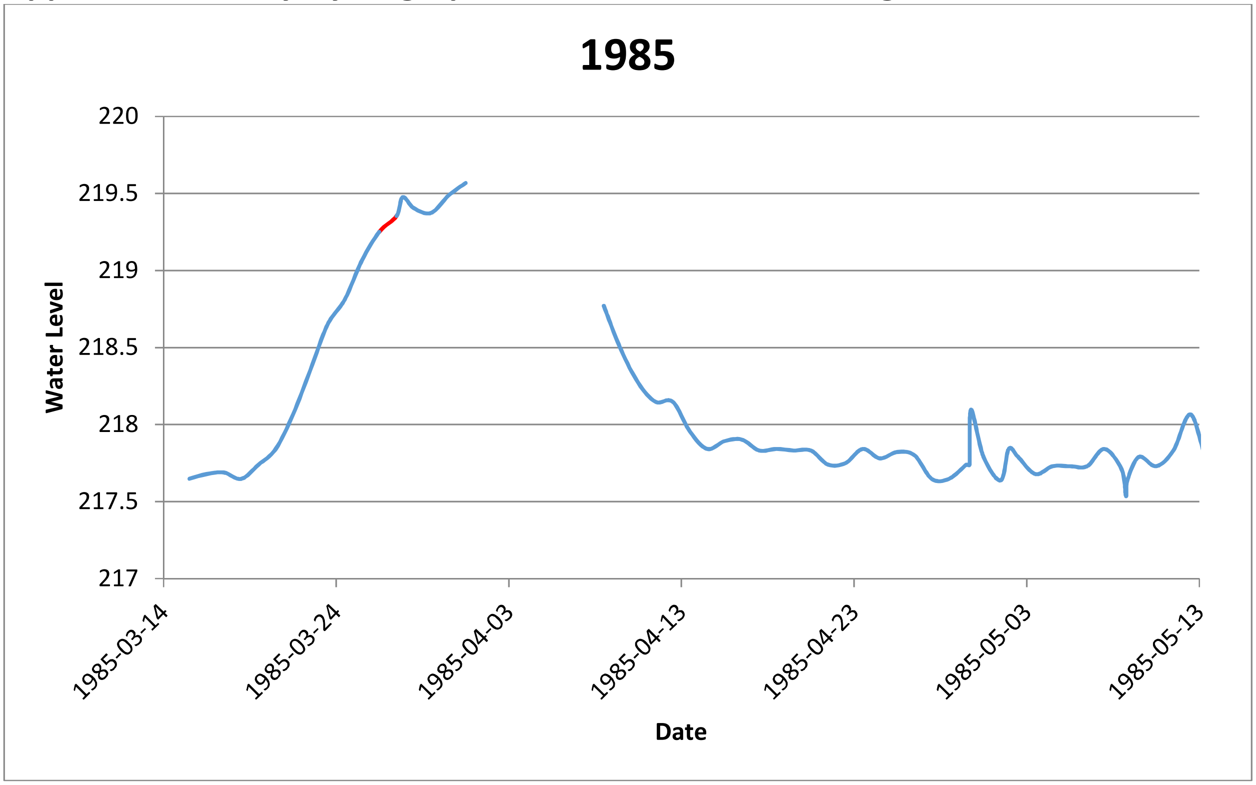

Figure B.18: Spring hydrograph for the Selkirk Generating Station in 1985. The red section of the line is the assumed time of breakup.

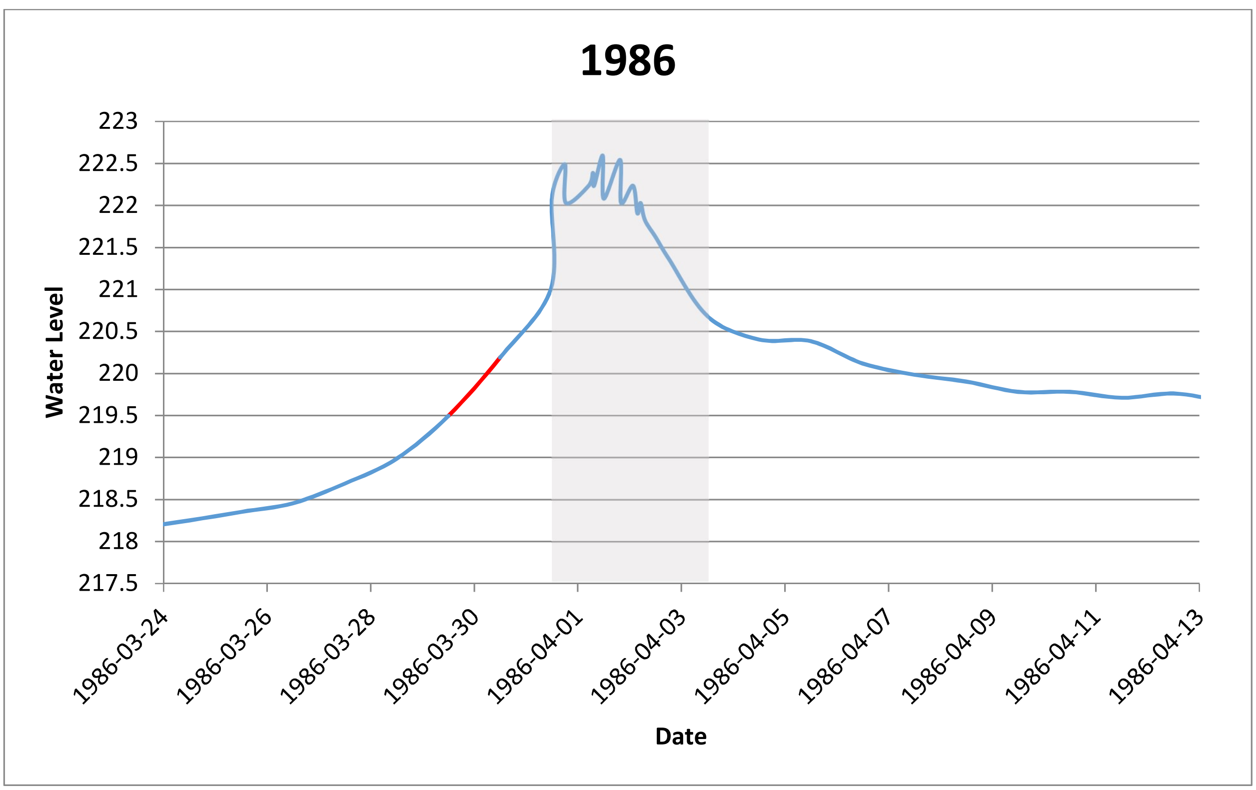

Figure B.19: Spring hydrograph for the Selkirk Generating Station in 1986.The red section of the line is the assumed time of breakup. The grey section of the graph indicates when an ice jam occurred.

Appendix B: Yearly Hydrographs at the Selkirk Generating Station

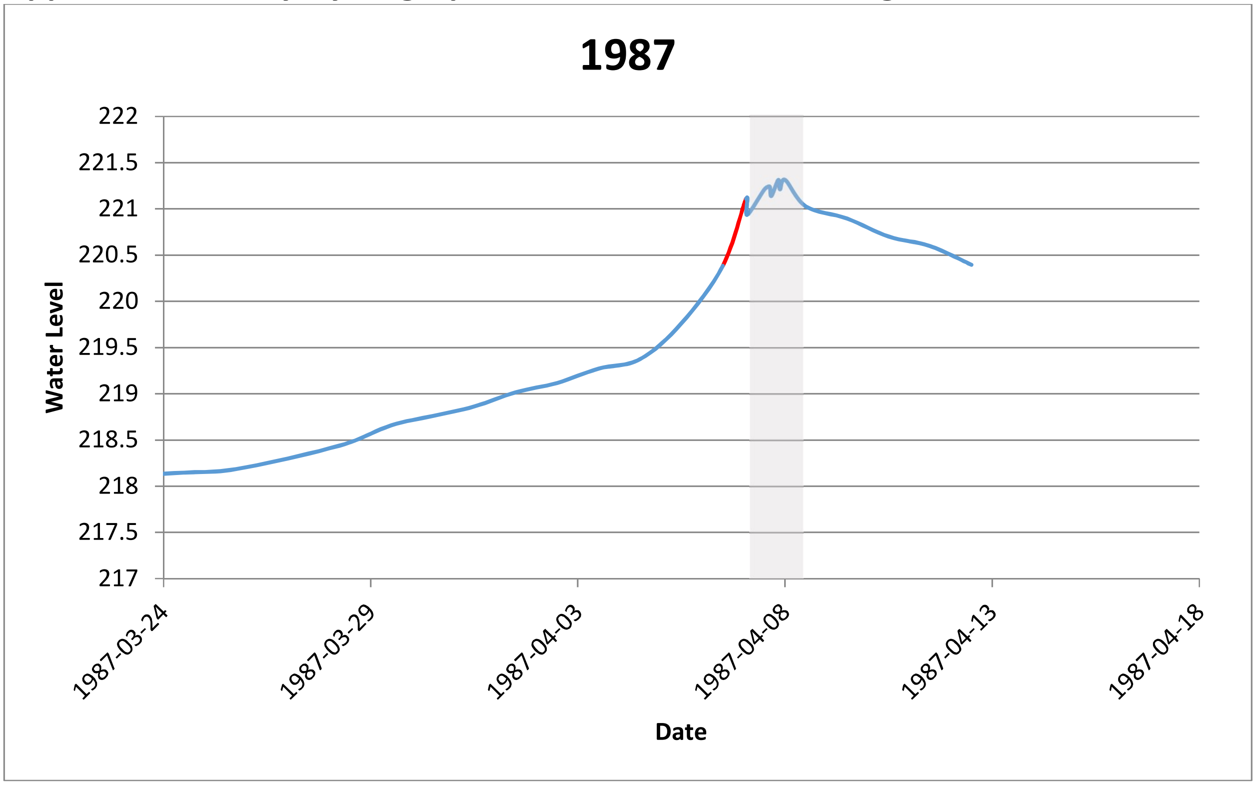

Figure B.20: Spring hydrograph for the Selkirk Generating Station in 1987.The red section of the line is the assumed time of breakup. The grey section of the graph indicates when an ice jam occurred.

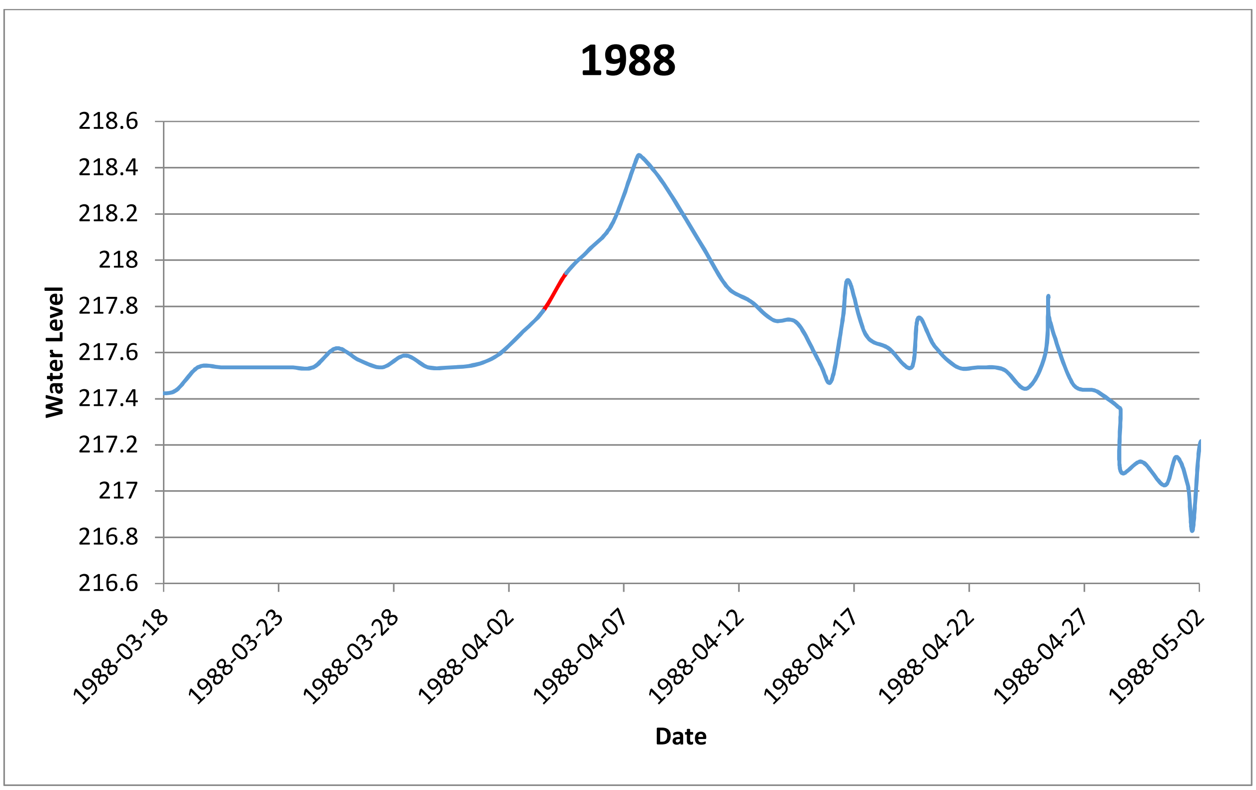

Figure B.21: Spring hydrograph for the Selkirk Generating Station in 1988.The red section of the line is the assumed time of breakup.

Appendix B: Yearly Hydrographs at the Selkirk Generating Station

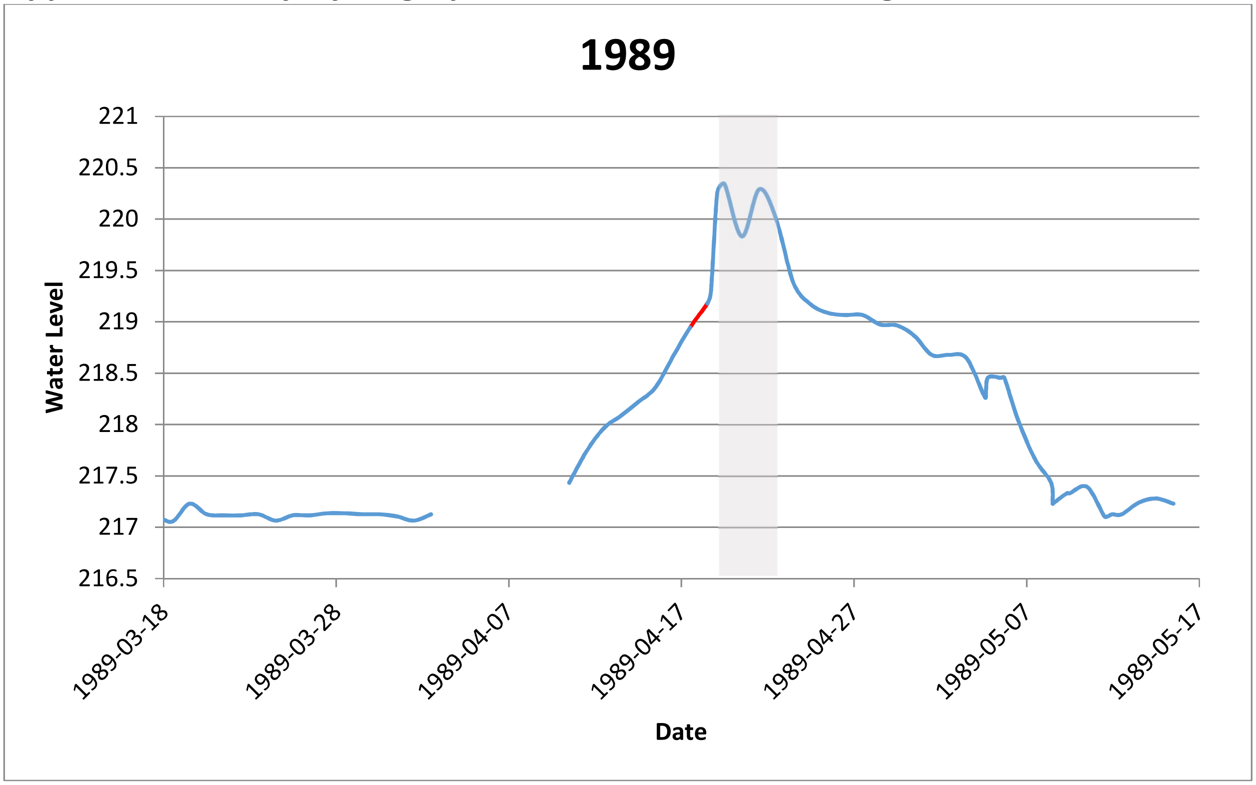

Figure B.22: Spring hydrograph for the Selkirk Generating Station in 1989.The red section of the line is the assumed time of breakup. The grey section of the graph indicates when an ice jam occurred.

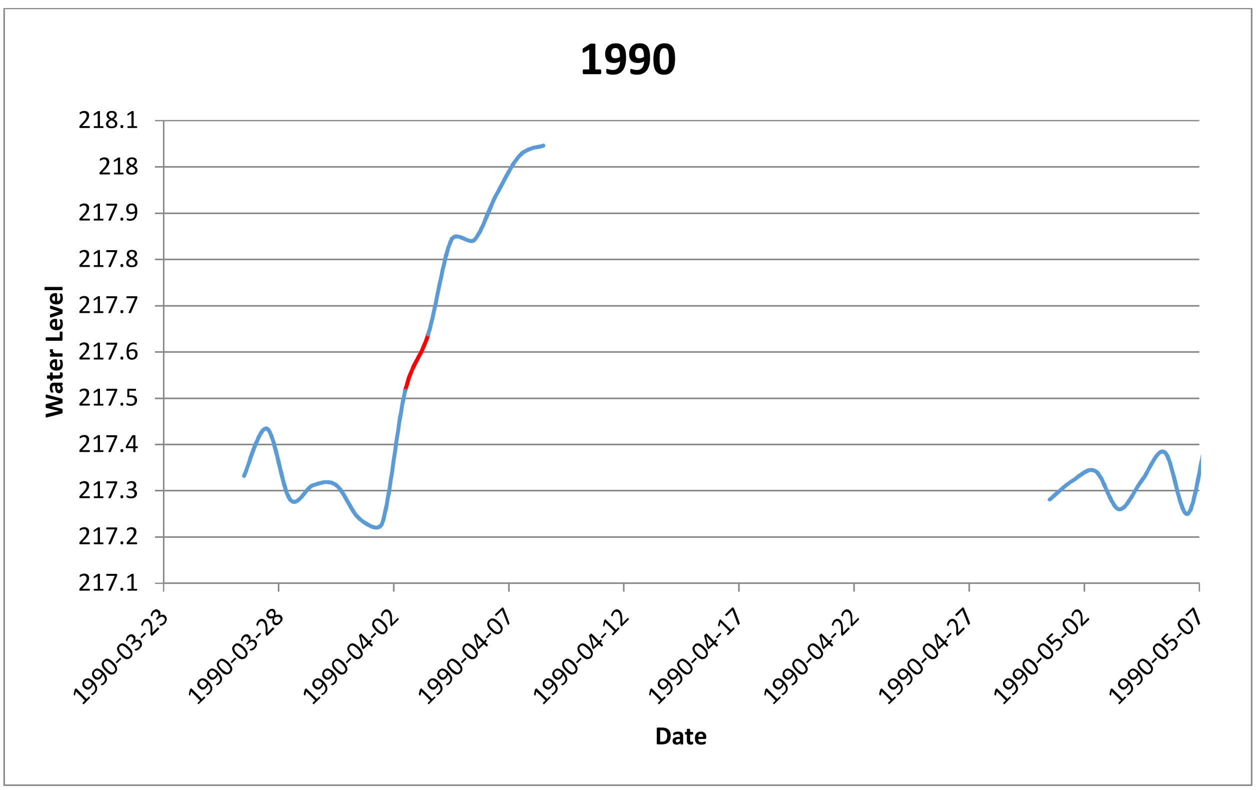

Figure B.23: Spring hydrograph for the Selkirk Generating Station in 1990.The red section of the line is the assumed time of breakup.

Appendix B: Yearly Hydrographs at the Selkirk Generating Station

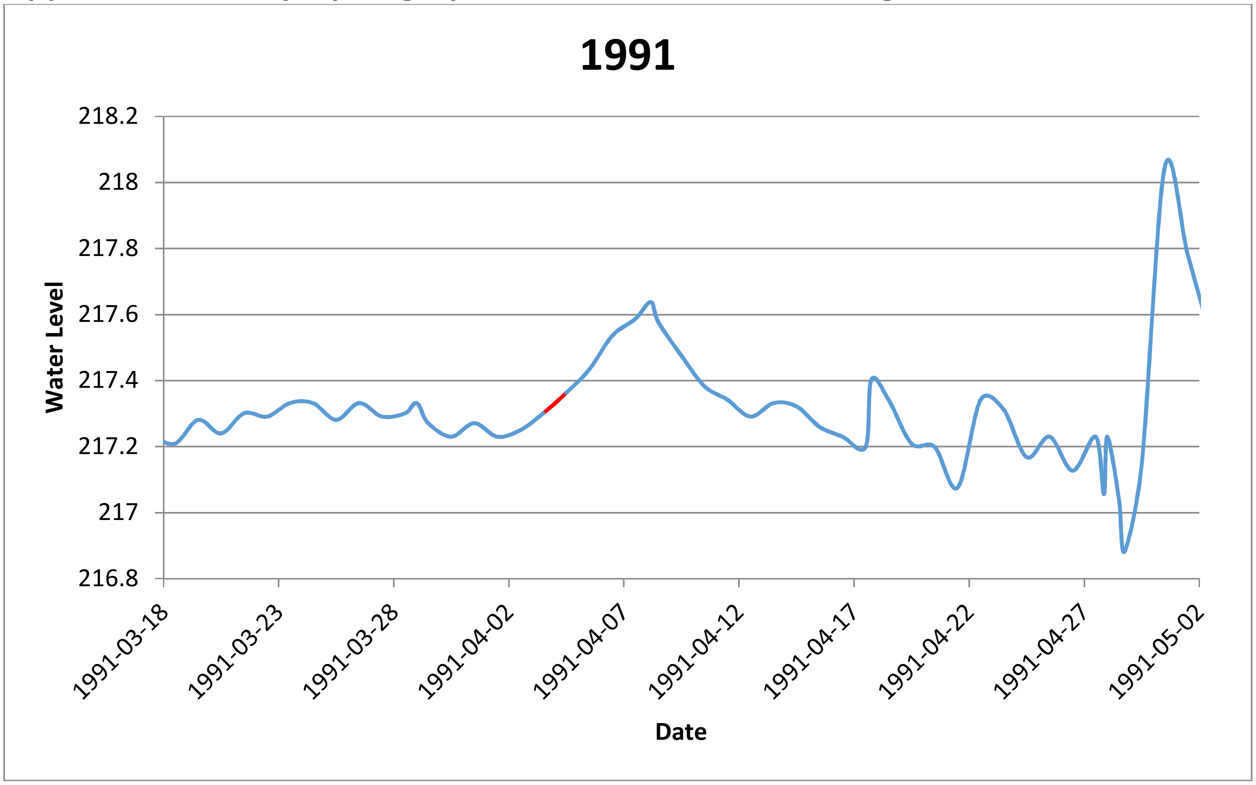

Figure B.24: Spring hydrograph for the Selkirk Generating Station in 1991.The red section of the line is the assumed time of breakup.

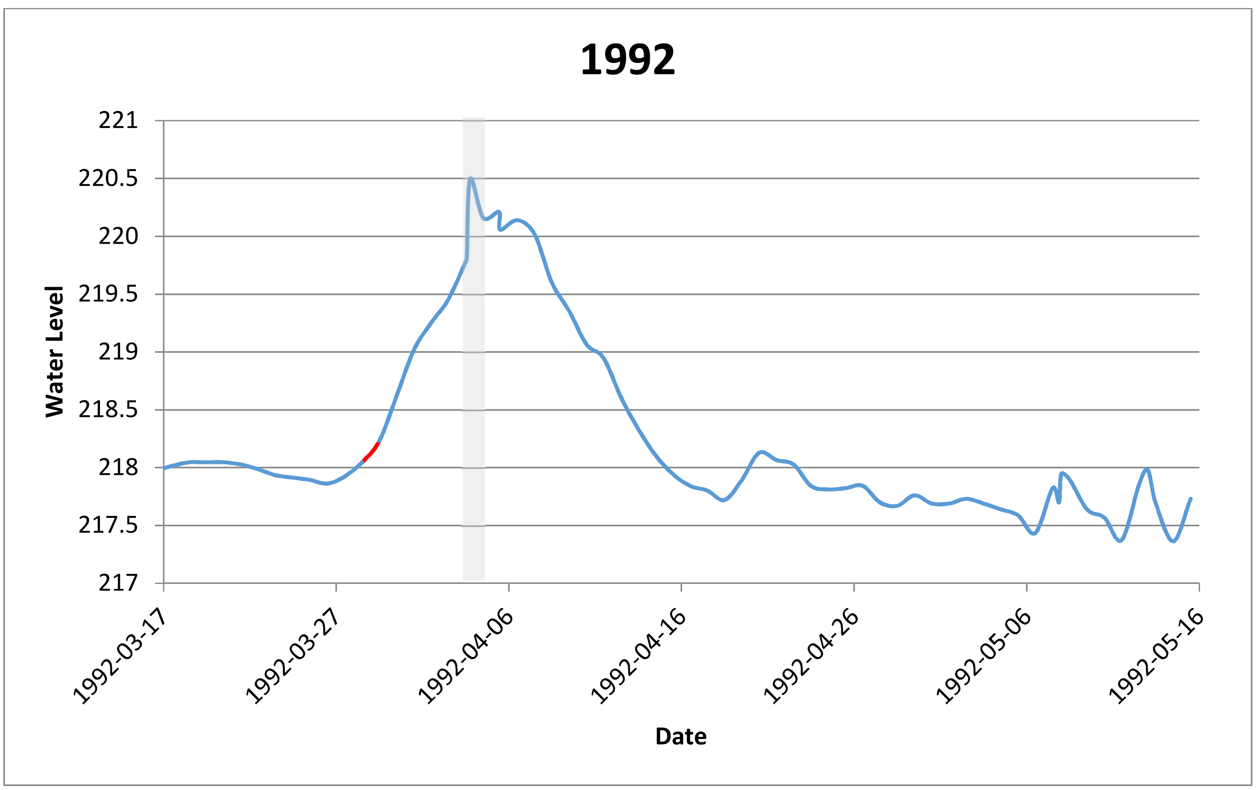

Figure B.25: Spring hydrograph for the Selkirk Generating Station in 1992.The red section of the line is the assumed time of breakup. The grey section of the graph indicates when an ice jam occurred.

Appendix B: Yearly Hydrographs at the Selkirk Generating Station

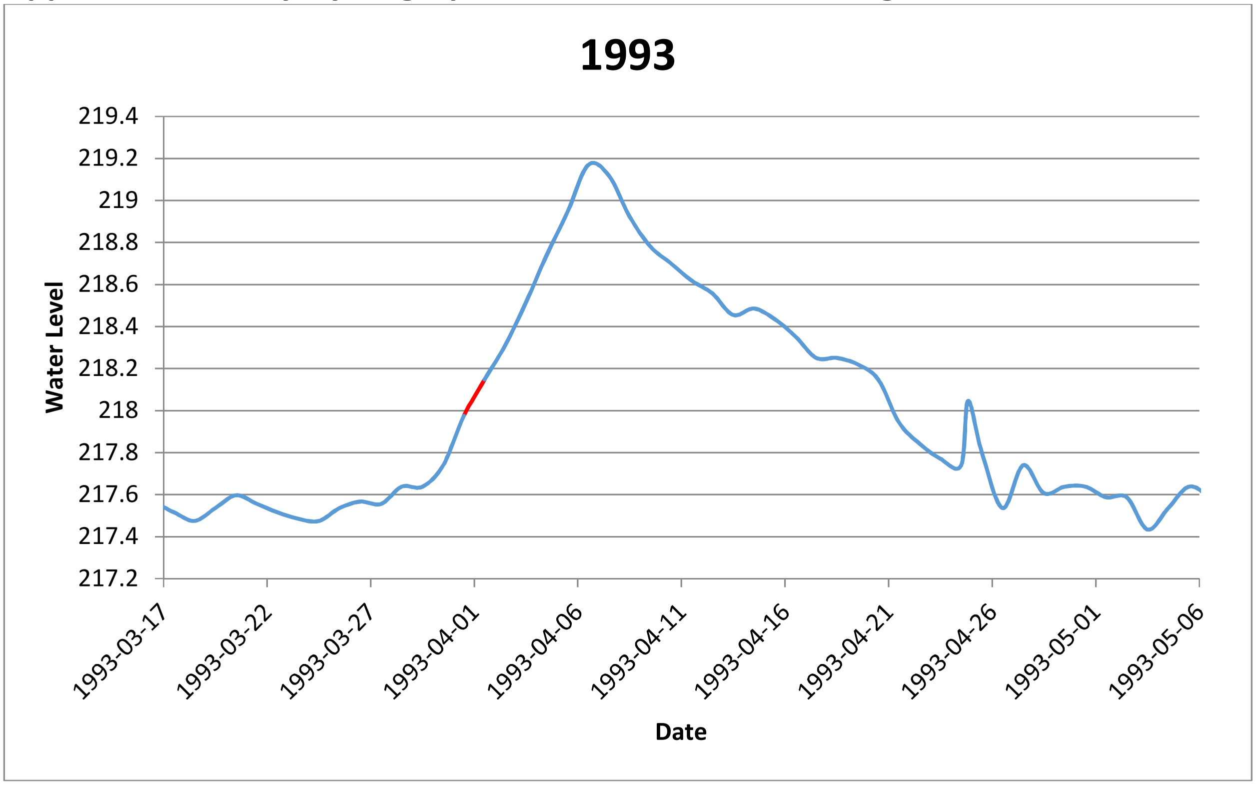

Figure B.26: Spring hydrograph for the Selkirk Generating Station in 1993.The red section of the line is the assumed time of breakup.

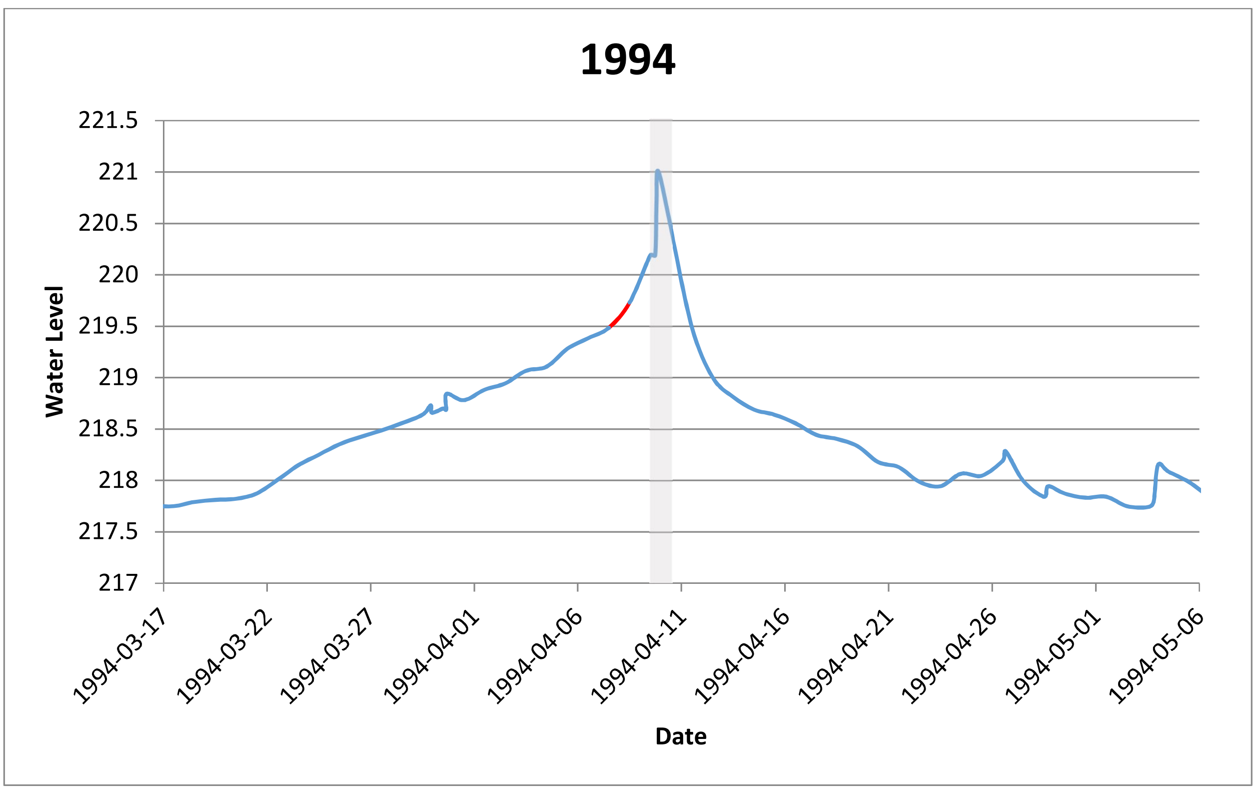

Figure B.27: Spring hydrograph for the Selkirk Generating Station in 1994.The red section of the line is the assumed time of breakup. The grey section of the graph indicates when an ice jam occurred.

Appendix B: Yearly Hydrographs at the Selkirk Generating Station

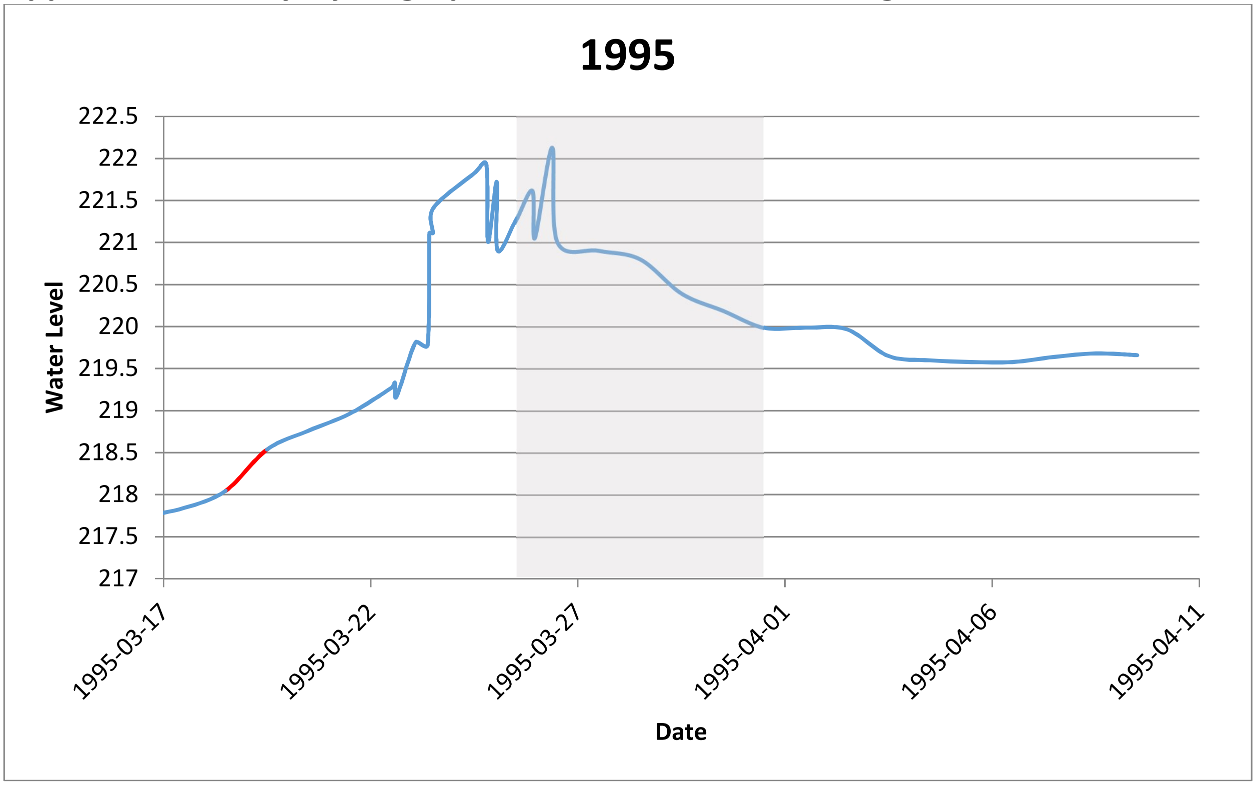

Figure B.28: Spring hydrograph for the Selkirk Generating Station in 1995.The red section of the line is the assumed time of breakup. The grey section of the graph indicates when an ice jam occurred.

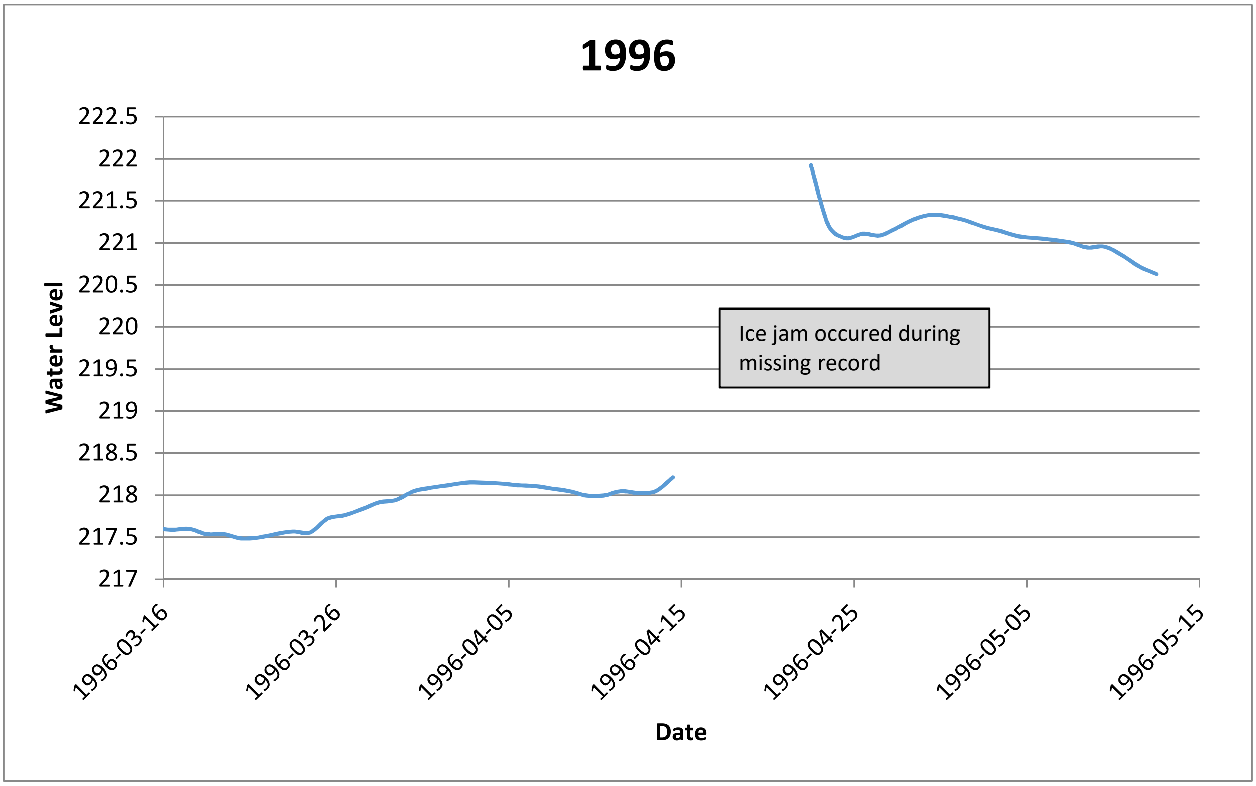

Figure B.29: Spring hydrograph for the Selkirk Generating Station in 1996.

Appendix B: Yearly Hydrographs at the Selkirk Generating Station

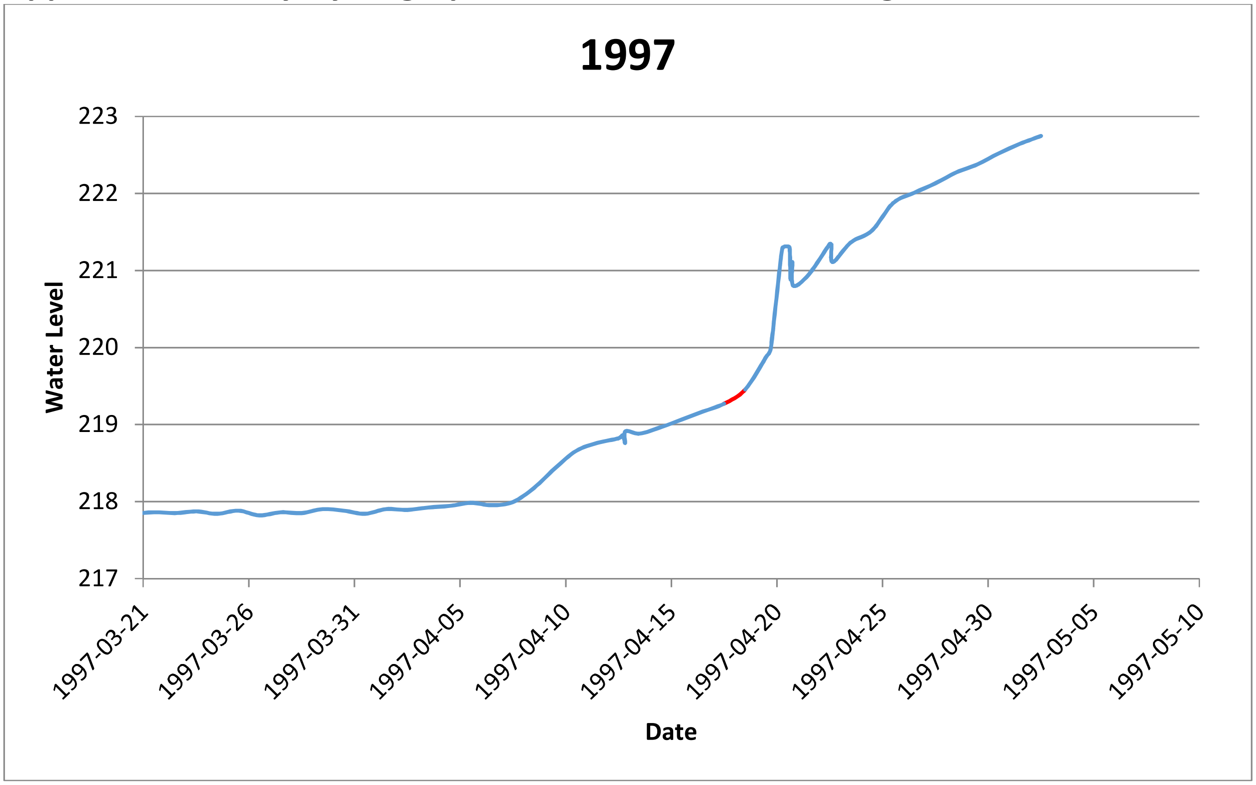

Figure B.30: Spring hydrograph for the Selkirk Generating Station in 1997.The red section of the line is the assumed time of breakup.

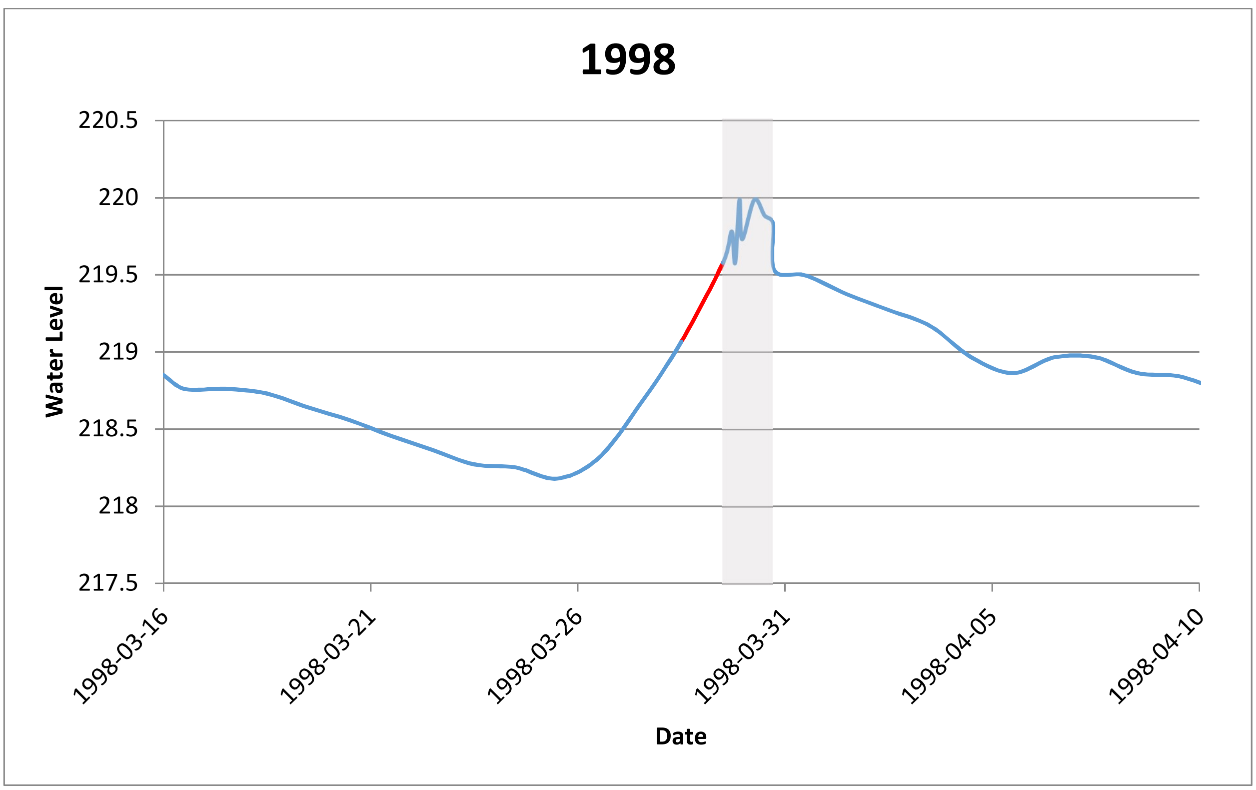

Figure B.31: Spring hydrograph for the Selkirk Generating Station in 1998.The red section of the line is the assumed time of breakup. The grey section of the graph indicates when an ice jam occurred.

Appendix B: Yearly Hydrographs at the Selkirk Generating Station

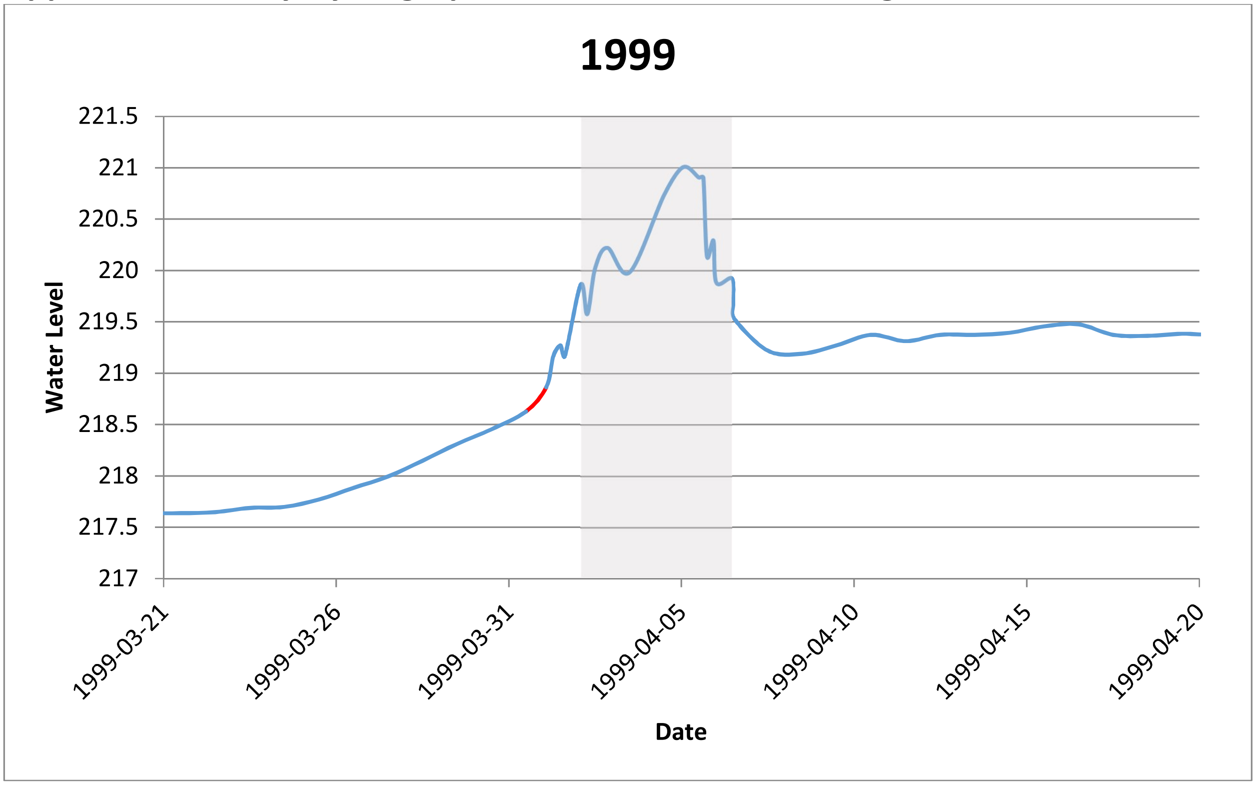

Figure B.32: Spring hydrograph for the Selkirk Generating Station in 1999.The red section of the line is the assumed time of breakup. The grey section of the graph indicates when an ice jam occurred.

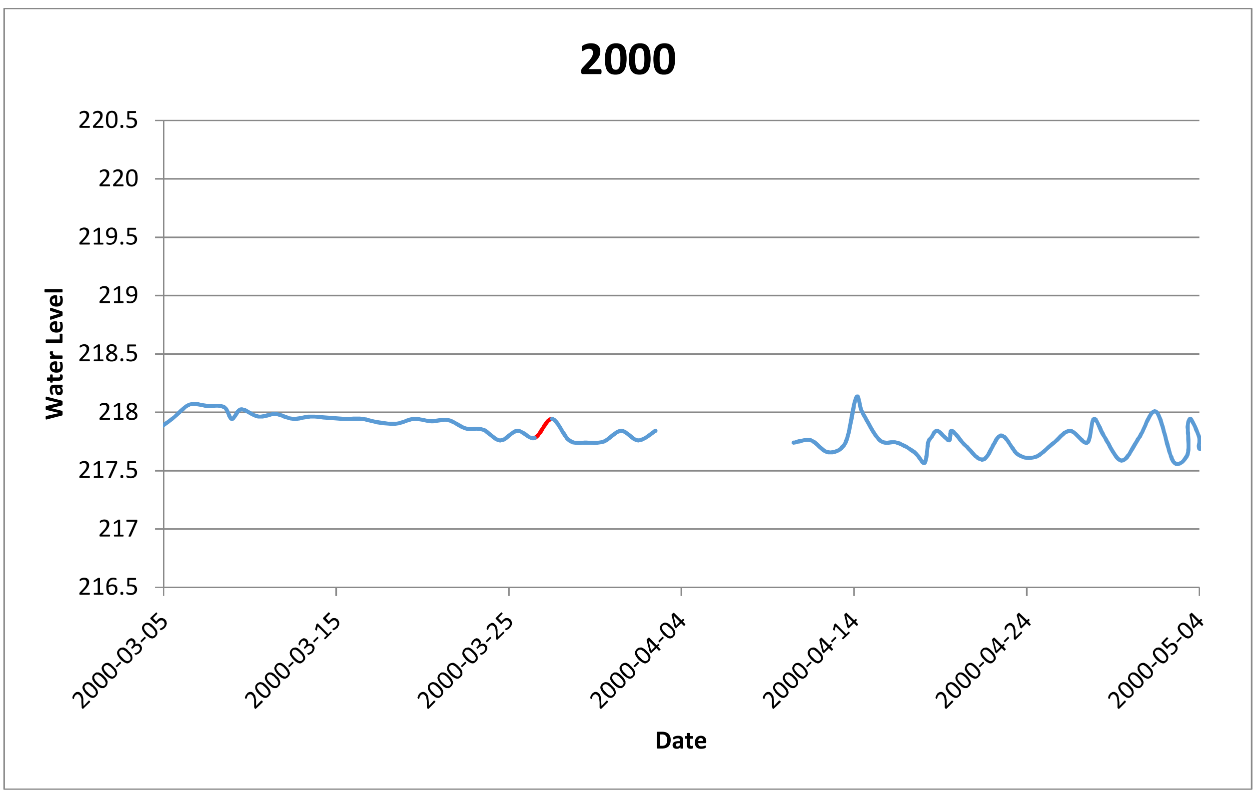

Figure B.33: Spring hydrograph for the Selkirk Generating Station in 2000.The red section of the line is the assumed time of breakup.

Appendix B: Yearly Hydrographs at the Selkirk Generating Station

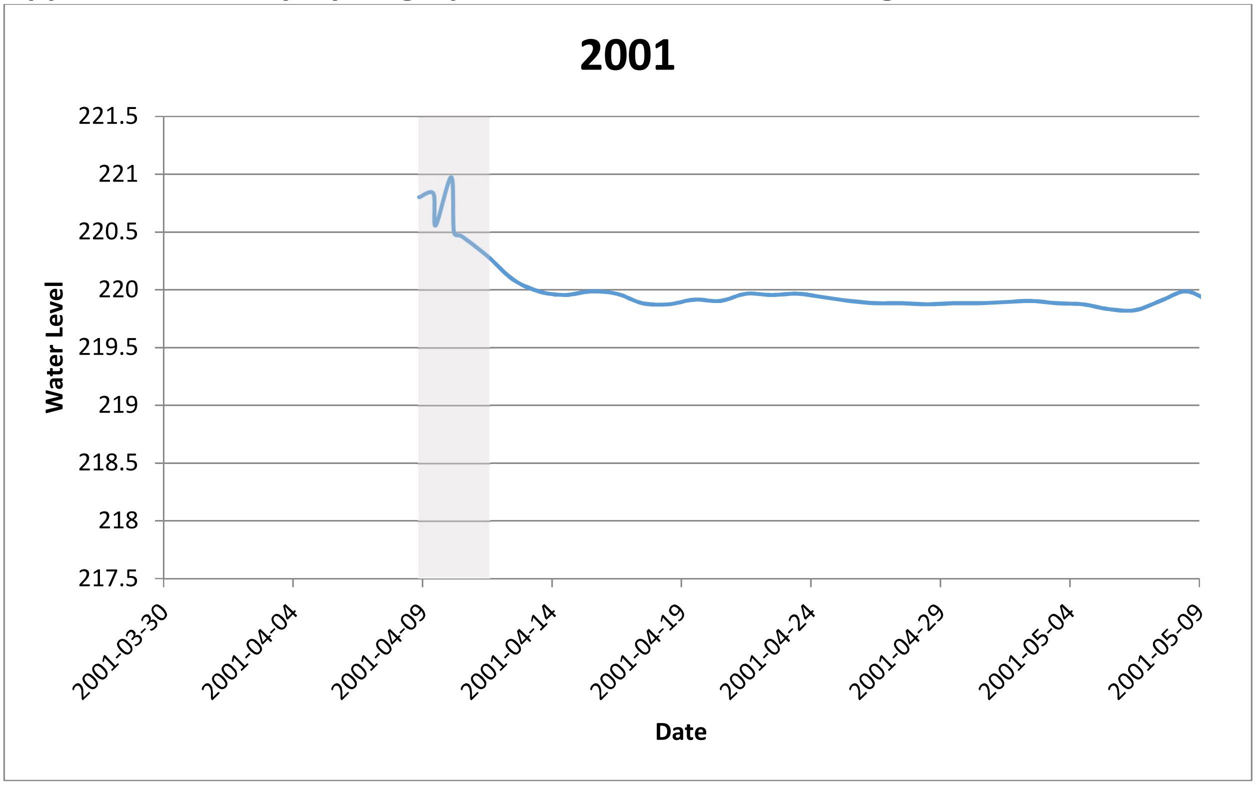

Figure B.34: Spring hydrograph for the Selkirk Generating Station in 2001.The grey section of the graph indicates when an ice jam occurred.

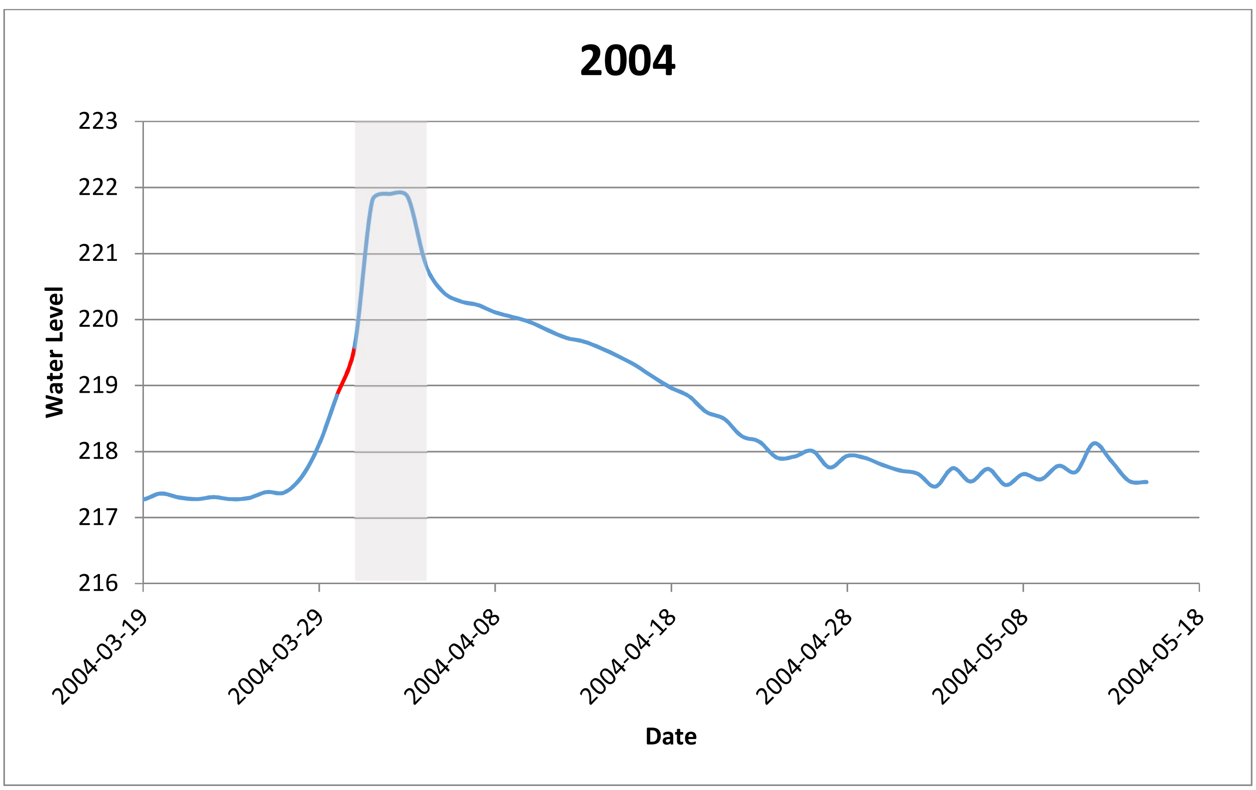

Figure B.35: Spring hydrograph for the Selkirk Generating Station in 2004. The red section of the line is the assumed time of breakup. The grey section of the graph indicates when an ice jam occurred.

Appendix B: Yearly Hydrographs at the Selkirk Generating Station

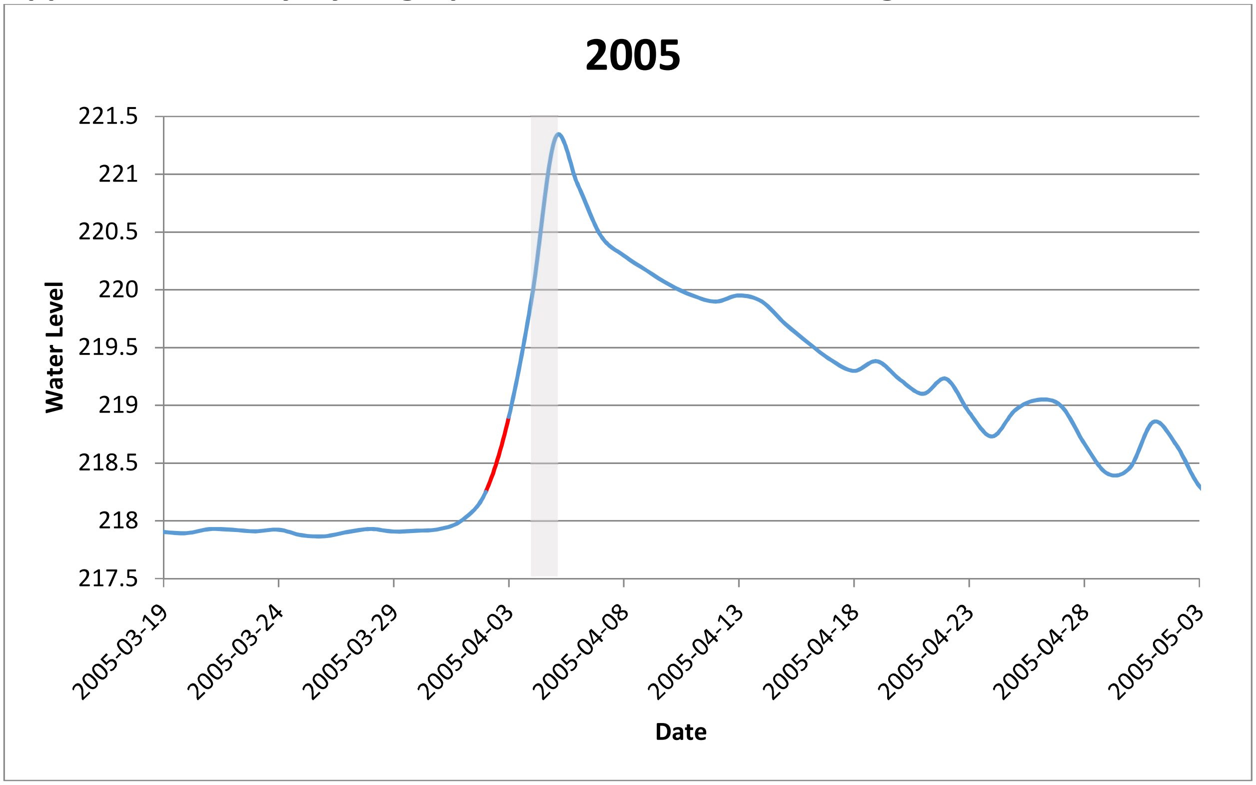

Figure B.36: Spring hydrograph for the Selkirk Generating Station in 2005.The red section of the line is the assumed time of breakup. The grey section of the graph indicates when an ice jam occurred.

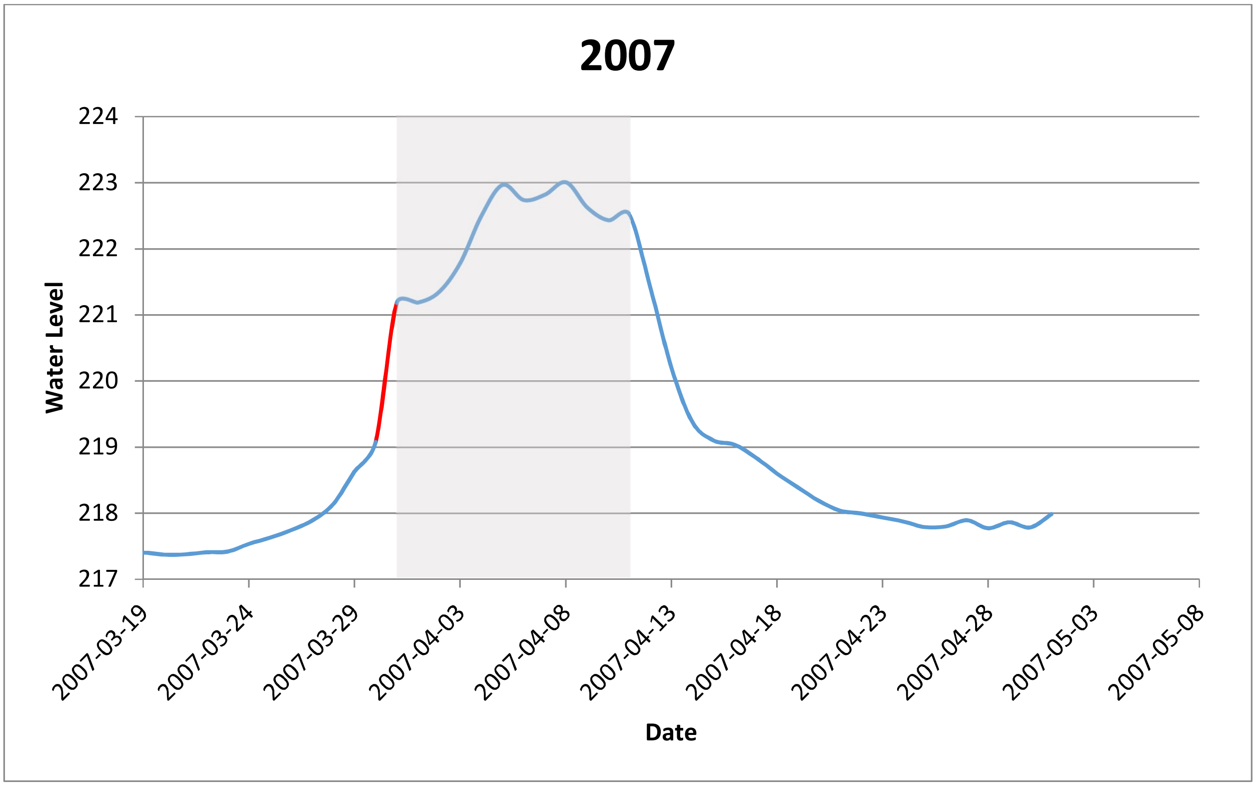

Figure B.37: Spring hydrograph for the Selkirk Generating Station in 2007.The red section of the line is the assumed time of breakup. The grey section of the graph indicates when an ice jam occurred.

Appendix B: Yearly Hydrographs at the Selkirk Generating Station

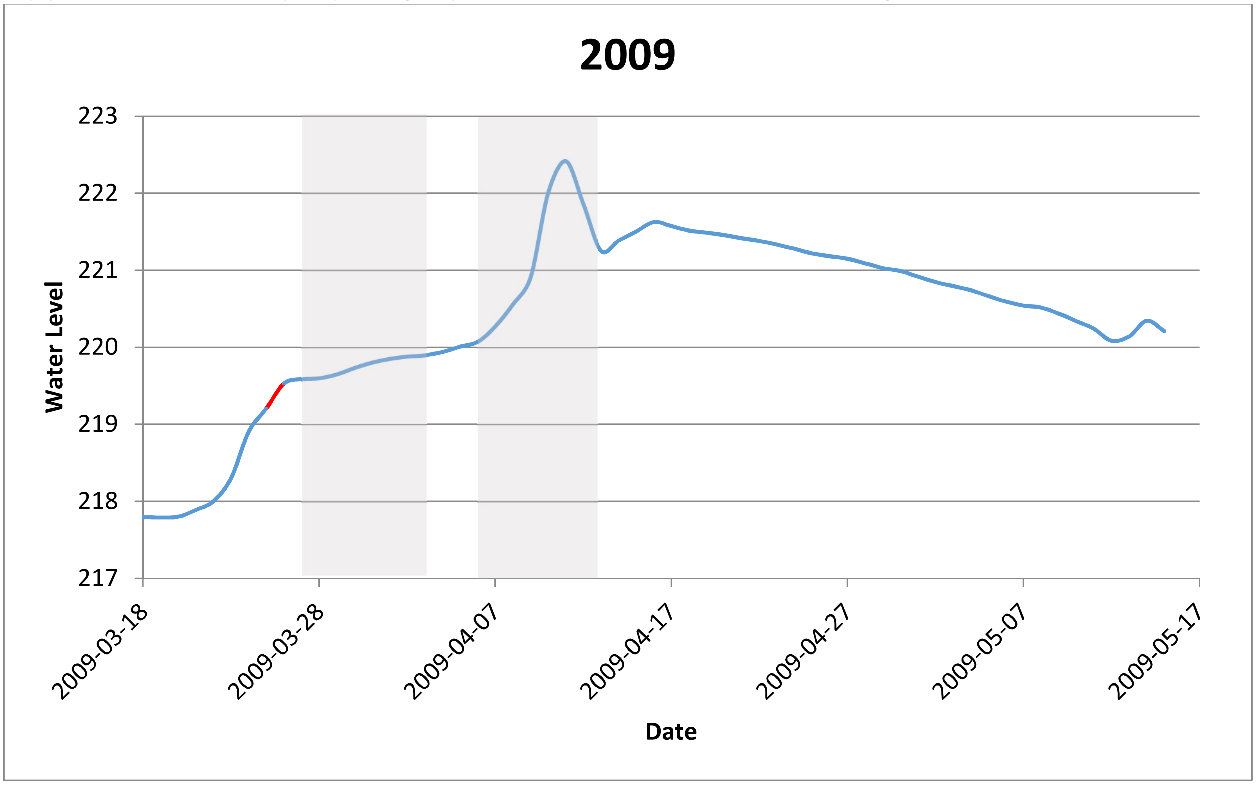

Figure B.38: Spring hydrograph for the Selkirk Generating Station in 2009.The red section of the line is the assumed time of breakup. The grey section of the graph indicates when an ice jam occurred.

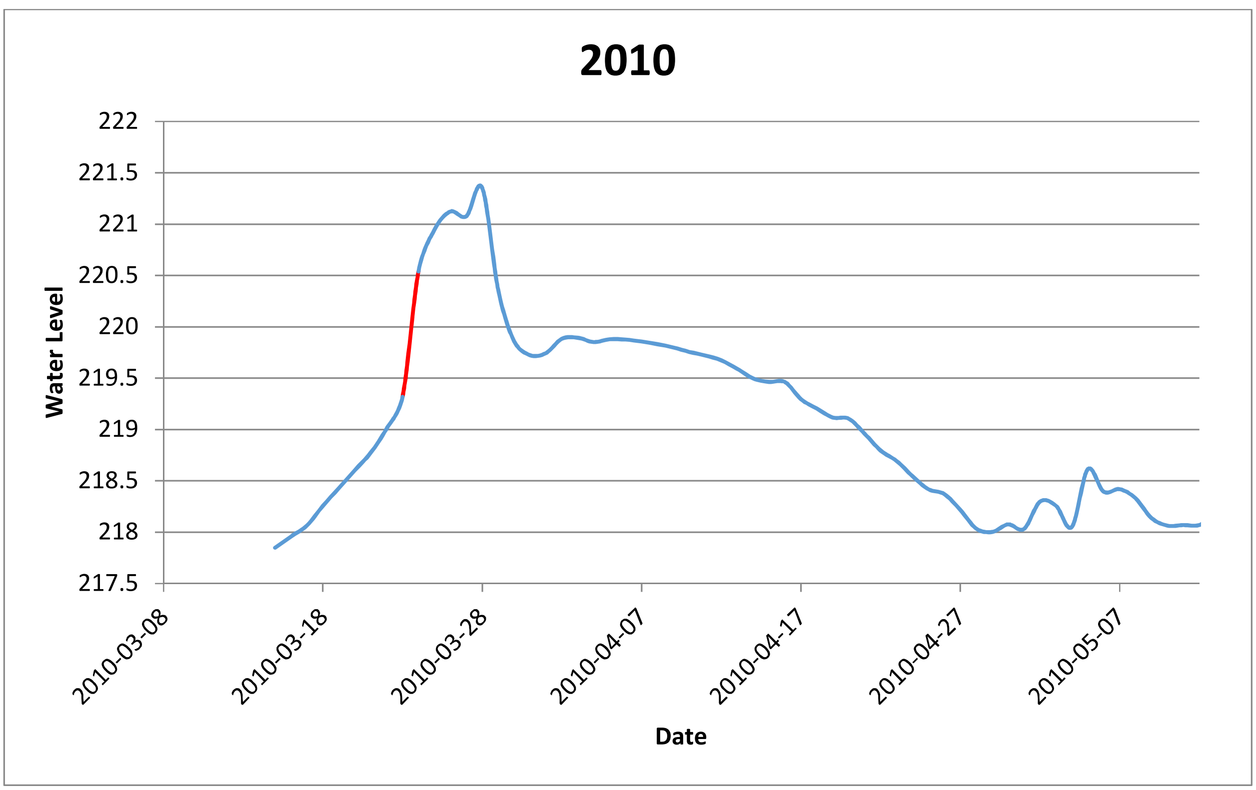

Figure B.39: Spring hydrograph for the Selkirk Generating Station in 2010.The red section of the line is the assumed time of breakup.

Appendix B: Yearly Hydrographs at the Selkirk Generating Station

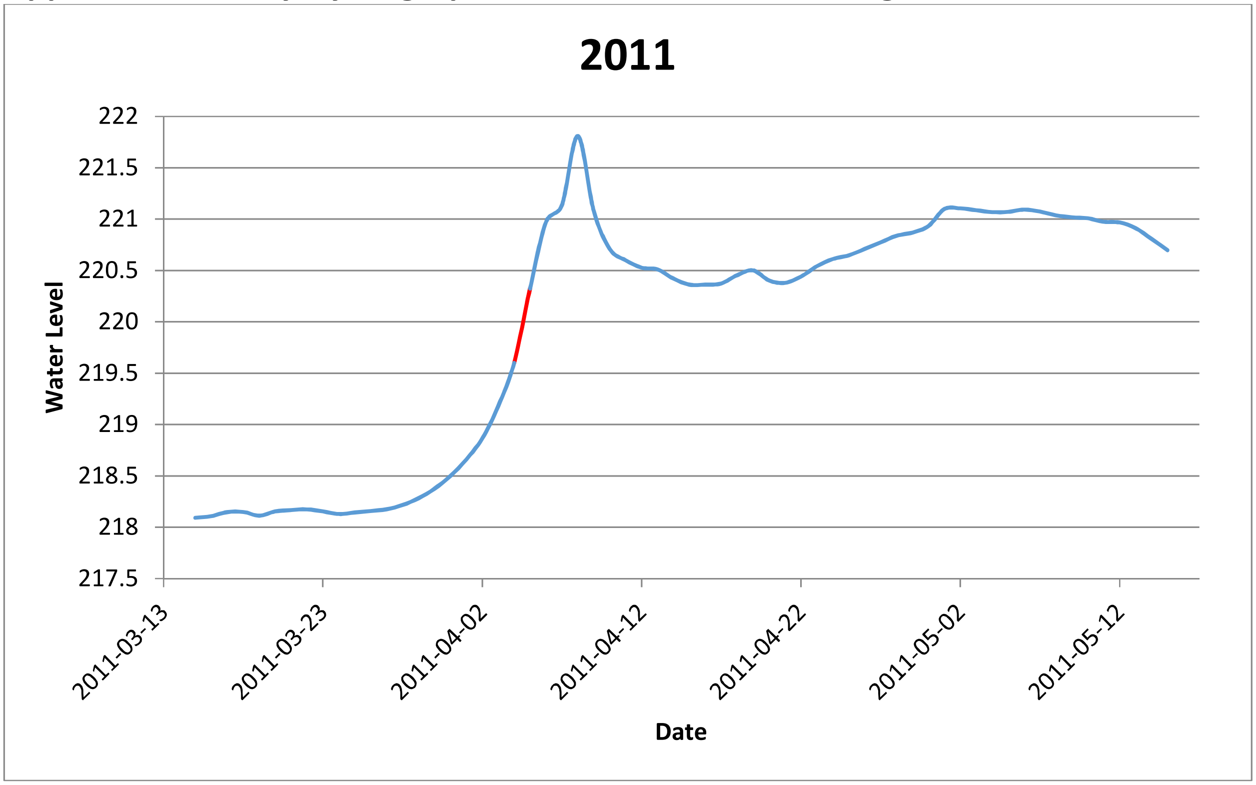

Figure B.40: Spring hydrograph for the Selkirk Generating Station in 2011.The red section of the line is the assumed time of breakup.

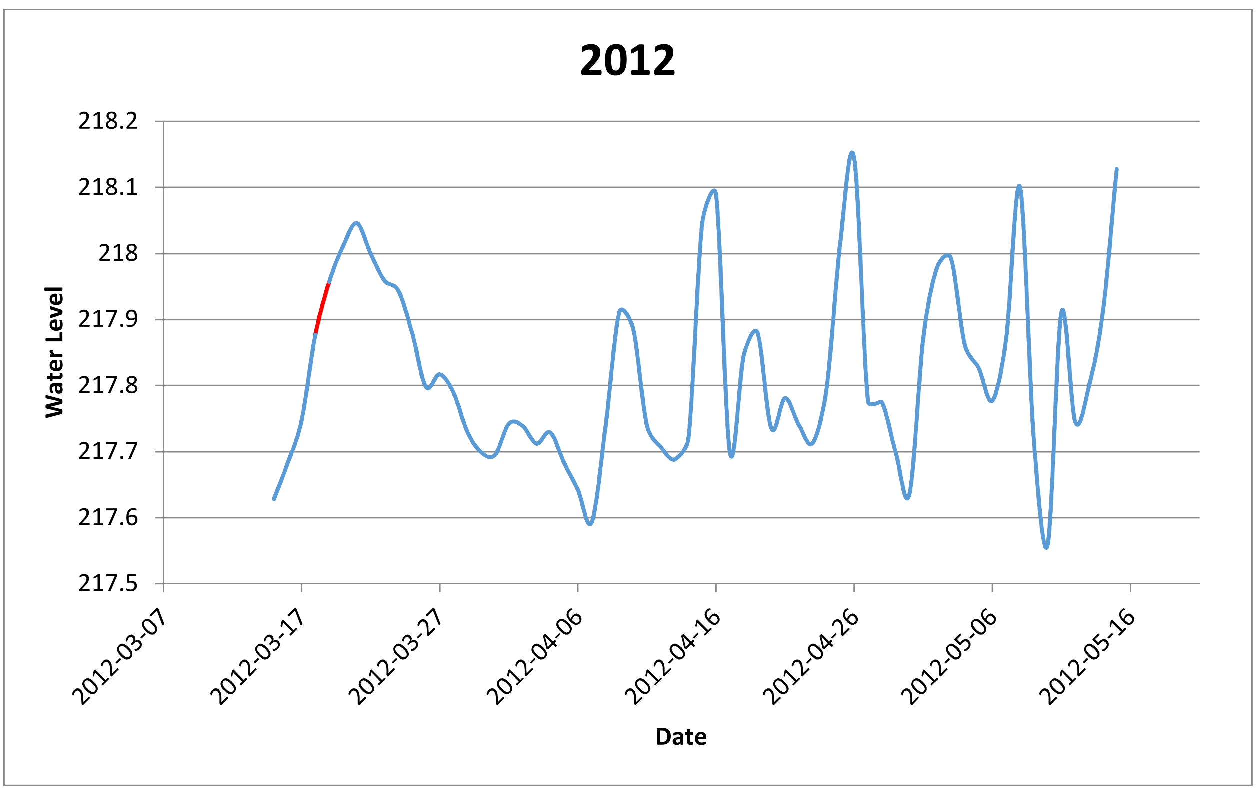

Figure B.41: Spring hydrograph for the Selkirk Generating Station in 2012.The red section of the line is the assumed time of breakup.

Appendix B: Yearly Hydrographs at the Selkirk Generating Station

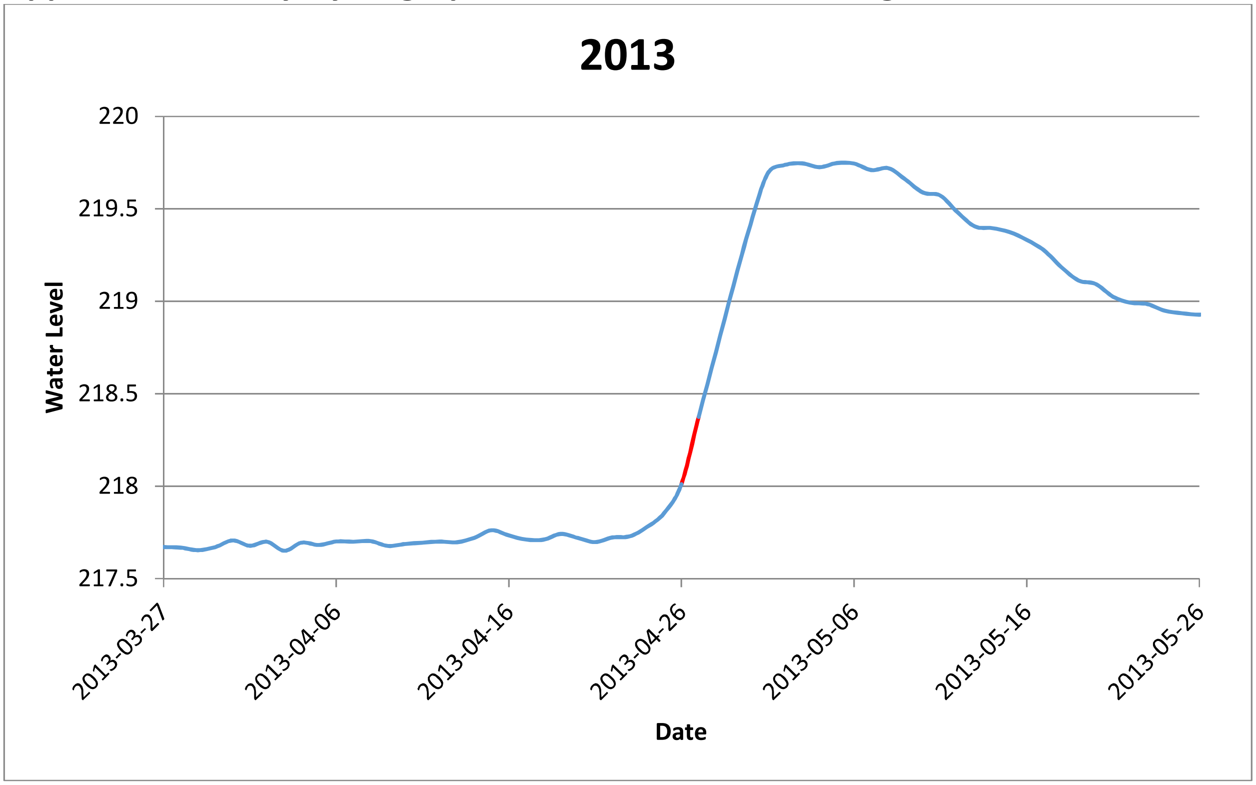

Figure B.42: Spring hydrograph for the Selkirk Generating Station in 2013.The red section of the line is the assumed time of breakup.

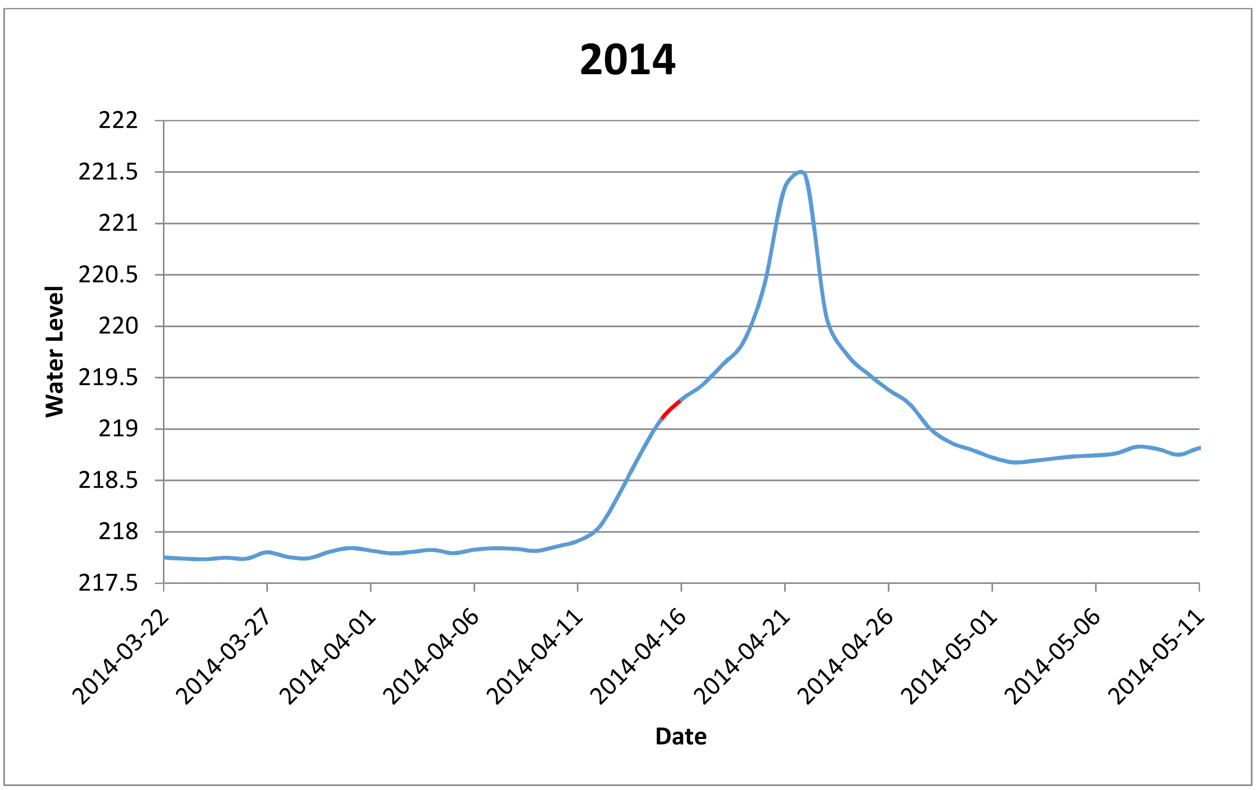

Figure B.43: Spring hydrograph for the Selkirk Generating Station in 2014.The red section of the line is the assumed time of breakup.

Appendix B: Yearly Hydrographs at the Selkirk Generating Station

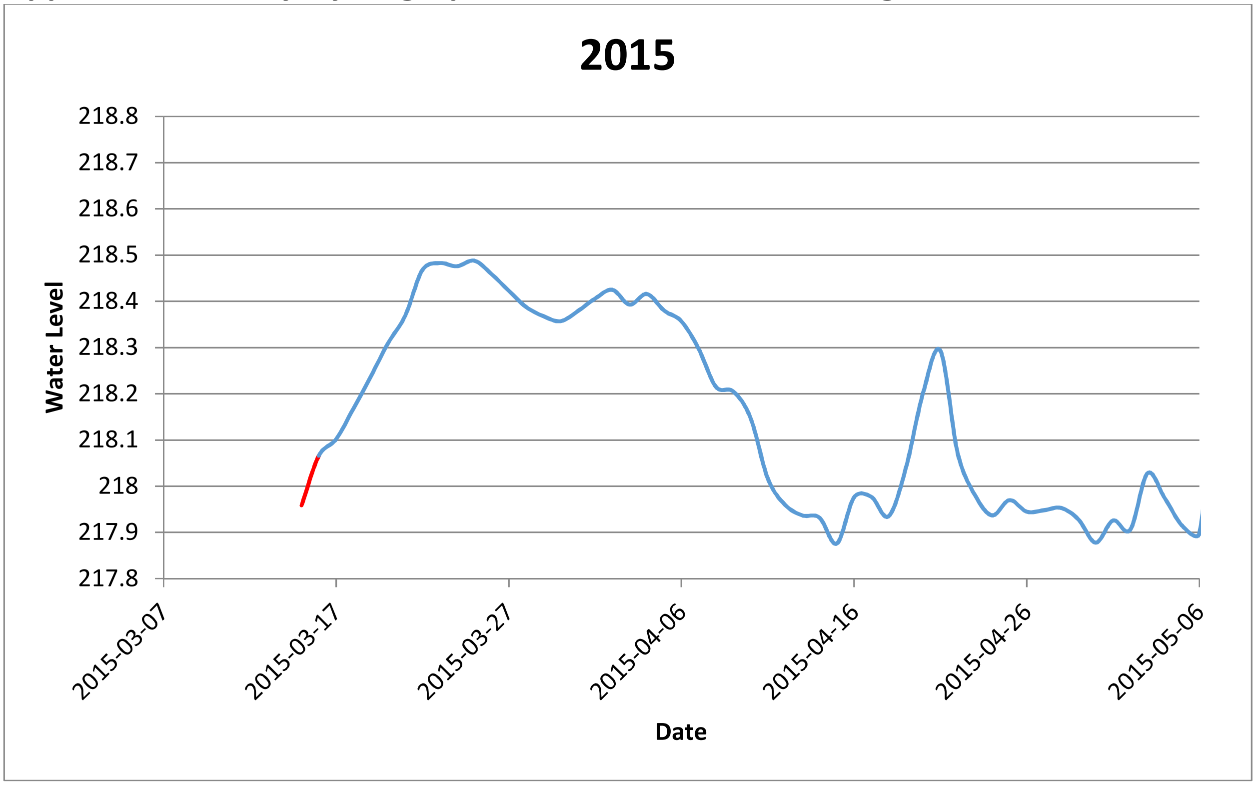

Figure B.44: Spring hydrograph for the Selkirk Generating Station in 2015.The red section of the line is the assumed time of breakup.

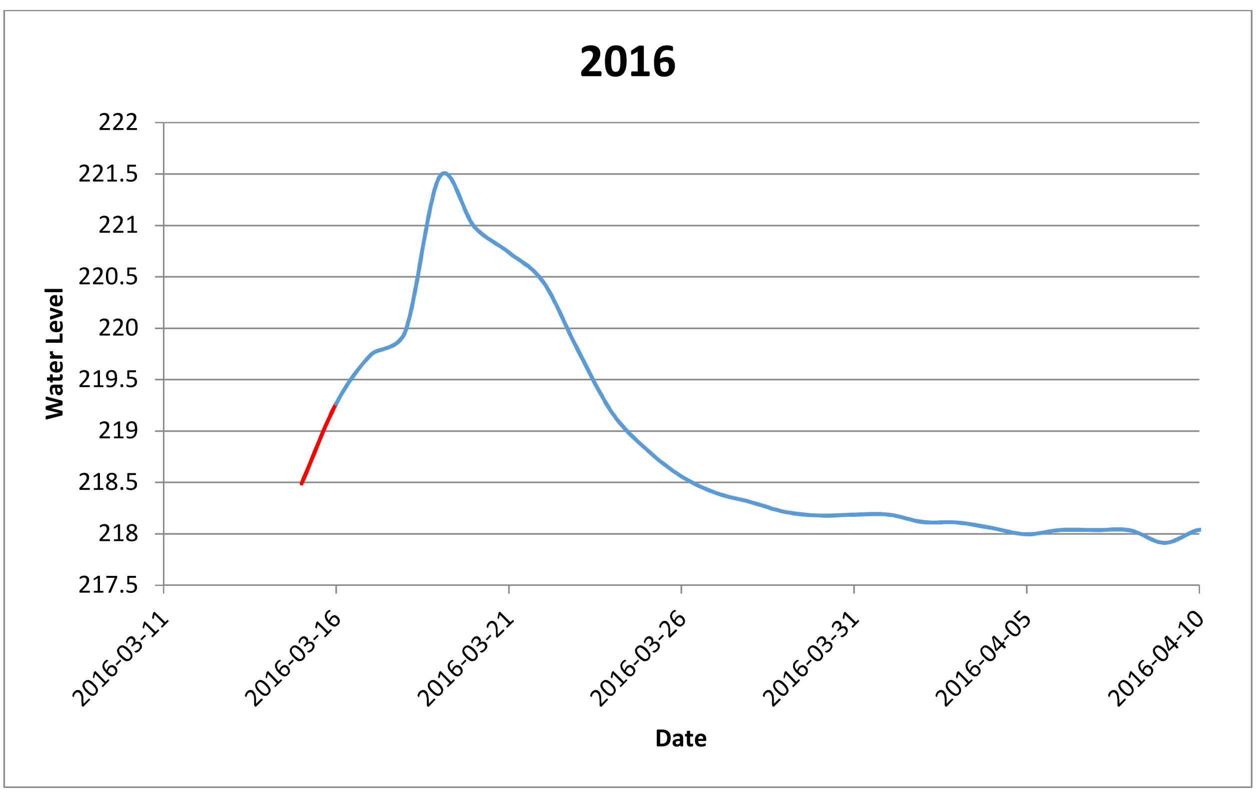

Figure B.45: Spring hydrograph for the Selkirk Generating Station in 2016.The red section of the line is the assumed time of breakup.

Appendix B: Yearly Hydrographs at the Selkirk Generating Station

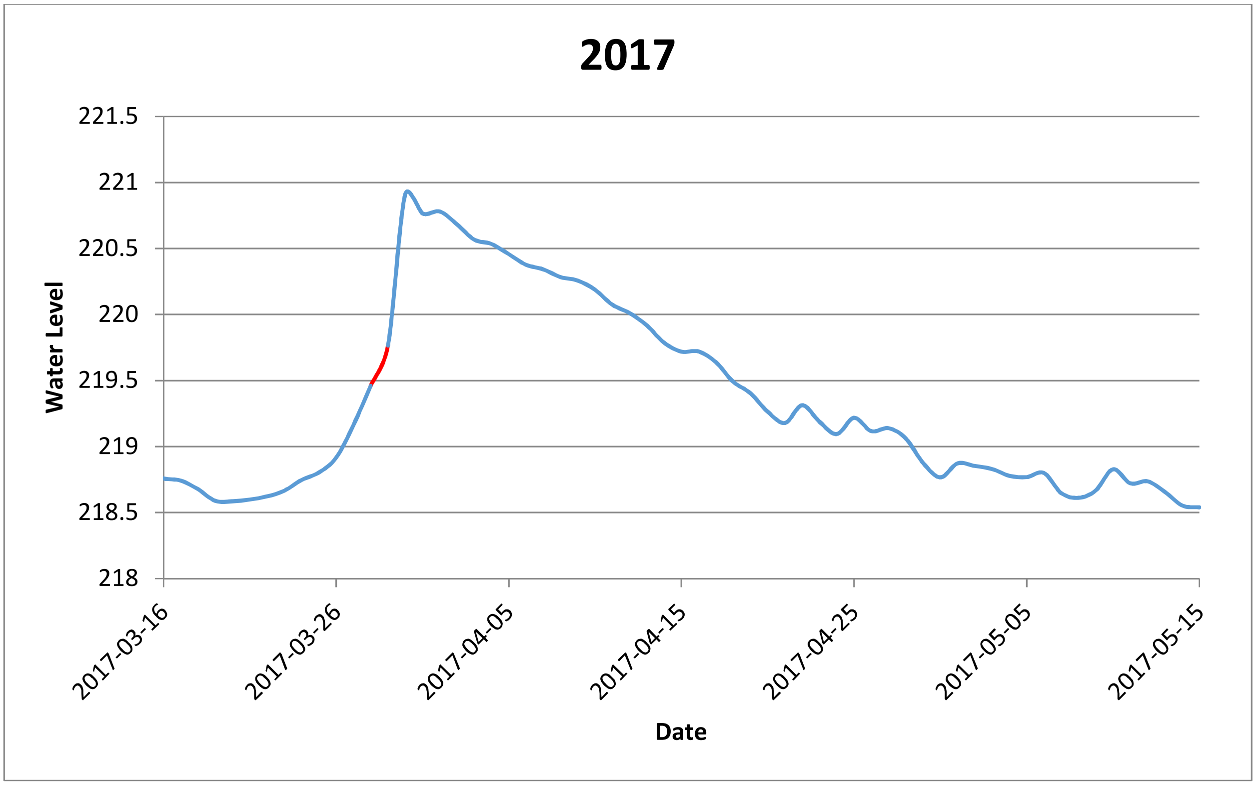

Figure B.46: Spring hydrograph for the Selkirk Generating Station in 2017.The red section of the line is the assumed time of breakup.

Appendix C: Breakup Initiation Dates

Table C.1: Breakup initiation dates on the Lower Red River from 1962-2017.

Breakup Initiation Dates
1962-04-20
1963-03-24
1964-04-16
1965-04-13
1966-04-02
1967-04-08
1968-04-08
1969-04-10
1970-04-17
1971-04-10
1972-04-09
1973-03-26
1974-04-18
1975-04-20
1976-04-05
1977-04-10
1978-04-06
1979-04-19
1980-04-12
1981-04-03
1982-01-01
1983-04-03
1984-04-07
1985-03-27
1986-03-30
1987-04-07
1988-04-04
1989-04-18
1990-04-05
1991-04-04
1992-03-29
1993-04-01
1994-04-08
1995-03-19
1996-04-17
1997-04-18
1998-03-29

Appendix C: Breakup Initiation Dates

1999-04-01
2000-03-27
2001-04-08
2002-04-11
2003-04-01
2004-03-30
2005-04-04
2006-04-02
2007-03-31
2008-04-11
2009-03-26
2010-03-24
2011-04-05
2012-03-19
2013-04-27
2014-04-16
2015-03-16
2016-03-16
2017-03-29

Appendix D: Discriminate Function Analysis Results

Table D.1: Discriminate function analysis results for the three-outcome model.

		LDA – With Flow			QDA – With Flow			QDA - Without Flow		
Year	Observed	No Jam	Minor Jam	Severe Jam	No Jam	Minor Jam	Severe Jam	No Jam	Minor Jam	Severe Jam
2017	Minor	15%	59%	26%	40%	55%	5%	60%	36%	4%
2016	Minor	17%	75%	8%	4%	93%	3%	7%	74%	19%
2015	No Jam	35%	49%	16%	99%	1%	0%	19%	72%	9%
2014	Severe	9%	11%	80%	0%	6%	94%	0%	4%	96%
2013	No Jam	40%	34%	25%	13%	81%	6%	22%	63%	15%
2012	No Jam	66%	34%	0%	97%	3%	0%	41%	59%	0%
2011	Severe	8%	31%	62%	26%	6%	68%	44%	4%	52%
2010	Minor	35%	60%	4%	8%	92%	0%	29%	70%	0%
2009	Severe	1%	24%	75%	2%	0%	98%	2%	7%	91%
2008	No Jam	56%	36%	8%	97%	3%	0%	28%	67%	5%
2007	Severe	38%	43%	19%	0%	5%	95%	1%	16%	83%
2006	No Jam	24%	58%	18%	20%	80%	0%	43%	57%	0%
2004	Severe	2%	3%	95%	0%	0%	100%	0%	0%	100%
2001	Minor	30%	62%	7%	28%	72%	0%	57%	43%	0%
2000	No Jam	81%	19%	0%	100%	0%	0%	66%	34%	0%
1999	Minor	48%	52%	1%	10%	90%	0%	47%	53%	0%
1998	Minor	23%	72%	5%	13%	87%	1%	41%	12%	47%
1997	No Jam	7%	64%	29%	100%	0%	0%	31%	68%	1%
1996	Severe	14%	76%	10%	8%	1%	91%	17%	54%	30%
1995	Severe	20%	58%	22%	14%	70%	15%	28%	57%	14%
1994	Minor	59%	38%	3%	85%	15%	0%	35%	65%	0%
1993	No Jam	69%	19%	12%	85%	1%	14%	30%	67%	3%
1992	Minor	28%	68%	5%	22%	70%	7%	40%	54%	6%
1991	No Jam	90%	10%	0%	100%	0%	0%	82%	18%	0%
1990	No Jam	82%	7%	11%	45%	0%	55%	59%	38%	3%
1989	Minor	70%	20%	10%	57%	43%	0%	64%	36%	0%
1988	No Jam	56%	43%	1%	84%	16%	0%	48%	51%	1%
1987	Minor	41%	59%	0%	3%	97%	0%	72%	28%	0%
1986	Minor	15%	82%	3%	2%	98%	0%	10%	90%	0%
1985	No Jam	44%	49%	7%	48%	52%	0%	20%	64%	16%
1979	No Jam	13%	58%	29%	96%	4%	0%	98%	2%	0%
1978	Minor	15%	76%	9%	12%	88%	0%	7%	93%	0%
1977	No Jam	95%	5%	0%	100%	0%	0%	99%	1%	0%
1976	Minor	28%	67%	5%	10%	89%	1%	23%	69%	8%
1975	No Jam	63%	33%	4%	100%	0%	0%	96%	4%	0%
1974	Severe	27%	18%	55%	10%	36%	54%	9%	12%	79%
1973	No Jam	75%	24%	0%	96%	4%	0%	73%	27%	0%
1972	Minor	24%	56%	20%	14%	86%	0%	18%	72%	10%

Appendix D: Discriminate Function Analysis Results

		LDA – With Flow			QDA – With Flow			QDA - Without Flow		
Year	Observed	No Jam	Minor Jam	Severe Jam	No Jam	Minor Jam	Severe Jam	No Jam	Minor Jam	Severe Jam
1971	Minor	24%	67%	8%	7%	93%	0%	16%	84%	0%
1970	Minor	14%	79%	8%	8%	92%	0%	19%	80%	1%
1969	Minor	17%	30%	53%	3%	31%	66%	4%	20%	76%
1968	No Jam	79%	20%	1%	99%	1%	0%	63%	37%	0%
1967	Severe	33%	34%	33%	3%	31%	66%	3%	16%	81%
1966	Minor	22%	22%	56%	28%	72%	0%	18%	35%	47%
1965	Minor	25%	45%	30%	0%	99%	1%	0%	98%	1%
1964	Minor	65%	34%	1%	16%	84%	0%	25%	75%	0%
1963	No Jam	25%	73%	1%	100%	0%	0%	100%	0%	0%
1962	No Jam	77%	17%	6%	100%	0%	0%	100%	0%	0%

Table D.2: Discriminate function analysis results for the two-outcome model.

		LDA - With Flow		QDA - With Flow		QDA - Without Flow	
Year	Observed	Non-event	Severe Jam	Non-event	Severe Jam	Non-event	Severe Jam
2017	Non-event	75%	25%	95%	5%	97%	3%
2016	Non-event	93%	7%	94%	6%	75%	25%
2015	Non-event	86%	14%	100%	0%	90%	10%
2014	Severe Jam	21%	79%	2%	98%	3%	97%
2013	Non-event	76%	24%	88%	12%	82%	18%
2012	Non-event	100%	0%	100%	0%	100%	0%
2011	Severe Jam	39%	61%	43%	57%	59%	41%
2010	Non-event	96%	4%	100%	0%	100%	0%
2009	Severe Jam	19%	81%	9%	91%	14%	86%
2008	Non-event	92%	8%	100%	0%	94%	6%
2007	Severe Jam	83%	17%	10%	90%	18%	82%
2006	Non-event	84%	16%	100%	0%	100%	0%
2004	Severe Jam	5%	95%	0%	100%	0%	100%
2001	Non-event	94%	6%	100%	0%	100%	0%
2000	Non-event	99%	1%	100%	0%	100%	0%
1999	Non-event	99%	1%	100%	0%	100%	0%
1998	Non-event	96%	4%	99%	1%	99%	1%
1997	Non-event	68%	32%	100%	0%	59%	41%
1996	Severe Jam	90%	10%	24%	76%	65%	35%
1995	Severe Jam	79%	21%	75%	25%	84%	16%
1994	Non-event	97%	3%	100%	0%	100%	0%
1993	Non-event	85%	15%	92%	8%	96%	4%

Appendix D: Discriminate Function Analysis Results

		LDA - With Flow		QDA - With Flow		QDA - Without Flow	
Year	Observed	Non-event	Severe Jam	Non-event	Severe Jam	Non-event	Severe Jam
1992	Non-event	96%	4%	93%	7%	96%	4%
1991	Non-event	99%	1%	100%	0%	100%	0%
1990	Non-event	77%	23%	59%	41%	97%	3%
1989	Non-event	87%	13%	100%	0%	100%	0%
1988	Non-event	99%	1%	100%	0%	99%	1%
1987	Non-event	100%	0%	100%	0%	100%	0%
1986	Non-event	97%	3%	100%	0%	100%	0%
1985	Non-event	94%	6%	100%	0%	82%	18%
1979	Non-event	72%	28%	100%	0%	100%	0%
1978	Non-event	92%	8%	100%	0%	100%	0%
1977	Non-event	100%	0%	100%	0%	100%	0%
1976	Non-event	96%	4%	98%	2%	90%	10%
1975	Non-event	96%	4%	100%	0%	100%	0%
1974	Severe Jam	45%	55%	34%	66%	20%	80%
1973	Non-event	100%	0%	100%	0%	100%	0%
1972	Non-event	82%	18%	100%	0%	89%	11%
1971	Non-event	93%	7%	100%	0%	99%	1%
1970	Non-event	93%	7%	100%	0%	99%	1%
1969	Non-event	49%	51%	18%	82%	18%	82%
1968	Non-event	99%	1%	100%	0%	100%	0%
1967	Severe Jam	69%	31%	17%	83%	14%	86%
1966	Non-event	46%	54%	100%	0%	50%	50%
1965	Non-event	73%	27%	94%	6%	97%	3%
1964	Non-event	99%	1%	100%	0%	100%	0%
1963	Non-event	99%	1%	100%	0%	100%	0%
1962	Non-event	92%	8%	100%	0%	100%	0%